The Pennsylvania State University

The Graduate School

John and Willie Leone Family Department of Energy and Mineral Engineering

# A SEMI-ANALYTICAL ANALYSIS OF THE GAS AND WATER FORECASTS FROM UNCONVENTIONAL RESERVOIRS

A Thesis in

Energy and Mineral Engineering

by

Abdulla Alzaabi



Submitted in Partial Fulfillment
of the Requirements
for the Degree of

Master of Science

May 2019

The thesis of Abdulla Alzaabi was reviewed and approved* by the following:

Gregory King
Professor of Practice Petroleum and Natural Gas Engineering
Thesis Advisor

Turgay Ertekin
Professor Emeritus of Petroleum and Natural Gas Engineering

John Wang
Associate Professor
Undergraduate Program Chair for Petroleum and Natural Gas Engineering

Luis F. Ayala H.
Professor of Petroleum and Natural Gas Engineering
Associate Head for Graduate Education
Energi Simulation Chair in Fluid Behavior and Rock Interactions

*Signatures are on file in the Graduate School

# ABSTRACT

Material balance is an essential reservoir engineering tool that is used to determine original hydrocarbon in place and the production performance of a reservoir. There are several types of material-balance approaches developed, each with its own application. Such approaches include integral material balance, differential material balance and flowing material balance. In this thesis, a form of differential material balance, similar to the one developed by Muskat for Solution Gas Drive Reservoirs, has been derived for unconventional gas-water reservoirs impacted by adsorption. Originally, the developed Muskat-type equation is in the pressure domain, but it can also be derived in other domains such as the time domain and the cumulative produced fluids domains. The resulting system of ordinary differential equations (ODEs) are then solved using fourth order Runge-Kutta method which is a traditional ODE solver.

The system of two differential equations for the Muskat-type equation in the time domain (time as an independent variable), are formulated with pressure and water saturation as the dependent variables. These resulting ODEs are then used to forecast and analyze the production profiles of a gas-water reservoir considering adsorption. The semi-analytical model is then validated internally using finite difference and analytical rate derivative equations, and externally by benchmarking it with a numerical simulator. The significant factor that caused the disparity between the semi-analytical model proposed in this study and the numerical simulator is the time it takes to reach pseudo-steady state flow ($t_{pss}$) with lower times producing better results. At $t_{pss}$ less than 0.111 days[1], numerical simulation is almost replaceable in forecasting rates. However, at $t_{pss}$ less than 0.717 days[1], cumulative gas produced can be accurately forecasted. This is to be expected and a reservoir simulator is fully transient, while material balance is based on the pseudo steady-state flow regime.

This study provided a unique opportunity to investigate the characteristics of the production profile such as the peak rate and the observed inflection points while also identifying the reservoir parameters that affect them. Moreover, an equation has been developed that can be used to identify and describe the peak rate. This equation makes use of the byproduct of the Muskat-type equation ($\frac{dS_w}{dP}$) which can be modified in terms of rock and fluid properties to aid in history matching. Furthermore, three well specifications were investigated (constant well pressure,

[1] This is not a general recommendation but was based off the limited amount of cases analyzed within this thesis. For a more general range of applicability, more cases will need to developed and analyzed.

constant drawdown, and constant water production rate) with only two of the three producing a peak rate – no peak gas production rate was observed for water rate specified wells. This study also showed that material balance can be used to replace decline curve analysis under certain conditions. This is mainly due to the reduced time to pseudo-steady state ($t_{pss}$) caused by the low total compressibility (rock and water), high permeability, low water viscosity, and low drainage area. At a threshold of $t_{pss}$ less than 0.178 days[1], an accurate late-time forecast can be attained.

Since the proposed semi-analytical model provided water saturation values for different pressures, a non-iterative methodology has been developed to improve upon King's (G. R. King, 1993) iterative integral material balance equation for unconventional reservoirs.

Through this study, a number of significant observations were made. It was found that at a low rock compressibility, the change in saturation over time can be estimated using the water production profile and initial porosity and water formation volume factor. Also, the saturation of gas can be estimated using the percentage of water produced from the original water in place (OWIP), adjusted for desorption time, at an increasing accuracy as the rock compressibility is decreased. Additionally, the cause of a phenomenon known as "dual peaking" which occurs in field and simulation data of CBM reservoirs has been identified to be due to the transient-state production.

# TABLE OF CONTENTS

# LIST OF FIGURES

# LIST OF TABLES

# ACKNOWLEDGEMENTS

All praise is due to Allah, the most merciful and most generous, for his blessings and giving me the strength to complete this thesis.

I would like to thank my parents and siblings for their immense support. If it was not for them, I would not have the strength and conviction to pursue my graduate studies. I could not thank them enough.

I would also like to thank my country, the United Arab Emirates, and ADNOC for providing me with the necessary means to continue my studies by covering all my expenses. A special thanks to His Highness Sheikh Khalifa bin Zayed Al Nahyan, His Highness Sheikh Mohammed bin Zayed Al Nahyan, His Highness Sheikh Mohammed bin Rashid Al Maktoum, and His Highness Sheikh Saud bin Saqr Al Qassimi for setting up funds, scholarships and opportunities for people like me to pursue their goals.

I owe a deep gratitude to Dr. Gregory King for accepting me as his student and taking me under his guidance. His constant encouragement has kept me striving to learn and develop skills that will surely be beneficial for me in the future. I also would like to extend my sincere thanks to Dr. Corina Drapaca for providing me with insight for my research.

I would like to thank Dr. Turgay Ertekin and Dr. John Wang for taking time out of their schedules and agreeing to be members of my committee.

# Chapter 1

# Introduction

In 1976, the U.S. government funded the Unconventional Gas Research Program in order to develop the U.S. domestic natural gas resource base. This step was in response to the OPEC oil embargo and as a consequence of the declining gas production. Unlike unconventional gas reservoirs, conventional gas reservoirs consist of drilling conventional vertical wells to tap into reservoirs of natural gas. In contrast, unconventional gas reservoirs are much more complicated to produce from. In order to extract unconventional gas at an economically desirable rate, a combination of techniques such as horizontal drilling and hydraulic fracturing needs to be used. In the 1990s, after years of innovation and federal support, these combined techniques became economically viable and common practice (American Energy Innovation Council, 2013). **Figure 1-1** shows the historical production before 2012 and the forecasted production of natural gas from different sources in the United States. More importantly, **Figure 1-1** shows that there is a decline in production from conventional reservoirs and a large increase in production from unconventional reservoirs, especially from shale gas.

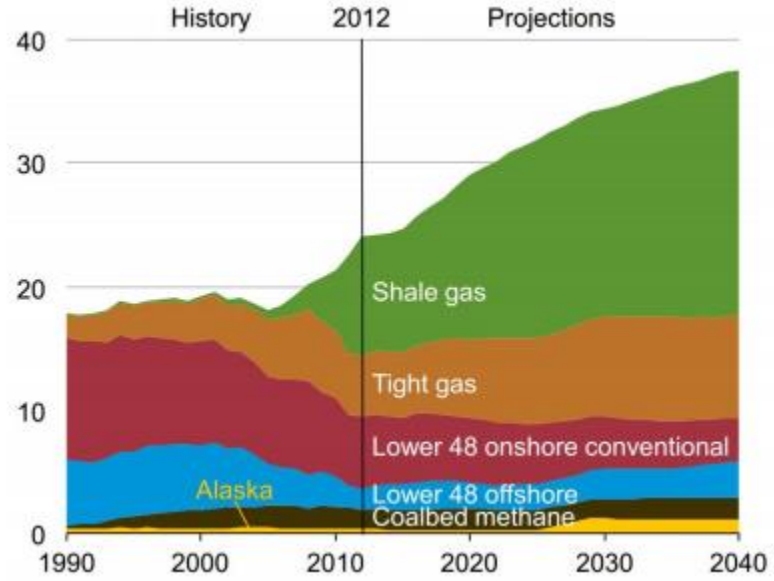


**Figure 1-1** - Natural gas production from different sources in the United States, in trillion cubic feet. (http://www.eia.gov)

The importance of unconventional gas reserves cannot be stressed enough, and its dramatic impact is changing the future energy landscape. Through advancements in technology and the development of innovative tools, a better economical output can be achieved from unconventional reserves.

In this study, a unique approach was attempted to characterize unconventional reservoirs. This was done analytically through the use of material balance which is a powerful tool that is used to determine original-fluids-in-place (OFIP) and forecast future reservoir performance. Then numerically through the utilization of a robust numerical method called Runge-Kutta which is used to solve ordinary differential equations (ODEs). Through the proposed model, a quick characterization of the reservoir performance and determination of OFIP can be carried out with minimal input and computational time. Moreover, this study provides the tools necessary to examine unique production profile phenomena that can help reservoir engineers achieve a better forecast of future production.

# Chapter 2

# Literature Review

## 2.1 Unconventional Gas Reservoirs

Unconventional reservoirs are characterized by their unique storage and transport properties including adsorption and diffusion. Unlike conventional reservoirs, they cannot be easily produced at an economically desirable flow rates or volumes to justify the costs of production. This is due to their special reservoir rock properties such as the low matrix permeability that makes it economically exploitable only with the assistance of stimulation techniques such as "hydraulic fracturing". Typical unconventional reservoirs are tight-gas, coalbed methane, gas shales. (Holditch, 2003)

### 2.1.1 Coalbed Methane

Coalbed methane is a form of unconventional gas reservoir that has distinct form of storage where most of the gas is stored through a process called adsorption on the organic matter. It is the source and reservoir (self-sourcing reservoir) for methane gas (with a very small amount of heavier hydrocarbons and no natural gas condensate).

Coalbed methane reservoirs are typically modeled as a dual porosity system: they contain macro-pore (primary porosity) and micro-pore (secondary porosity) system. The macro-pore system is made up of cleats. There are two types of cleats: face and butt cleats. The face cleats are continuous across the coal seam while the butt cleats are discontinuous and usually ends at the intersection with another face cleat as depicted in **Figure 2-1**. Each cleat type is generally

perpendicular to each other and they serve the role of transporting the fluids consisting of water and gas to the wellbore

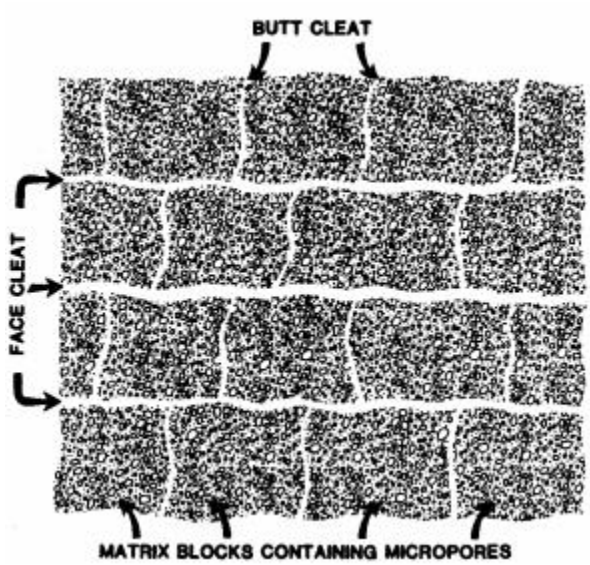


**Figure 2-1** - View of the dual-porosity nature of coal. (Gregory R. King, Ertekin, & Schwerer, 1986)

On the other hand, the micro-pores are inaccessible to water and serve as the main source of gas storage by the effect of adsorption on the coal matrix surface. Free gas can also exist in the micro-pores as well as the macro-pores. (Gregory R. King et al., 1986)

## 2.2 Adsorption

There are several concepts used to capture the process of adsorption. One of the most commonly used concepts was introduced by Langmuir in 1918. This simple sorption model is defined by the sorption pressure and sorption volume/capacity. The major assumptions in deriving the equation that represents this concept are as follow:

- One gas molecule is adsorbed at a single adsorption site (monolayer adsorption).

- An adsorbed molecule does not affect the molecule on the neighboring site.
- All adsorption sites are equivalent and are indistinguishable by the gas molecule.
- Adsorption is on an open surface with no resistance to gas access to adsorption site.

For coalbed methane (CBM) reservoirs, a Langmuir Adsorption Isotherm is commonly used to model the adsorption phenomena (Gregory R. King et al., 1986). The adsorbed gas volume at the average reservoir pressure, $V_d(P_{avg})$, in standard cubic feet of gas per cubic feet $[\mathrm{SCF/ft^3}]$, is given by the following equation:

$$V_d(P_{avg}) = \frac{V_L P_{avg}}{P_L + P_{avg}} \tag{2.1}$$

Where $V_L$ $[\mathrm{SCF/ft^3}]$ and $P_L$ [psia] are constants that correspond to the Langmuir Volume and Langmuir Pressure, respectively, and are properties of the coal seam. Langmuir Volume is the maximum adsorption capacity of the rock and the Langmuir Pressure is the pressure at which the gas content of the rock is equal to half the maximum adsorption capacity ($V_L$).

## 2.3 Material Balance

In petroleum engineering, the Material Balance Equation (MBE), which is based on the law of mass conservation, is used to determine original-fluids-in-place (OFIP) and making estimated predictions of future reservoir performance based on production and static pressure data. It is a model that considers the reservoir to have an isotropic tank behavior at any depth. Hence, the reservoir is assumed to have the same fluid properties and pressure at any location within it (Fekete Associates Inc., 2012). The MBE is usually represented with a crossplot of $P/z$ (pressure over gas compressibility factor) vs $G_p$ (cumulative gas production) which generally results in a straight line from which the original-fluid-in-place can be determined (Dake, 1978). However, when

considering unconventional reservoirs, alterations and assumptions have to be made, otherwise, inaccurate estimations of the OFIP will be made.

King (G. R. King, 1993) formulated a material balance equation that is applicable to unconventional gas reservoirs such as shales and coal seams. The MBE considers the fact that there is a dual porosity system made up of matrix and fractures within the reservoir. The equation also includes the effects of adsorbed gas.

Traditional material balance shows the relationship between the average pressure in the reservoir and the amount of gas produced. At the beginning, the reservoir is at initial reservoir pressure and no gas has been produced. When all the gas has been produced, the pressure in the reservoir is zero at which point the original-gas-in-place (OGIP) can be determined. In order to perform traditional material balance, the average reservoir pressure must be determined. This requires the well to be shut-in to obtain built-up reservoir pressures. This procedure causes the loss of valuable production. (Mattar & McNeil, 1998) presents a material balance method that does not require the well to be shut-in. This method consists of using “flowing” pressure instead of the average “shut-in” reservoir pressure. The method is considered to be very practical and provides results within reasonable certainty.

In 1945, Muskat developed the MBE in a differential form. The equation was given in terms of oil saturation as a function of pressure ($\frac{dS_o}{dP}$) and was solved using previously known pressures and new chosen lower pressure. The average of the two differential values was then used to determine the oil saturation at the new pressure. With the oil saturation known, it is possible to calculate the cumulative oil production. (Mosobalaje, Onuh, & Seteyeobot, 2015)

# Chapter 3

# Problem Statement

The objective of this thesis is to develop a differential material balance equation (Muskat-type equation) for gas reservoirs impacted by desorption. A MATLAB code will be developed to solve the derived system of differential equations using Runge-Kutta; a numerical method. This code will then be used to attempt to characterize a water-gas reservoir and the results will be benchmarked against a numerical simulator. The deliverables of this thesis are:

- Formulate the Muskat-type equation into a system of equations different domains.
    - Pressure domain.
    - Time domain.
    - Cumulative gas produced and cumulative water produced domain.
- Apply a traditional ODE solver such as Runge-Kutta to the differential mass balance equation in the pressure domain and the system of equations in the time domain.
- Analyze the production profiles for the gas and water in unconventional gas reservoirs using these equations.
    - Develop rate derivative equations ($\frac{dq}{dt}$).
    - Develop semi-analytical equations for time to peak gas production.
        - Specified (constant) well pressure, $P_{wf}$.
        - Specified (constant) water production, $q_w$.
        - Specified (constant) pressure drawdown, $(\bar{P} - P_{wf})$.

    - Develop methodology for time to peak gas rate.
        - Perform similar analysis in other domains.

- Explore the use of the developed equation as an alternative to decline curve analysis.
- Explore the use of these equations to develop a non-iterative $\frac{P}{Z^*}$ method for integral material balance.
- Explore the possibility of developing a transient version of all equations.
- Compare the developed equations and Runge-Kutta analysis against a numerical simulator.

# Chapter 4

# Coalbed Rock and Fluid Properties

Coalbed Methane was selected to be the unconventional reservoir used to evaluate the developed model. The reason for this is because adsorption plays a larger role in the production life of a coalbed methane reservoir. Also, unlike shale which spend most of its production life in the transient state flow regime, coalbed methane has a short transient state period. This provides the advantage of being able to model both transient state and pseudo-steady state flow regimes.

## 4.1 Rock Properties

### 4.1.1 Porosity

Coal is a compressible rock. Therefore, as the reservoir is depleted, porosity decreases (Seidle, 2011). This relationship is expressed as a ratio through the following equation:

$$\frac{\phi}{\phi_i} = 1 + c_\phi (P - P_i) \qquad \textbf{(4.1)}$$

Where

$\phi = porosity\ at\ reservoir\ pressure, fraction$
$\phi_i = porosity\ at\ initial\ reservoir\ pressure, fraction$
$P = reservoir\ pressure, psia$
$P_i = initial\ reservoir\ pressure, psia$
$c_\phi = cleat\ volume\ compressibility, psia^{-1}$

It is clear that porosity is a pressure dependent term that is also affected by the compressibility of the reservoir rock. Using the developed base case for this thesis, **Figure 4-1** has been generated to show the changes in porosity with a linear pressure decline.

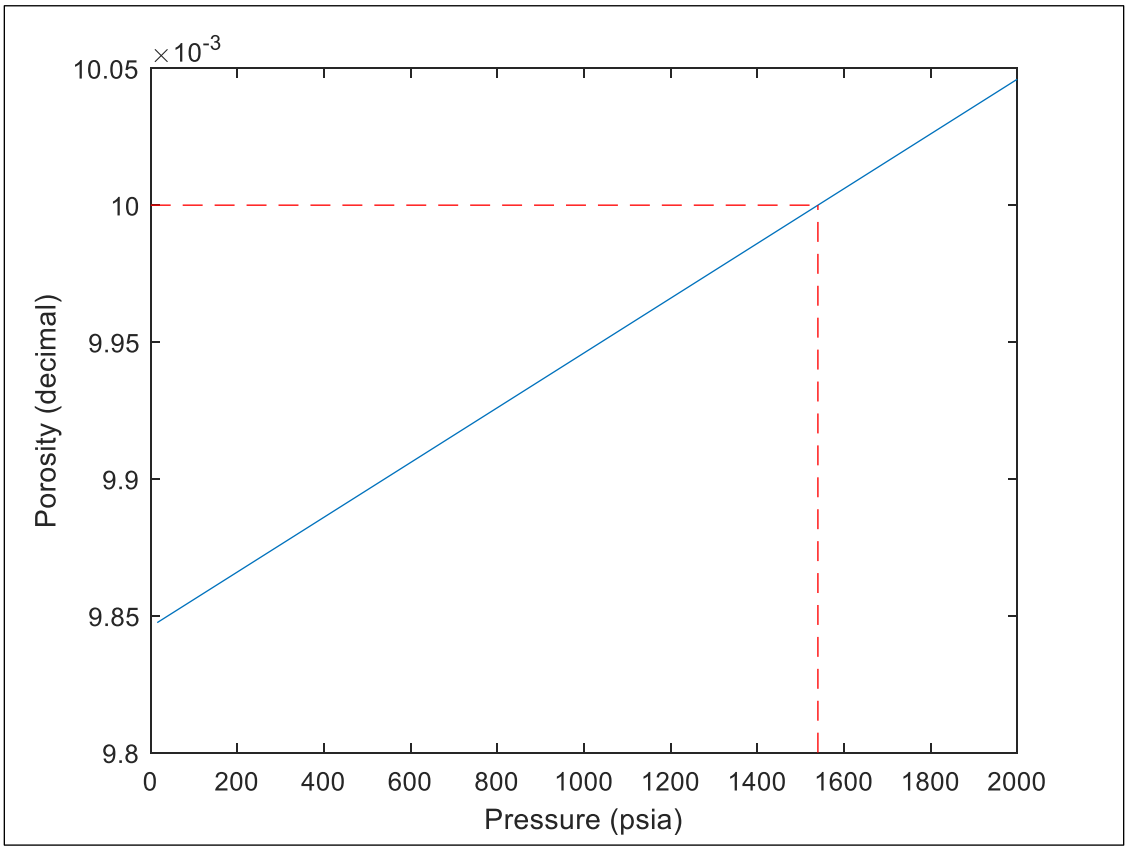


**Figure 4-1** - Porosity vs pressure using base case values of initial pressure (1540 psia) and rock compressibility (0.00001 psia^-1). The red dashed line signifies the initial values.

### 4.1.2 Permeability

Permeability was evaluated using the cubic power law model. This cubic relation between porosity and permeability can be applied to many naturally fractured reservoirs such as coals and shales (Liu & Harpalani, 2012).

Assuming that the coal matrix is stiff and that the cleat spacing remains constant as stress changes, permeability can be expressed using the following equation:

$$\frac{k}{k_i} = \left(\frac{\phi}{\phi_i}\right)^n \tag{4.2}$$

Where

$k = permeability, md$
$k_i = initial\ reservoir\ permeability, md$
$n = power\ law\ exponent, dimensionless$

The power exponent is usually assumed to be 3 but not necessarily since the exponent is a fitting parameter that can be varied accordingly. The porosity ratio model used is the one discussed in the previous section. **Figure 4-2** shows the permeability changes with a linear pressure decline.

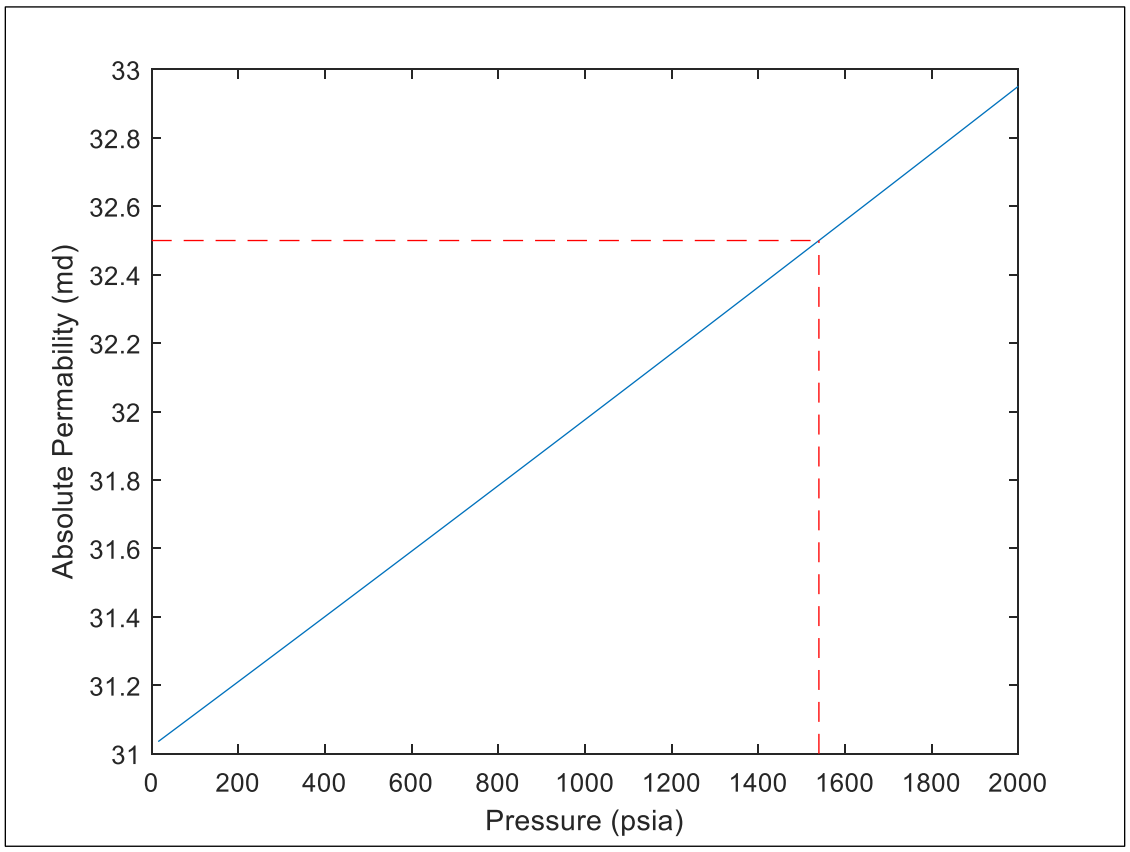


**Figure 4-2** - Permeability vs pressure using base case values for pressure (1540 psia) and rock compressibility (0.00001 psia^-1) in the porosity model. The red dashed line signifies the initial values.

## 4.2 Gas Properties

### 4.2.1 Gas Compressibility Factor (Z)

Due to the fact that this problem employs gas in the form of methane, the gas compressibility factor (z-factor) needs to be evaluated at different reservoir pressures. The z-factor is used to calculate the gas formation volume factor and gas density at different reservoir pressures through the real-gas law. It is also used in material balance in order to estimate gas reserves (Dune & Bright N, 2012).

In 1973, Hall and Yarborough developed an accurate correlation to be used to estimate the gas compressibility factor (z-factor) for natural gas (Fatoorehchi, Abolghasemi, Rach, & Assar, 2014). This correlation was designed to fit the Standing-Katz gas compressibility factor charts (Dune & Bright N, 2012)The Hall-Yarborough equation is defined through the following parameters:

$$t_r = \frac{1}{T_{pr}} \tag{4.3}$$

$$A = 0.06125\ t_r\ e^{-1.2(1-t_r)^2} \tag{4.4}$$

$$B = t_r\ (14.76 - 9.76\ t_r + 4.58\ t_r^2) \tag{4.5}$$

$$C = t_r\ (90.7 - 242.2\ t_r + 42.4\ t_r^2) \tag{4.6}$$

$$D = 2.18 + 2.82\ t_r \tag{4.7}$$

And

$$z = \frac{A\ P_{pr}}{Y} \tag{4.8}$$

$$f(Y) = \frac{Y + Y^2 + Y^3 - Y^4}{(1-Y)^3} - A\ P_{pr} - B\ Y^2 + C\ Y^D = 0 \tag{4.9}$$

Pseudo-reduced pressure $P_{pr}$ and pseudo-reduced temperature $T_{pr}$ can be calculated through the following equations:

$$P_{pr} = \frac{P}{P_c} \tag{4.10}$$

$$T_{pr} = \frac{T}{T_c} \tag{4.11}$$

Where $T$ and $P$ are the reservoir temperature and pressure respectively, and $P_c$ and $T_c$ are the gas critical values.

In order to calculate Y, Newton-Raphson iterative algorithm is generally used. Newton-Raphson is a powerful iterative algorithm that finds the roots of a real-valued function (Press, 2007). The Newton-Raphson algorithm is as follows:

$$x_{i+1} = x_i - \frac{f(x)}{f'(x)} \tag{4.12}$$

Where $x_i$ is the initial guess. The solution is then found through iterating until the error converges to a very small number.

The derivative $f'(Y)$ needed to solve the equation for Y is:

$$f'(Y) = \frac{1 + 4\,Y + 4\,Y^2 - 4\,Y^3 + Y^4}{(1 - Y)^4} - 2\,B\,Y + C\,D\,Y^{D-1} \tag{4.13}$$

A MATLAB function has been developed for this model which takes in pressure and temperature values to solve for z-factor. **Figure 4-3** shows the changes in z-factor with a linear pressure decline and a constant temperature (581°R) derived from the base case that is used in this analysis.

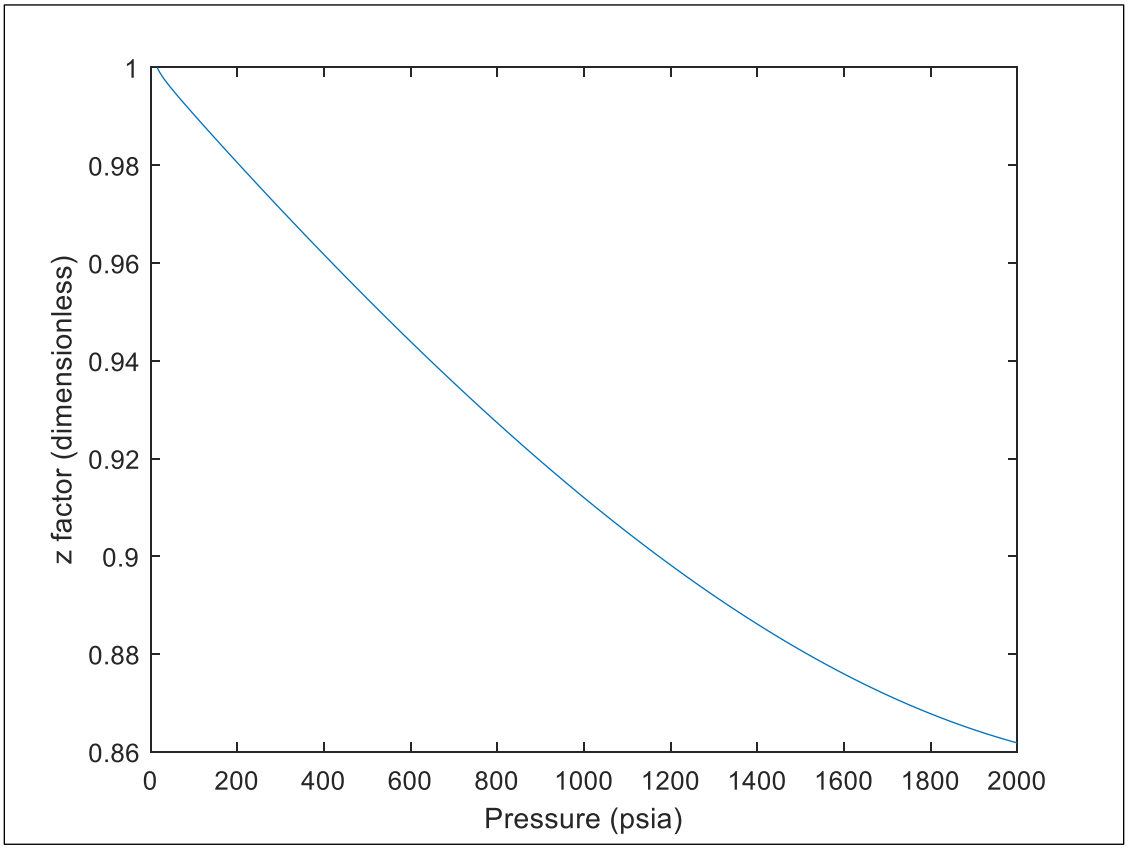


**Figure 4-3** - z-factor vs pressure evaluated using Newton-Raphson with the base case reservoir temperature of 581 Rankine.

### 4.2.2 Gas Viscosity

In this study, the gas viscosity of methane is a pressure and temperature dependent variable. The gas viscosity is obtained by using the Lee-Gonzalez-Eakin empirical correlation (A. L. Lee, Gonzalez, & Eakin, 1966).

$$\mu_g = K\, e^{(X\, \rho_g{}^{Y})} \tag{4.14}$$

Where

$$K = \frac{(7.77 + 0.0063\, M)\, T^{1.5}}{122.4\ + 12.9\, M + T} \tag{4.15}$$

$$X = 2.57 + \frac{1941.5}{T} + 0.0095\, M \tag{4.16}$$

$$Y = 1.11 + 0.04\, X \tag{4.17}$$

And

$\mu_g = gas\ viscosity, cp$
$\rho_g = gas\ density, gm/cc$
$T = absolute\ temperature, R$
$M = molecular\ weight$

The molecular weight of methane is 16.04.

The density of gas in g/cc, which is a pressure dependent variable, can be obtained from the real-gas law.

$$\rho_g = 0.00149406\, \frac{P\, M}{z\, T} \tag{4.18}$$

As discussed previously for z-factor, a MATLAB function has been developed that requires the inputs of pressure, z-factor for the corresponding pressure, and reservoir temperature to calculate the gas viscosity at that specified pressure and temperature. **Figure 4-4** shows the changes

in gas viscosity with a linear pressure decline and a constant temperature (581°R) derived from the base case that is used in this analysis.

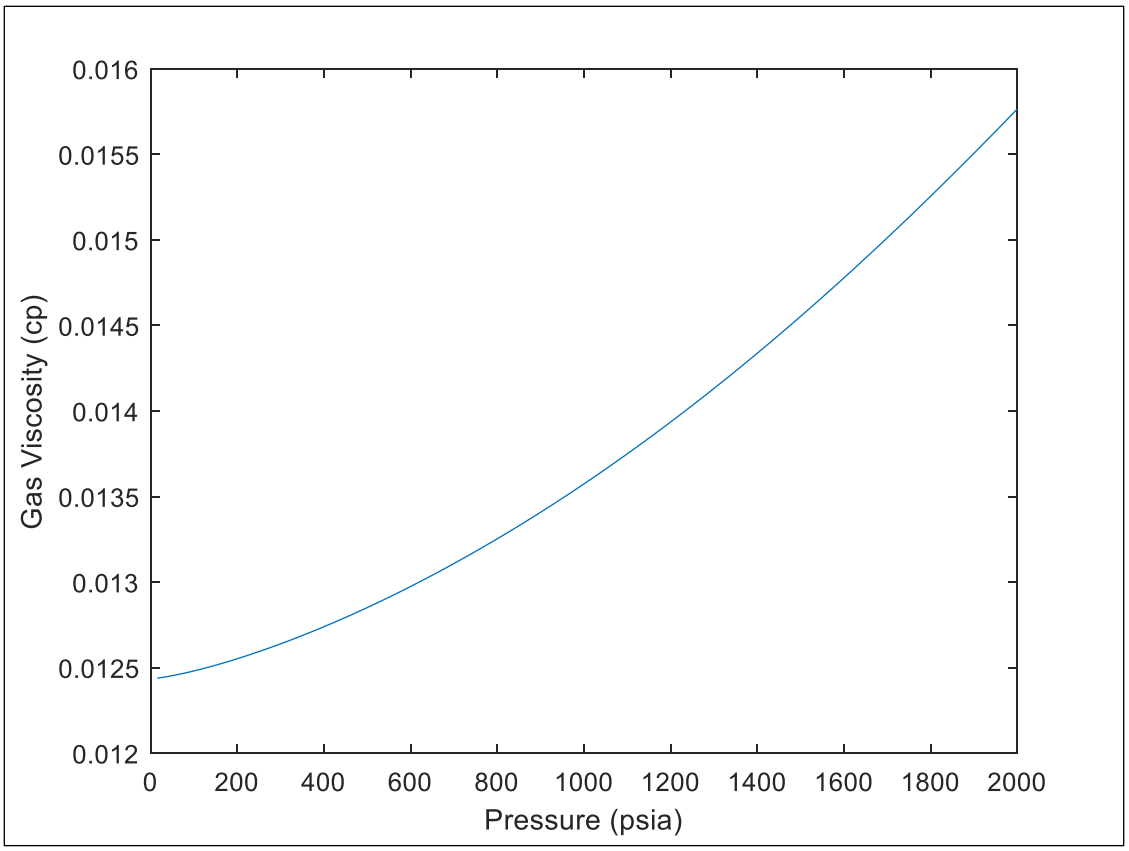


**Figure 4-4** - Gas viscosity vs pressure.

### 4.2.3 Gas Formation Volume Factor

The real-gas law is used to give the expression for gas formation volume factor $B_g$ in terms of the volume ratio of gas at reservoir conditions and standard conditions (Ertekin, Abou-Kassem, & King, 2001).

$$B_g = \frac{P_{sc}\, T\, z}{T_{sc}\, P} \tag{4.19}$$

Where

$B_g = gas\ formation\ volume\ factor, ft^3/SCF$
$P_{sc} = pressure\ at\ standard\ conditions, psia$
$T_{sc} = temperature\ at\ standard\ conditions, R$
$z = gas\ compressibility\ factor, dimensionless$

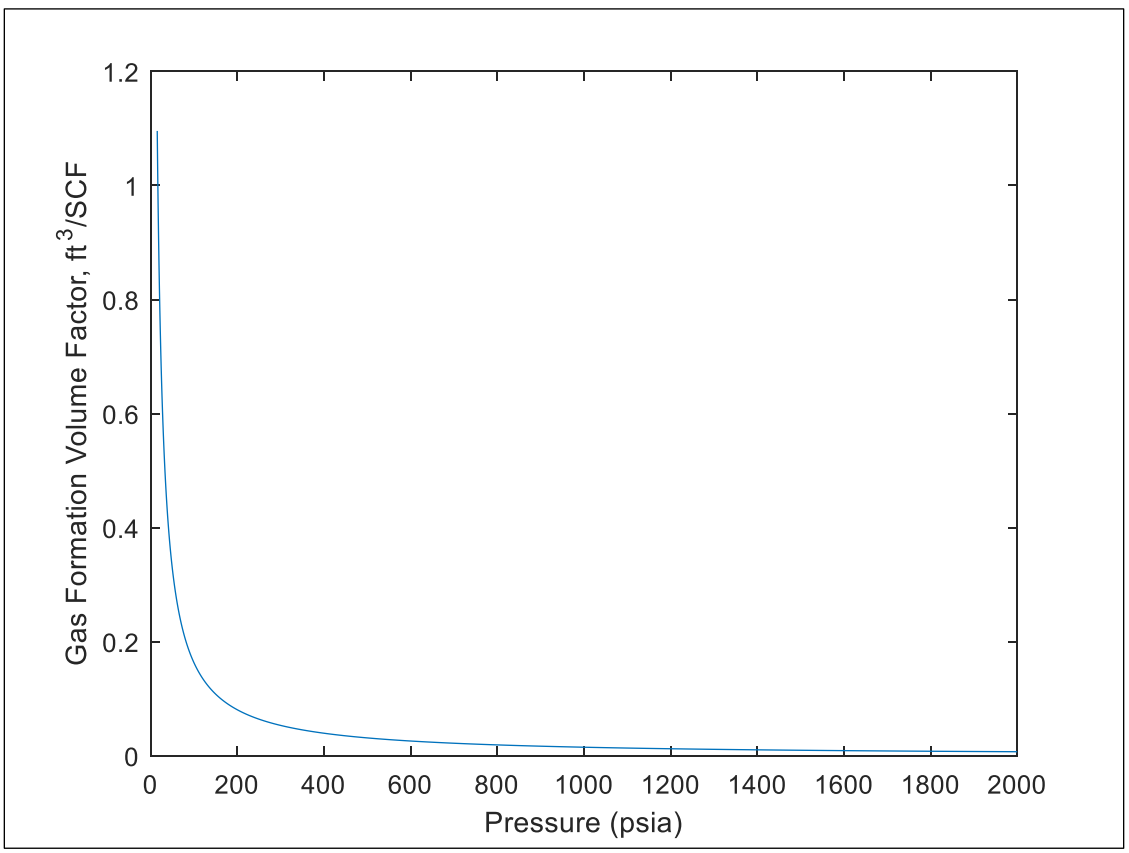


**Figure 4-5** - Gas formation volume factor vs pressure.

**Figure 4-5** shows the changes in the gas formation volume factor with pressure. It seems that at high pressures, the gas has a very low formation volume factor which is expected since formation volume factor is a ratio between the volume of gas at standard conditions versus the volume of gas in the reservoir. Therefore, at high pressures, the gas is compressed and occupies a smaller volume than at low pressures.

## 4.3 Water Properties

Without loss of generality, in this study, the water compressibility is assumed to be a constant of $3.2 * 10^{-6}$ $[psia^{-1}]$. Also, water viscosity is assumed to be a constant of 1 $[cp]$.

### 4.3.1 Water Formation Volume Factor

For slightly compressible fluids, such as water, the water formation volume factor can be approximated using the following equation (Ertekin et al., 2001):

$$B_w = \frac{B_{wi}}{[1 + c_w(P - P_i)]} \tag{4.20}$$

Where

$B_w = water\ formation\ volume\ factor, bbl/STB$
$B_{wi} = initial\ water\ formation\ volume\ factor, bbl/STB$
$c_w = water\ compressibility, psia^{-1}$

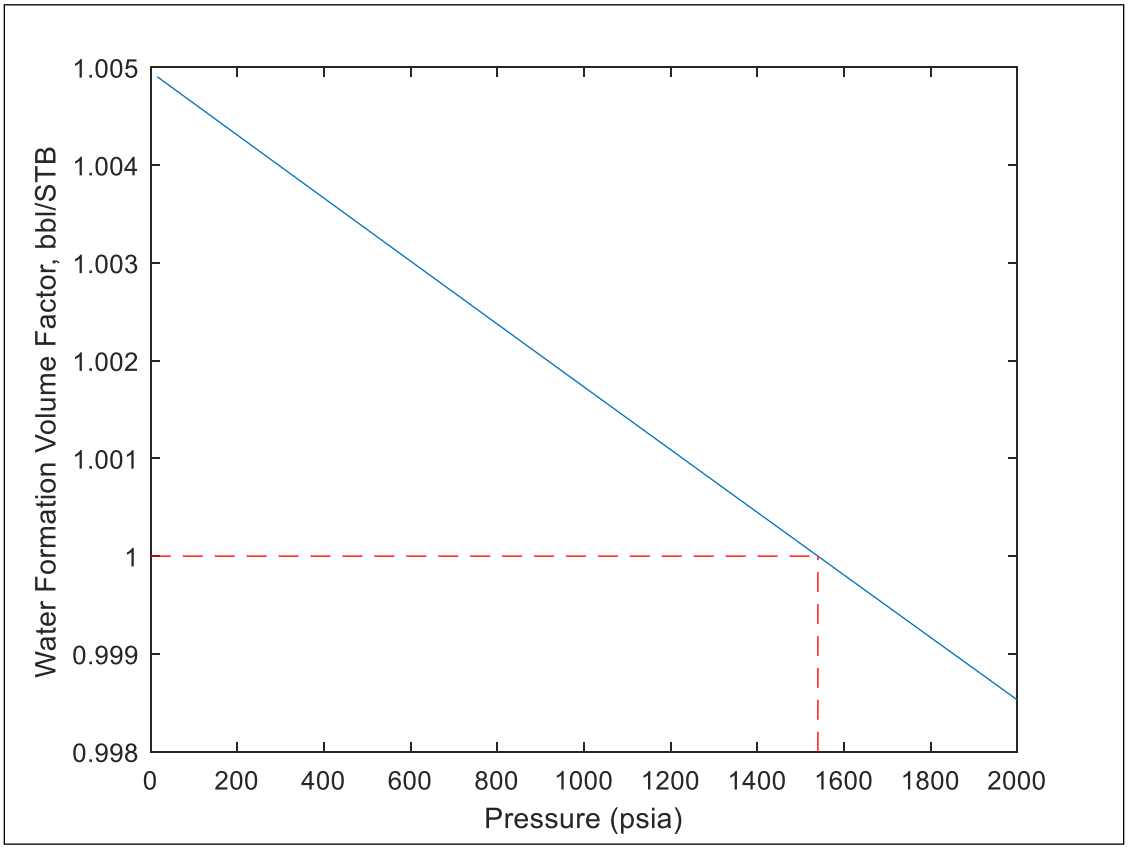


**Figure 4-6** - Water formation volume factor vs pressure. The red dashed line signifies initial conditions.

### 4.4 Fluids Relative Permeabilities

Since there are two fluids present during production, the movement of one fluid is restricted due to movement of the other. Relative permeabilities are used to quantify the movement of one fluid relative to the other. The values of the relative permeability range between 0 and 1 where 1 is considered maximum mobility. In this case, modified Brooks-Corey relative permeability model is used. This model is also known as the "power-law" model. For a gas-water system, the relationships are as follows:

$$k_{rg} = k_{rg,max}\left(\frac{S_g - S_{gc}}{1 - S_{wir} - S_{gc}}\right)^{N_g} \quad \textbf{(4.21)}$$

$$k_{rw} = k_{rw,max}\left(\frac{S_w - S_{wir}}{1 - S_{wir}}\right)^{N_w} \quad \textbf{(4.22)}$$

Where

$k_{rg} = relative\ permeability\ of\ gas, decimal$
$k_{rg,max} = maximum\ possible\ relative\ permeability\ of\ gas, decimal$
$S_g = saturation\ of\ gas, decimal$
$S_{gc} = critical\ saturation\ of\ gas, decimal$
$N_g = gas\ permeability\ exponent, dimensionless$
$k_{rw} = relative\ permeability\ of\ water, decimal$
$k_{rw,max} = maximum\ possible\ relative\ permeability\ of\ water, decimal$
$S_w = saturation\ of\ water, decimal$
$S_{gc} = irreducible\ water\ saturation, decimal$
$N_w = water\ permeability\ exponent, dimensionless$

The permeability exponents $N_w$ and $N_g$ range from 1 to 6. The maximum relative permeability of water ($k_{rw,max}$) is 1 since it is possible to have all the gas adsorbed at some point with no fluid in the pore volume except water. As for the maximum relative permeability of gas ($k_{rg,max}$), in the base case for this model, it is assumed to be 0.8. The

critical saturation of gas ($S_{gc}$) is the saturation at which gas starts to mobilize. Using base case values, **Figure 4-7** is generated to show the changes in permeability of a fluid relative to the other.

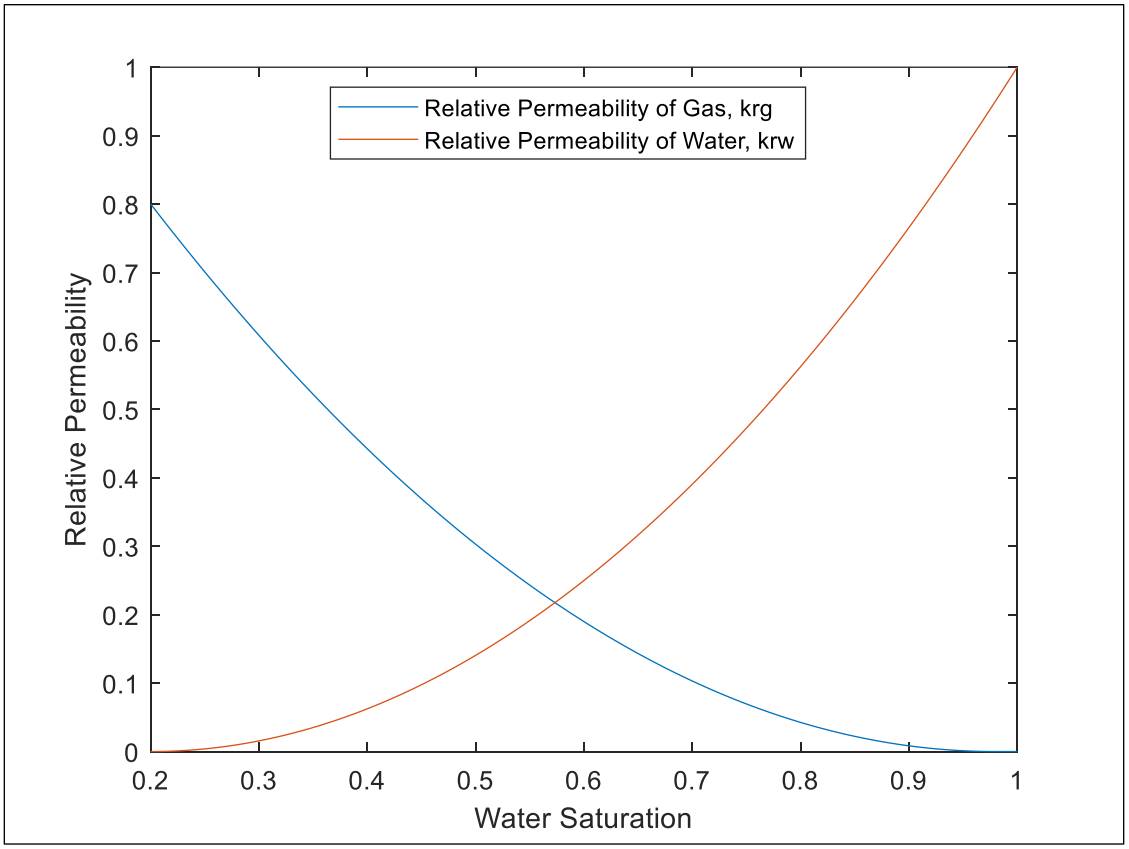


**Figure 4-7** - Relative permeabilities plot with base case values (Swir = 0.2, Nw = 2, Ng = 2, Sgc = 0.02).

### 4.5 Range of Properties Investigated

To validate the developed model, different ranges of reservoir properties have been derived from literatures. The data have been separated into three ranges; lower range, mid-range (which is also the base case), and an upper range. This ensures that the model provides valid results for the different range of properties while also exemplifies the effects of the change in properties with the results pursued. In this case, the Fruitland formation in the San Juan basin located in western United States has been selected to be used as the base case to validate the developed model. This specific

selection enables the results from the developed model to be compared with the reported production data provided in literatures in order to further validate the results.

The process for determining the range of properties involved taking a set of data for a given property that is reported by literatures. The property values are usually determined from different samples from different reservoirs. After that, through MATLAB's "prctile" function, the 10$^{th}$ percentile and 90$^{th}$ percentile of the collective data are calculated and determined to be the minimum and maximum values respectively. The way that MATLAB's "prctile" function works is that it sorts the data set in ascending order and then it uses an algorithm and linear interpolation to compute the desired percentile. To keep the range symmetric and avoid inconsistency, the base case was calculated to be the average of the minimum and maximum range values when appropriate.

Using data sourced from (Seidle, 2011), (Ayers, 2001), (Palmer & Mansoori, 1996) and (Mavor, Owen, & Pratt, 1990), the same process in determining the range is applied for other reservoir properties such as langmuir pressure and volume. Some of the reservoir parameters such as the area of the reservoir and the desorption pressure have been assumed.

According to (Ayers, 2001), the temperature of the Fruitland formation in San Juan basin is less than 140°F. Using this information, a temperature gradient of 0.02°F$/ft$ has been derived using the maximum depth which is stated to be 3600 $ft$ and corresponds to the maximum temperature of 140°F. Ayers also states that the basin contains a mixture of overpressured and underpressured zones. For overpressured zones, the bottomhole pressure is equivalent to a simple pressure gradient of 0.44 – 0.63 $psi/ft$ and it is 0.30 – 0.40 $psi/ft$ in the underpressured zones. Therefore, for consistency, the bottomhole pressure/initial reservoir pressure is calculated using an averaged pressure gradient of 0.5 $psi/ft$.

Operating conditions such as the well flowing pressure were also assumed. For the well flowing pressure, the base case was assumed to be 40% of the initial reservoir pressure while the minimum and maximum are 35% and 45% of the initial reservoir pressure respectivily.

For simplicity, the numerical values were rounded to the nearest integer when appropriate and the results are summarized in **Table 4-1**.

**Table 4-1 - Reservoir Parameters' Ranges**

| Parameter's Name | | Min | Base Case | Max | Unit |
|---|---|---|---|---|---|
| Area | A | 60 | 80 | 100 | $[Acres]$ |
| Depth | | 2500 | 3050 | 3600 | $[ft]$ |
| Thickness | h | 30 | 50 | 70 | $[ft]$ |
| Porosity | Ø | 0.005 | 0.01 | 0.02 | $[Fraction]$ |
| Permeability | k | 5 | 32.5 | 60 | $[md]$ |
| Rock Compressibility | $C_{\emptyset}$ | $1 * 10^{-6}$ | $1 * 10^{-5}$ | $1 * 10^{-4}$ | $[psia^{-1}]$ |
| Langmuir Pressure | $P_L$ | 91 | 309 | 389 | $[psia]$ |
| Langmuir Volume | $V_L$ | 611 | 756 | 1471 | $[\frac{SCF}{ton}]$ |
| Initial Pressure | $P_i$ | 1265 | 1540 | 1815 | $[psia]$ |
| Reservoir Temperature | T | 116 | 121 | 140 | $[°F]$ |
| Desorption Pressure | $P_d$ | 1165 | 1490 | 1815 | $[psia]$ |
| Well Flowing Pressure | $P_{wf}$ | 443 | 616 | 817 | $[psia]$ |

The developed model uses correlations in order to calculate relative permeabilities for the fluid present in the reservoir. The correlations contain coefficients which vary within a certain range. **Table 4-2** summarizes the fluid properties and correlation coefficients assumed range.

**Table 4-2 - Fluid Parameters' Ranges**

| Parameter's Name | | Min | Base Case | Max |
|---|---|---|---|---|
| Critical Gas Saturation | $S_{gc}$ | 0 | 2 | 4 |
| Irreducible Water Saturation | $S_{wir}$ | 0.15 | 0.20 | 0.25 |
| Exponential Coefficient for Gas | $N_g$ | 3 | 2 | 1 |
| Exponential Coefficient for Water | $N_w$ | 3 | 2 | 1 |

# Chapter 5

# Formulation

This chapter shows the derivation of the Muskat-type equation for pseudo-steady state in the pressure domain, and then in the time domain, and in other domains such as the cumulative gas and water produced domain. It also shows the derivation of the same equation but for "pseudo-transient" state with a variable bulk volume and drainage radius as the pressure wave travels across the reservoir.

## 5.1 Derivation of Muskat-type Equation

### 5.1.1 Derivation of Differential Material Balance (Muskat-type) From in Place Volumes

Starting with the equations for Original Gas in Place (OGIP) and Original Water in Place (OWIP), an equation for the production rate can be derived.

$$OGIP = G = \frac{V_b\, \phi_i\, S_{gi}}{\alpha_c\, B_{gi}} + V_b V_d \qquad \textbf{(5.1)}$$

Where

$G = Gas\ in\ Place, SCF$
$V_b = reservoir\ bulk\ volume, ft^3$
$\phi_i = initial\ porosity, decimal$
$S_{gi} = initial\ gas\ saturation, decimal$
$B_{gi} = initial\ gas\ formation\ volume\ factor, bbl/SCF$
$V_d = adsorption\ isotherm, SCF/ft^3$
And $\alpha_c$ is a conversion factor equal to $5.615\ ft^3/bbl$ in order to maintain consistent units.

The Langmuir adsorption isotherm is given by the following equation:

$$V_d = \frac{V_L\, P}{P + P_L} \tag{5.2}$$

Where,

$V_L = Langmuir\ volume, SCF/ft^3$
$P_L = Langmuir\ pressure, psia$
$P = reservoir\ pressure, psia$

This isotherm gives a measure of the amount of gas adsorbed on the reservoir rock.

The rate of gas produced can be linked to the amount of gas available in the reservoir over the time of production using the following equation:

$$q_g = \frac{dG_p}{dt} = -\frac{dG}{dt} = -\frac{1}{\alpha_c}\frac{d}{dt}\left(V_b\left[\frac{\phi\, S_g}{B_g} + V_d\right]\right) \tag{5.3}$$

Where

$q_g = gas\ production\ rate, SCF/ft^3$
$S_g = gas\ saturation, decimal$

The same can be done for Original Water in Place (OWIP) to determine the water production rate.

$$OWIP = W = \frac{V_b\, \phi_i\, S_{wi}}{\alpha_c\, B_{wi}} \tag{5.4}$$

Where

$S_{wi} = initial\ water\ saturation, decimal$

$$q_w = \frac{dW_p}{dt} = -\frac{dW}{dt} = -\frac{1}{\alpha_c}\frac{d}{dt}\left(\frac{V_b\, \phi\, S_w}{B_w}\right) \tag{5.5}$$

Where

$q_w = gas\ production\ rate, bbl/day$
$S_w = water\ saturation, decimal$

### 5.1.2 Derivation of Differential Material Balance (Muskat-type) From the Definition of Pseudo-Steady State Flow

During pseudo-steady state flow, which generally occurs at the late time region of production, the outer boundaries of the reservoir is assumed to be no flow boundaries. Therefore, the reservoir can be assumed to behave like a tank and the pressure gradient is constant throughout the reservoir. However, the absolute reservoir pressure varies with time (Slider, 1966). This justifies the use of the average reservoir pressure when calculating rates using Darcy's equation. The advantage of using pseudo-steady state flow assumption instead of steady-state flow assumption is because steady-state flow assumes that the pressure and flow rate throughout the reservoir remain constant with time. Basically, the amount of mass entering the reservoir is the same amount of leaving the reservoir. This assumption is simply unrealistic. On the other hand, there is unsteady-state flow which assumes that the rate and pressure do change with time. This assumption is ideal, however, the solutions to unsteady-state flow equations are generally very complex and hard to apply (Slider, 1966). Instead, pseudo-steady state flow assumption, which is simpler to apply, can be used to give an acceptable approximation.

Equations **(5.3)** and **(5.5)** can be modified to represent pseudo-steady state flow. Since it is assumed that the pressure wave has reached the boundary of the reservoir and the drainage radius is fixed. Thus, the reservoir bulk volume can be moved out of the derivative.

$$q_g = -\frac{V_b}{\alpha_c}\frac{d}{dt}\left[\left(\frac{\phi\, S_g}{B_g}\right) + V_d\right] \tag{5.6}$$

$$q_w = -\frac{V_b}{\alpha_c}\frac{d}{dt}\left(\frac{\phi\, S_w}{B_w}\right) \tag{5.7}$$

### 5.1.3 Derivation of Differential Material Balance (Muskat-type) From the Diffusivity Equation With Standard Well Test Assumptions

From mass balance, the continuity equation can be used to describe one-dimensional, radial flow in porous media. By introducing Darcy's flow law into the continuity equation, the resulting equation for gas flow is (J. Lee, 1981)

$$\frac{1}{r}\frac{\partial}{\partial r}\left(r\frac{\rho_g\, k_{rg}\, k}{\mu_g}\frac{dP}{dr}\right) = \frac{1}{\alpha_c}\frac{\partial}{\partial t}\left(\rho_g\, \phi\right) \qquad \textbf{(5.8)}$$

Where,

$\rho_g = density\ of\ gas, lb/ft^3$
$\mu_g = gas\ viscosity, cp$
$k = absolute\ permeability, md$

The goal is to develop the Muskat-type equation from the continuity equation which provides a stronger relationship that proves the validity of the Muskat-type equation than that derived using fluids in place equations and pseudo-steady state assumptions. This would also prove that the Muskat-type equation can be used for transient flow with common assumption used in pressure transient analysis which are that the pressure and saturation gradients are small.

The formation volume factor of gas can be introduced using the following equation:

$$\rho_g = \frac{\rho_{scg}}{B_g} \qquad \textbf{(5.9)}$$

Where

$\rho_{scg} = density\ of\ gas\ at\ standard\ conditions, lb/ft^3$

$$\frac{1}{r}\frac{\partial}{\partial r}\left(r\frac{\rho_{scg}\, k_{rg}\, k}{B_g\, \mu_g}\frac{\partial P}{\partial r}\right) = \frac{1}{\alpha_c}\frac{\partial}{\partial t}\left(\frac{\rho_{scg}\, \phi}{B_g}\right) \qquad \textbf{(5.10)}$$

Since $\rho_{scg}$ is a constant, it can be eliminated from both sides of the equation.

$$\frac{1}{r}\frac{\partial}{\partial r}\left(r\frac{k_{rg}\, k}{B_g\, \mu_g}\frac{dP}{dr}\right) = \frac{1}{\alpha_c}\frac{\partial}{\partial t}\left(\frac{\phi}{B_g}\right) \qquad \textbf{(5.11)}$$

The equation can also be modified further in order to include gas desorption and saturation changes over time on the right-hand side of the equation.

$$\frac{1}{r}\frac{\partial}{\partial r}\left(r\frac{k_{rg}\,k}{B_g\,\mu_g}\frac{\partial P}{\partial r}\right)=\frac{1}{\alpha_c}\frac{\partial}{\partial t}\left(\frac{\phi\,S_g}{B_g}+V_d\right) \tag{5.12}$$

On the left-hand side of the equation, $k_{rg}$ is a saturation dependent term while $\frac{k}{B_g\,\mu_g}$ is a pressure dependent term. Defining pressure and saturation dependent functions:

$$f_{gP}=\frac{k}{B_g\,\mu_g} \tag{5.13}$$

$$f_{gS}=k_{rg} \tag{5.14}$$

Therefore,

$$\frac{1}{r}\frac{\partial}{\partial r}\left(r\,f_{gS}\,f_{gP}\,\frac{\partial P}{\partial r}\right)=\frac{1}{\alpha_c}\frac{\partial}{\partial t}\left(\frac{\phi\,S_g}{B_g}+V_d\right) \tag{5.15}$$

First, the left-hand side of the equation can be expanded using the product rule for derivation:

$$\frac{1}{r}\left[r\frac{\partial}{\partial r}\left(f_{gS}\,f_{gP}\frac{\partial P}{\partial r}\right)+\,f_{gS}\,f_{gP}\frac{\partial P}{\partial r}\frac{\partial}{\partial r}(r)\right]=\frac{1}{\alpha_c}\frac{\partial}{\partial t}\left(\frac{\phi\,S_g}{B_g}+V_d\right) \tag{5.16}$$

$$\frac{1}{r}\left[r\left\{f_{gS}\,\frac{\partial}{\partial r}\left(\,f_{gP}\frac{\partial P}{\partial r}\right)+\,f_{gP}\frac{\partial P}{\partial r}\frac{\partial f_{gS}}{\partial r}\right\}+\,f_{gS}\,f_{gP}\frac{\partial P}{\partial r}\right]=\frac{1}{\alpha_c}\frac{\partial}{\partial t}\left(\frac{\phi\,S_g}{B_g}+V_d\right) \tag{5.17}$$

The derivative of $f_{gS}$ is separated in terms of its saturation dependency.

$$\frac{1}{r}\left[r\left\{f_{gS}\,\frac{\partial}{\partial r}\left(\,f_{gP}\frac{\partial P}{\partial r}\right)+\,f_{gP}\frac{\partial P}{\partial r}\frac{\partial f_{gS}}{\partial S}\frac{\partial S}{\partial r}\right\}+\,f_{gS}\,f_{gP}\frac{\partial P}{\partial r}\right]=\frac{1}{\alpha_c}\frac{\partial}{\partial t}\left(\frac{\phi\,S_g}{B_g}+V_d\right) \tag{5.18}$$

Expand using product rule again.

$$\frac{1}{r}\left[r\left\{f_{gS}\,\left(\,f_{gP}\frac{\partial^2 P}{\partial r^2}+\frac{\partial P}{\partial r}\frac{\partial f_{gP}}{\partial r}\right)+\,f_{gP}\frac{\partial P}{\partial r}\frac{\partial f_{gS}}{\partial S}\frac{\partial S}{\partial r}\right\}+\,f_{gS}\,f_{gP}\frac{\partial P}{\partial r}\right]=\frac{1}{\alpha_c}\frac{\partial}{\partial t}\left(\frac{\phi\,S_g}{B_g}+V_d\right) \tag{5.19}$$

The derivative of $f_{gP}$ is separated again in terms of its saturation dependency.

$$\frac{1}{r}\left[r\left\{f_{gS}\,\left(\,f_{gP}\frac{\partial^2 P}{\partial r^2}+\frac{\partial P}{\partial r}\frac{\partial f_{gP}}{\partial P}\frac{\partial P}{\partial r}\right)+\,f_{gP}\frac{\partial P}{\partial r}\frac{\partial f_{gS}}{\partial S}\frac{\partial S}{\partial r}\right\}+\,f_{gS}\,f_{gP}\frac{\partial P}{\partial r}\right]=\frac{1}{\alpha_c}\frac{\partial}{\partial t}\left(\frac{\phi\,S_g}{B_g}+V_d\right) \tag{5.20}$$

Simplifying,

$$\frac{1}{r}\left[r\left\{f_{gS}\left[f_{gP}\frac{\partial^2 P}{\partial r^2}+\frac{\partial f_{gP}}{\partial P}\left(\frac{\partial P}{\partial r}\right)^2\right]+f_{gP}\frac{\partial P}{\partial r}\frac{\partial f_{gS}}{\partial S}\frac{\partial S}{\partial r}\right\}+f_{gS}\,f_{gP}\frac{\partial P}{\partial r}\right]=\frac{1}{\alpha_c}\frac{\partial}{\partial t}\left(\frac{\phi\,S_g}{B_g}+V_d\right) \quad \textbf{(5.21)}$$

Assuming that the pressure gradients are small, then the second order pressure gradients are small and can be neglected, thus, $\left(\frac{dP}{dr}\right)^2$ can be eliminated. Also, saturation changes are assumed to be small as well, therefore, $\frac{dP}{dr}\frac{dS}{dr}$ can be considered a second order gradient and can also be eliminated.

$$\frac{1}{r}\left[r\left\{f_{gS}\,f_{gP}\frac{\partial^2 P}{\partial r^2}\right\}+f_{gS}\,f_{gP}\frac{\partial P}{\partial r}\right]=\frac{1}{\alpha_c}\frac{\partial}{\partial t}\left(\frac{\phi\,S_g}{B_g}+V_d\right) \quad \textbf{(5.22)}$$

Simplifying,

$$\frac{f_{gS}\,f_{gP}}{r}\left[r\frac{\partial^2 P}{\partial r^2}+\frac{dP}{dr}\right]=\frac{1}{\alpha_c}\frac{\partial}{\partial t}\left(\frac{\phi\,S_g}{B_g}+V_d\right) \quad \textbf{(5.23)}$$

Since

$$\frac{\partial}{\partial r}\left(r\frac{dP}{dr}\right)=r\frac{\partial^2 P}{\partial r^2}+\frac{\partial P}{\partial r} \quad \textbf{(5.24)}$$

Then

$$\frac{f_{gS}\,f_{gP}}{r}\left[\frac{\partial}{\partial r}\left(r\frac{\partial P}{\partial r}\right)\right]=\frac{1}{\alpha_c}\frac{\partial}{\partial t}\left(\frac{\phi\,S_g}{B_g}+V_d\right) \quad \textbf{(5.25)}$$

Similarly, an equation can be derived for water flow:

$$\frac{f_{wS}\,f_{wP}}{r}\left[\frac{\partial}{\partial r}\left(r\frac{\partial P}{\partial r}\right)\right]=\frac{1}{\alpha_c}\frac{\partial}{\partial t}\left(\frac{\phi\,S_w}{B_w}\right) \quad \textbf{(5.26)}$$

$$f_{wP}=\frac{k}{B_w\,\mu_w} \quad \textbf{(5.27)}$$

$$f_{wS}=k_{rw} \quad \textbf{(5.28)}$$

Where

$\mu_w = water\ viscosity, cp$
$k_{rw} = relative\ permeability\ of\ water, decimal$

Dividing equation **(5.25)** by **(5.26)** yields the gas-water ratio on the right-hand side and the Muskat-type equation on the left-hand side.

$$\frac{f_{gS}\, f_{gP}}{f_{wS}\, f_{wP}} = \frac{\frac{\partial}{\partial t}\left(\frac{\phi\, S_g}{B_g} + V_d\right)}{\frac{\partial}{\partial t}\left(\frac{\phi\, S_w}{B_w}\right)} \tag{5.29}$$

The derivation of left-hand side of equation **(5.29)** into $\frac{dS_w}{dP}$ (Muskat-type equation) will be shown in the section (5.2).

The significance of the derivation from the diffusivity equation is that the saturation as a function of pressure obtained from the Muskat-type equation is valid for evaluating relative permeabilities in pressure *transient* analysis (Camacho-V, 1991) provided the conditions of gradients are achieved.

### 5.1.4 Derivation of Differential Material Balance (Muskat-type) From the Diffusivity Equation Using the Divergence Theorem

The Muskat-type equation can also be evaluated with no restrictions such as the negligible pressure gradients assumption used in section (5.1.3) by using the divergence theorem. Equation **(5.8)** can be rewritten in terms of the divergence (Dake, 1978).

$$\nabla \cdot \left(f_{gS}\, f_{gP} \frac{\partial P}{\partial r}\right) = \frac{1}{\alpha_c} \frac{\partial}{\partial t}\left(\frac{\phi\, S_g}{B_g} + V_d\right) \tag{5.30}$$

The divergence theorem states that the volume integral of the divergence is equal to the integral of the surface surrounding the bulk volume (Arfken & Weber, 2005).

$$\int_{V_b} \nabla \cdot \vec{F}\; dV_b = \int_{\sigma} \hat{n}\, \vec{F}\, d\sigma \tag{5.31}$$

Where $\hat{n}$ is the normal vector to the vector field $\vec{F}$.

Applying this theorem to the left-hand side of equation **(5.30)**:

$$\int_{V_b} \nabla \cdot \left( f_{gS}\, f_{gP} \frac{\partial P}{\partial r} \right) dV_b = \int_{\sigma} \left( f_{gS}\, f_{gP} \frac{\partial P}{\partial r} \right) d\sigma \qquad \textbf{(5.32)}$$

$f_{gS}\, f_{gP} \frac{dP}{dr}$ is basically Darcy's law in terms of velocity and it is constant over the surface of the reservoir. Thus, it can be moved out of the integral.

$$\int_{V_b} \nabla \cdot \left( f_{gS}\, f_{gP} \frac{\partial P}{\partial r} \right) dV_b = \left( f_{gS}\, f_{gP} \frac{\partial P}{\partial r} \right) \int_{\sigma} d\sigma \qquad \textbf{(5.33)}$$

The integral of the surface of the entire reservoir yields area.

$$\int_{V_b} \nabla \cdot \left( f_{gS}\, f_{gP} \frac{\partial P}{\partial r} \right) dV_b = \left( f_{gS}\, f_{gP} \frac{\partial P}{\partial r} \right) A \qquad \textbf{(5.34)}$$

Where A is the area of the reservoir in units squared.

The right-hand side of the equation is now Darcy's law in terms of rate since velocity multiplied by area yields rate.

$$q_g = \frac{\partial}{\partial t} \int_{V_b} \frac{1}{\alpha_c} \left( \frac{\phi\, S_g}{B_g} + V_d \right) dV_b \qquad \textbf{(5.35)}$$

Multiplying and dividing by $V_b$ , and exporting the constant $\alpha_c$ outside the integral and derivative.

$$q_g = \frac{V_b}{\alpha_c} \frac{\partial}{\partial t} \left( \frac{1}{V_b} \int_{V_b} \left( \frac{\phi\, S_g}{B_g} + V_d \right) dV_b \right) \qquad \textbf{(5.36)}$$

Integrating each term separately.

$$q_g = \frac{V_b}{\alpha_c} \frac{\partial}{\partial t} \left( \frac{1}{V_b} \left[ \int_{V_b} \frac{\phi\, S_g}{B_g} dV_b + \int_{V_b} V_d\, dV_b \right] \right) \qquad \textbf{(5.37)}$$

Since

$$\bar{F} = \frac{1}{V_b} \int_{V_b} F\, dV_b \qquad \textbf{(5.38)}$$

Then the same can be applied to equation **(5.37)**.

$$q_g = \frac{V_b}{\alpha_c}\frac{\partial}{\partial t}\left(\overline{\frac{\phi\, S_g}{B_g}} + \overline{V_d}\right) \tag{5.39}$$

Where

$$\frac{\partial}{\partial t}\left(\overline{\frac{\phi\, S_g}{B_g}} + \overline{V_d}\right) \neq \frac{\partial}{\partial t}\left(\frac{\phi\, S_g}{B_g} + V_d\right) \tag{5.40}$$

The difference in the derived Muskat-type equation using the divergence theorem is that it is an approximation by using the average of the entire derivative while the previous derivation developed in (5.1.3) is evaluated with $\bar{P}$ and $\bar{S}$ only.

The same method can be applied to derive water rate.

$$q_w = \frac{V_b}{\alpha_c}\frac{\partial}{\partial t}\left(\overline{\frac{\phi\, S_w}{B_w}}\right) \tag{5.41}$$

## 5.2 Derivation of Muskat-type Equation for Pseudo-Steady State

This section shows the derivation of the Muskat-type equation for pseudo-steady state in different domains.

### 5.2.1 Pseudo-Steady State in the Time Domain

$$q_g = \frac{V_b}{\alpha_c}\frac{d}{dt}\left[\left(\frac{\phi\, S_g}{B_g}\right) + V_d\right] \tag{5.42}$$

$$q_w = \frac{V_b}{\alpha_c}\frac{d}{dt}\left(\frac{\phi\, S_w}{B_w}\right) \tag{5.43}$$

Gas production rate can be rewritten to be given in terms of water saturation:

$$q_g = \frac{V_b}{\alpha_c}\frac{d}{dt}\left[\left(\frac{\phi\,(1-S_w)}{B_g}\right) + V_d\right] \quad \textbf{(5.44)}$$

To evaluate the derivative present in both production equations, each variable needs to be broken down depending on their pressure dependency.

Using the following derivation method:

$$f = \frac{a_1\,a_2\,a_3\,...}{b_1\,b_2\,b_3\,...} \quad \textbf{(5.45)}$$

Applying natural logarithm to both sides of the equation:

$$\ln f = \ln(\frac{a_1\,a_2\,a_3\,...}{b_1\,b_2\,b_3\,...}) \quad \textbf{(5.46)}$$

Using logarithm multiplication and division rule, the equation can be rewritten to:

$$\ln f = \ln a_1 + \ln a_2 + \ln a_3 - \ln b_1 - \ln b_2 - \ln b_3 \quad \textbf{(5.47)}$$

Taking the derivative of both sides of the equation:

$$\frac{1}{f}\frac{df}{dt} = \frac{d}{dt}(\ln a_1 + \ln a_2 + \ln a_3 - \ln b_1 - \ln b_2 - \ln b_3) \quad \textbf{(5.48)}$$

$$\frac{1}{f}\frac{df}{dt} = \frac{1}{a_1}\frac{da_1}{dt} + \frac{1}{a_2}\frac{da_2}{dt} + \frac{1}{a_2}\frac{da_2}{dt} - \frac{1}{b_1}\frac{db_1}{dt} - \frac{1}{b_2}\frac{db_2}{dt} - \frac{1}{b_3}\frac{db_3}{dt} \quad \textbf{(5.49)}$$

$$\frac{df}{dt} = f(\frac{a_1{}'}{a_1} + \frac{a_1{}'}{a_1} + \frac{a_1{}'}{a_1} - \frac{b_1{}'}{b_1} - \frac{b_2{}'}{b_2} - \frac{b_3{}'}{b_3}) \quad \textbf{(5.50)}$$

Therefore, by applying the same method to equation **(5.43)** and **(5.44)**. Starting with the water production equation:

$$q_w = \frac{V_b}{\alpha_c}\left(\frac{\phi\,S_w}{B_w}\right)(\frac{\phi'}{\phi} + \frac{S_w{}'}{S_w} - \frac{B_w{}'}{B_w}) \quad \textbf{(5.51)}$$

$$q_w = \frac{V_b}{\alpha_c}\left(\frac{\phi\,S_w}{B_w}\right)(\frac{1}{\phi}\frac{d\phi}{dP}\frac{dP}{dt} + \frac{1}{S_w}\frac{dS_w}{dt} - \frac{1}{B_w}\frac{dB_w}{dP}\frac{dP}{dt}) \quad \textbf{(5.52)}$$

$$q_w = \frac{V_b}{\alpha_c}\left[S_w\left(\frac{1}{B_w}\frac{d\phi}{dP} - \phi\frac{dB_w}{dP}\right)\frac{dP}{dt} + \frac{\phi}{B_w}\frac{dS_w}{dt}\right] \quad \textbf{(5.53)}$$

Likewise, the gas production equation can be expanded to the following:

$$q_g = \frac{V_b}{\alpha_c}\left[\left(\frac{\phi\,(1-S_w)}{B_g}\right)(\frac{\phi'}{\phi} + \frac{(1-S_w)'}{(1-S_w)} - \frac{B_g{}'}{B_g}) + \frac{dV_d}{dP}\frac{dP}{dt}\right] \quad \textbf{(5.54)}$$

$$q_g = \frac{V_b}{\alpha_c}\left[\left(\frac{\phi\,(1-S_w)}{B_g}\right)(\frac{1}{\phi}\frac{d\phi}{dP}\frac{dP}{dt} - \frac{1}{(1-S_w)}\frac{dS_w}{dt} - \frac{1}{B_g}\frac{dB_g}{dP}\frac{dP}{dt}) + \frac{dV_d}{dP}\frac{dP}{dt}\right] \quad \textbf{(5.55)}$$

$$q_g = \frac{V_b}{\alpha_c}\left\{\left[(1-S_w)\left(\frac{1}{B_g}\frac{d\phi}{dP} - \phi\frac{dB_w}{dP}\right) + \frac{dV_d}{dP}\right]\frac{dP}{dt} - \frac{\phi}{Bg}\frac{dS_w}{dt}\right\} \quad \textbf{(5.56)}$$

The two equations can then be presented in a simplified format by grouping up the terms with respect to pressure and saturation:

$$q_w = C_{wP}\frac{dP}{dt} + C_{wS}\frac{dS_w}{dt} \quad \textbf{(5.57)}$$

$$q_g = C_{gP}\frac{dP}{dt} + C_{gS}\frac{dS_w}{dt} \quad \textbf{(5.58)}$$

Where

$$C_{wP} = \frac{V_b S_w}{\alpha_c}\left[\frac{1}{B_w}\frac{d\phi}{dP} - \phi\frac{dB_w}{dP}\right] \quad \textbf{(5.59)}$$

$$C_{wS} = \frac{V_b\phi}{\alpha_c B_w} \quad \textbf{(5.60)}$$

$$C_{gP} = \frac{V_b}{\alpha_c}\left[(1-S_w)\left(\frac{1}{B_g}\frac{d\phi}{dP} - \phi\frac{dB_w}{dP}\right) + \frac{dV_d}{dP}\right] \quad \textbf{(5.61)}$$

$$C_{gS} = -\frac{V_b\emptyset}{\alpha_c B_g} \quad \textbf{(5.62)}$$

Now, equations **(5.57)** and **(5.58)** can be solved simultaneously to derive the two ordinary differential equations of pressure and saturation in the time domain.

Multiply equation **(5.57)** by $C_{gS}$:

$$C_{gS}\, q_w = C_{gS}\, C_{wP} \frac{dP}{dt} + C_{gS}\, C_{wS} \frac{dS_w}{dt} \qquad \textbf{(5.63)}$$

Multiply equation **(5.58)** by $C_{wS}$:

$$C_{wS}\, q_g = C_{wS}\, C_{gP} \frac{dP}{dt} + C_{wS}\, C_{gS} \frac{dS_w}{dt} \qquad \textbf{(5.64)}$$

Subtract equation **(5.64)** from **(5.63)**:

$$C_{gS}\, q_w - C_{wS}\, q_g = \left(C_{gS}\, C_{wP} - C_{wS}\, C_{gP}\right) \frac{dP}{dt} \qquad \textbf{(5.65)}$$

Therefore, the equation for pressure in the time domain is:

$$\frac{dP}{dt} = \frac{C_{gS}\, q_w - C_{wS}\, q_g}{\left(C_{gS}\, C_{wP} - C_{wS}\, C_{gP}\right)} \qquad \textbf{(5.66)}$$

The equation can be also written in terms of one production variable by substituting in a gas-water ratio which is given by the following equation:

$$Gas - Water\ Ratio = \frac{q_g}{q_w} = R = \alpha_c \frac{k_{rg}}{\mu_g\, B_g} \frac{\mu_w\, B_w}{k_{rw}} \qquad \textbf{(5.67)}$$

Therefore,

$$\frac{dP}{dt} = \frac{(C_{gS} - C_{wS}\, R) q_w}{\left(C_{gS}\, C_{wP} - C_{wS}\, C_{gP}\right)} \qquad \textbf{(5.68)}$$

Likewise, equations **(5.57)** and **(5.58)** can be solved to give saturation in the time domain:

Multiply equation **(5.57)** by $C_{gP}$:

$$C_{gP}\, q_w = C_{gP}\, C_{wP} \frac{dP}{dt} + C_{gP}\, C_{wS} \frac{dS_w}{dt} \qquad \textbf{(5.69)}$$

Multiply equation **(5.58)** by $C_{wP}$:

$$C_{wP}\, q_g = C_{wP}\, C_{gP} \frac{dP}{dt} + C_{wP}\, C_{gS} \frac{dS_w}{dt} \qquad \textbf{(5.70)}$$

Subtract equation **(5.69)** from **(5.70)**:

$$C_{wP}\, q_g - C_{gP}\, q_w = \left(C_{gS}\, C_{wP} - C_{wS}\, C_{gP}\right)\frac{dS_w}{dt} \qquad \textbf{(5.71)}$$

Therefore, the equation for saturation in the time domain is:

$$\frac{dS_w}{dt} = \frac{C_{wP}\, q_g - C_{gP}\, q_w}{\left(C_{gS}\, C_{wP} - C_{wS}\, C_{gP}\right)} \qquad \textbf{(5.72)}$$

Substituting in the gas-water ratio:

$$\frac{dS_w}{dt} = \frac{\left(C_{wP}\, R - C_{gP}\right) q_w}{\left(C_{gS}\, C_{wP} - C_{wS}\, C_{gP}\right)} \qquad \textbf{(5.73)}$$

### 5.2.2 Pseudo-Steady-State in the Pressure Domain

By diving equation **(5.66)** from **(5.72)**, the Muskat type equation can be derived in order to give saturation as a function of pressure.

$$\frac{dS_w}{dP} = \frac{\frac{dS_w}{dt}}{\frac{dP}{dt}} = \frac{\frac{C_{wP}\, q_g - C_{gP}\, q_w}{\left(C_{gS}\, C_{wP} - C_{wS}\, C_{gP}\right)}}{\frac{C_{gS}\, q_w - C_{wS}\, q_g}{\left(C_{gS}\, C_{wP} - C_{wS}\, C_{gP}\right)}} = \frac{C_{wP}\, q_g - C_{gP}\, q_w}{C_{gS}\, q_w - C_{wS}\, q_g} \qquad \textbf{(5.74)}$$

The equation can be rewritten using the gas-water ratio:

$$\frac{dS_w}{dP} = \frac{C_{wP}\, R - C_{gP}}{C_{gS} - C_{wS}\, R} \qquad \textbf{(5.75)}$$

This is especially useful in material balance as it enables the calculation of z* in King's material balance equation in order to evaluate the original-gas-in-place (OGIP) within a reservoir using pressure data only.

### 5.2.3 Pseudo-Steady-State in Other Domains

The Muskat type equation can also be derived in domains other than pressure and time. It can be evaluated in the total gas produced domain. This can prove to be useful in observing the effects of pressure and saturation drops on the total gas produced from the reservoir.

Since the change in the total gas produced over the change in time is the rate of production as follows:

$$\frac{dG_p}{dt} = q_g \tag{5.76}$$

Where $G_p$ is the total gas produced from the reservoir.

Then by manipulating the equation,

$$\frac{dP}{dG_p} = \frac{\frac{dP}{dt}}{\frac{dG_p}{dt}} = (\frac{1}{q_g})\frac{dP}{dt} \tag{5.77}$$

$$\frac{dS_w}{dG_p} = \frac{\frac{dS_w}{dt}}{\frac{dG_p}{dt}} = (\frac{1}{q_g})\frac{dS_w}{dt} \tag{5.78}$$

The same can be done with the total water produced from the reservoir.

$$\frac{dW_p}{dt} = q_w \tag{5.79}$$

$$\frac{dP}{dW_p} = \frac{\frac{dP}{dt}}{\frac{dW_p}{dt}} = (\frac{1}{q_w})\frac{dP}{dt} \tag{5.80}$$

$$\frac{dS_w}{dW_p} = \frac{\frac{dS_w}{dt}}{\frac{dW_p}{dt}} = (\frac{1}{q_w})\frac{dS_w}{dt} \tag{5.81}$$

### 5.3 Derivation for Pseudo-Transient State

During the beginning of production from a reservoir, the pressure wave slowly begins to travel outwards with time. At this stage, the pressure wave has not reached the reservoir boundary and therefore, the behavior of the pressure is the same as that in an infinite reservoir (Matthews, 1986). Unlike pseudo-steady state, the pressure gradient is not constant throughout the reservoir which makes it difficult, or rather, inaccurate, to assume an average reservoir pressure. The difference between both flow states is presented in **Figure 5-1**. Nevertheless, the "pseudo-transient" state equation can be derived, and the solution can be compared to pseudo-steady state solution to evaluate its accuracy while benchmarked against a numerical simulator.

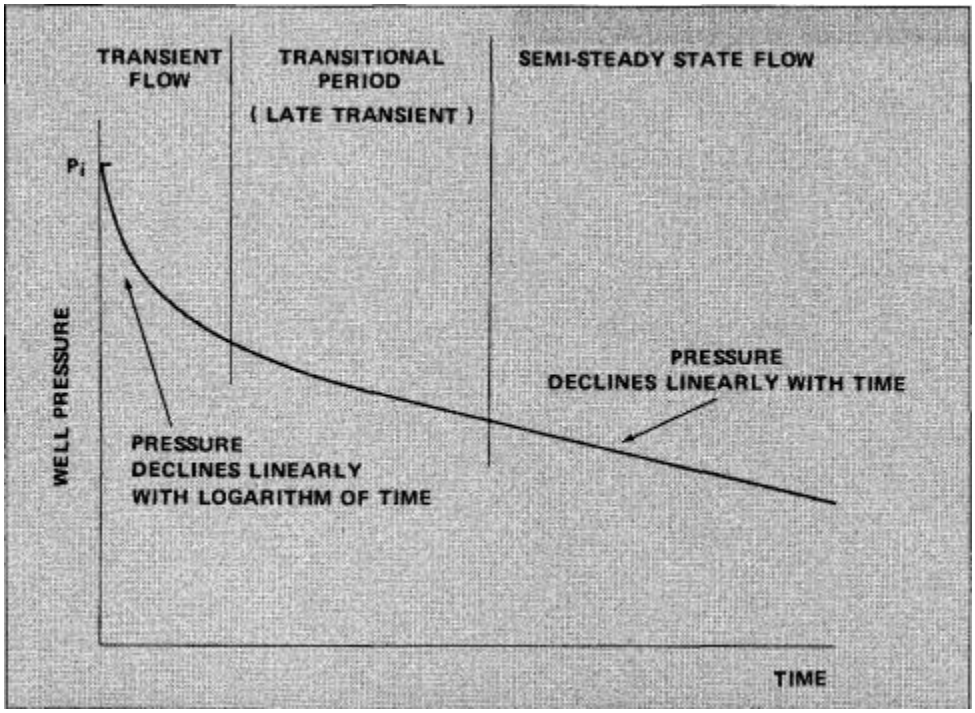


**Figure 5-1** - Plot of pressure decline at a well, bounded circular reservoir, constant rate case. (Matthews, 1986)

As the pressure wave moves outwards during transient state production, essentially, the drainage radius is increasing with time. Thus, the bulk volume of the reservoir cannot be assumed to be constant as it is in pseudo-steady state. The derivations starts with equations **(5.3)** and **(5.5)** and the reservoir bulk volume is kept inside the time derivative in order to capture the increasing drainage radius over time.

$$q_g = \frac{1}{\alpha_c}\frac{d}{dt}\left[\frac{V_b\,\phi\,(1-S_w)}{B_g} + V_b\,V_d\right] \tag{5.82}$$

$$q_w = \frac{1}{\alpha_c}\frac{d}{dt}\left(\frac{V_b\,\phi\,S_w}{B_w}\right) \tag{5.83}$$

From well testing, the changing radius with time can be expressed using the following equation (J. Lee, 1981):

$$r_i = \sqrt{\frac{24\,k\,t}{948\,\phi\,\mu_w\,c_t}} \tag{5.84}$$

Where,

$r_i = radius\ of\ investigation, ft$
$k = reservoir\ permeability, md$
$t = time, hours$
$c_t = total\ compressibility, psia^{-1}$

And the reservoir bulk volume is expressed using the following equation:

$$V_b = \pi\,{r_i}^2\,h \tag{5.85}$$

Where,

$h = thickness\ of\ the\ reservoir, ft$

The derivative of the reservoir bulk volume (radius of investigation included) with respect to time is:

$$\frac{dV_b}{dt} = 2\,\pi\,r_i\,h\,\frac{dr_i}{dt} \tag{5.86}$$

The derivative of the radius of investigation with respect to time can be evaluated using the u-substitution technique:

$$u = \frac{24\,k\,t}{948\,\phi\,\mu_w\,c_t} \tag{5.87}$$

$$r_i = u^{\frac{1}{2}} \tag{5.88}$$

$$\frac{dr_i}{dt} = \frac{1}{2}u^{-\frac{1}{2}}\frac{du}{dt} \tag{5.89}$$

Assuming that the viscosity of water is constant:

$$\frac{du}{dt} = \frac{24}{948\,\mu_w\,c_t}\frac{d}{dt}\left(\frac{k\,t}{\phi}\right) \tag{5.90}$$

$$\frac{du}{dt} = \frac{24}{948\,\mu_w\,c_t}\left(\frac{k\,t}{\phi}\right)\left(\frac{k'}{k} + \frac{1}{t} - \frac{\phi'}{\phi}\right) \tag{5.91}$$

$$\frac{du}{dt} = \frac{24\,k\,t}{948\,\phi\,\mu_w\,c_t}\left(\frac{1}{k}\frac{dk}{dP}\frac{dP}{dt} + \frac{1}{t} - \frac{1}{\phi}\frac{d\phi}{dP}\frac{dP}{dt}\right) \tag{5.92}$$

Substituting equation **(5.87)** and **(5.92)** into equation **(5.89)**:

$$\frac{dr_i}{dt} = \frac{1}{2}\left(\frac{24\,k\,t}{948\,\phi\,\mu_w\,c_t}\right)^{-\frac{1}{2}}\left[\frac{24\,k\,t}{948\,\phi\,\mu_w\,c_t}\left(\frac{1}{k}\frac{dk}{dP}\frac{dP}{dt} + \frac{1}{t} - \frac{1}{\phi}\frac{d\phi}{dP}\frac{dP}{dt}\right)\right] \tag{5.93}$$

Substituting equation **(5.93)** into equation **(5.86)**:

$$\frac{dV_b}{dt} = 2\,\pi\,r_i\,h\left\{\frac{1}{2}\left(\frac{24\,k\,t}{948\,\phi\,\mu_w\,c_t}\right)^{-\frac{1}{2}}\left[\frac{24\,k\,t}{948\,\phi\,\mu_w\,c_t}\left(\frac{1}{k}\frac{dk}{dP}\frac{dP}{dt} + \frac{1}{t} - \frac{1}{\phi}\frac{d\phi}{dP}\frac{dP}{dt}\right)\right]\right\} \tag{5.94}$$

The resulting equation after simplifying is:

$$\frac{dV_b}{dt} = V_b\left(\frac{1}{k}\frac{dk}{dP}\frac{dP}{dt} + \frac{1}{t} - \frac{1}{\phi}\frac{d\phi}{dP}\frac{dP}{dt}\right) \tag{5.95}$$

Evaluating $q_g$ assuming a time dependent bulk volume:

$$q_g = \frac{1}{\alpha_c}\frac{d}{dt}\left[\frac{V_b\,\phi\,(1-S_w)}{B_g} + V_b\,V_d\right] \tag{5.96}$$

$$q_g = \frac{1}{\alpha_c}\left[\left\{\left(\frac{V_b\,\phi\,(1-S_w)}{B_g}\right)\left(\frac{V_b{}'}{V_b} + \frac{\phi'}{\phi} + \frac{(1-S_w)'}{(1-S_w)} - \frac{B_g{}'}{B_g}\right)\right\} + V_b\frac{dV_d}{dP}\frac{dP}{dt} + V_d\frac{dV_b}{dt}\right] \tag{5.97}$$

$$q_g = \frac{1}{\alpha_c}\left[\left\{\left(\frac{V_b\,\phi\,(1-S_w)}{B_g}\right)\left(\frac{1}{V_b}\frac{dV_b}{dt} + \frac{1}{\phi}\frac{d\phi}{dP}\frac{dP}{dt} - \frac{1}{(1-S_w)}\frac{dS_w}{dt} - \frac{1}{B_g}\frac{dB_g}{dP}\frac{dP}{dt}\right)\right\} + V_b\frac{dV_d}{dP}\frac{dP}{dt} + V_d\frac{dV_b}{dt}\right] \tag{5.98}$$

$$q_g = \frac{1}{\alpha_c}\left[\left(\frac{\phi\,(1-S_w)}{B_g}\frac{dV_b}{dt} + \frac{V_b\,(1-S_w)}{B_g}\frac{d\phi}{dP}\frac{dP}{dt} - \frac{V_b\,\phi}{B_g}\frac{dS_w}{dt} - V_b\,\phi\,(1 - S_w)\frac{dB_g}{dP}\frac{dP}{dt}\right) + V_b\frac{dV_d}{dP}\frac{dP}{dt} + V_d\frac{dV_b}{dt}\right] \tag{5.99}$$

Substituting in $\frac{dV_b}{dt}$ from equation **(5.95)**.

$$q_g = \frac{1}{\alpha_c}\left[\left(\frac{\phi\,(1-S_w)}{B_g}V_b\left(\frac{1}{k}\frac{dk}{dP}\frac{dP}{dt} + \frac{1}{t} - \frac{1}{\phi}\frac{d\phi}{dP}\frac{dP}{dt}\right) - \frac{V_b\,(1-S_w)}{B_g}\frac{d\phi}{dP}\frac{dP}{dt} + \frac{V_b\,\phi}{B_g}\frac{dS_w}{dt} - V_b\,\phi\,(1-S_w)\frac{dB_g}{dP}\frac{dP}{dt}\right) + V_b\frac{dV_d}{dP}\frac{dP}{dt} + V_d\,V_b\left(\frac{1}{k}\frac{dk}{dP}\frac{dP}{dt} + \frac{1}{t} - \frac{1}{\phi}\frac{d\phi}{dP}\frac{dP}{dt}\right)\right] \tag{5.100}$$

Simplifying,

$$q_g = \frac{1}{\alpha_c}\left\{\left[(1-S_w)\left\{\frac{V_b}{B_g}\frac{d\phi}{dP} - V_b\,\phi\frac{dB_g}{dP} + \frac{V_b\,\phi}{B_g}\left(\frac{1}{k}\frac{dk}{dP} - \frac{1}{\phi}\frac{d\phi}{dP}\right)\right\} + V_b\frac{dV_d}{dP} + V_d\,V_b\left(\frac{1}{k}\frac{dk}{dP} - \frac{1}{\phi}\frac{d\phi}{dP}\right)\right]\frac{dP}{dt} - \frac{V_b\,\phi}{B_g}\frac{dS_w}{dt} + \frac{V_b}{t}\left(\frac{\phi\,(1-S_w)}{B_g} + V_d\right)\right\} \tag{5.101}$$

$$q_g = \frac{V_b}{\alpha_c}\left\{\left[(1-S_w)\left\{\frac{\phi}{B_g}\frac{dk}{k\,dP} - \phi\frac{dB_g}{dP}\right\} + \frac{dV_d}{dP} + V_d\left(\frac{1}{k}\frac{dk}{dP} - \frac{1}{\phi}\frac{d\phi}{dP}\right)\right]\frac{dP}{dt} - \frac{\phi}{B_g}\frac{dS_w}{dt} + \frac{1}{t}\left(\frac{\phi\,(1-S_w)}{B_g} + V_d\right)\right\} \quad \textbf{(5.102)}$$

Evaluating $q_w$ assuming a time dependent bulk volume:

$$q_w = \frac{1}{\alpha_c}\frac{d}{dt}\left(\frac{V_b\,\phi\,S_w}{B_w}\right) \quad \textbf{(5.103)}$$

$$q_w = \frac{1}{\alpha_c}\left(\frac{V_b\,\phi\,S_w}{B_w}\right)\left(\frac{V_b{}'}{V_b} + \frac{\phi'}{\phi} + \frac{S_w{}'}{S_w} - \frac{B_w{}'}{B_w}\right) \quad \textbf{(5.104)}$$

$$q_w = \frac{1}{\alpha_c}\left(\frac{V_b\,\phi\,S_w}{B_w}\right)\left(\frac{1}{V_b}\frac{dV_b}{dt} + \frac{1}{\phi}\frac{d\phi}{dP}\frac{dP}{dt} + \frac{1}{S_w}\frac{dS_w}{dt} - \frac{1}{B_w}\frac{dB_w}{dP}\frac{dP}{dt}\right) \quad \textbf{(5.105)}$$

$$q_w = \frac{1}{\alpha_c}\left(\frac{\phi\,S_w}{B_w}\frac{dV_b}{dt} + \frac{V_b\,S_w}{B_w}\frac{d\phi}{dP}\frac{dP}{dt} + \frac{V_b\,\phi}{B_w}\frac{dS_w}{dt} - V_b\,\phi\,S_w\frac{dB_w}{dP}\frac{dP}{dt}\right) \quad \textbf{(5.106)}$$

Substituting in $\frac{dV_b}{dt}$ from equation **(5.95)**.

$$q_w = \frac{1}{\alpha_c}\left(\frac{\phi\,S_w}{B_w}V_b\left(\frac{1}{k}\frac{dk}{dP}\frac{dP}{dt} + \frac{1}{t} - \frac{1}{\phi}\frac{d\phi}{dP}\frac{dP}{dt}\right) + \frac{V_b\,S_w}{B_w}\frac{d\phi}{dP}\frac{dP}{dt} + \frac{V_b\,\phi}{B_w}\frac{dS_w}{dt} - V_b\,\phi\,S_w\frac{dB_w}{dP}\frac{dP}{dt}\right) \quad \textbf{(5.107)}$$

Simplifying,

$$q_w = \frac{1}{\alpha_c}\left\{\left[(V_b\,S_w)\left(\frac{1}{B_w}\frac{d\phi}{dP} - \phi\frac{dB_w}{dP}\right) + \frac{\phi\,S_w\,V_b}{B_w}\left(\frac{1}{k}\frac{dk}{dP} - \frac{1}{\phi}\frac{d\phi}{dP}\right)\right]\frac{dP}{dt} + \frac{V_b\,\phi}{B_w}\frac{dS_w}{dt} + \frac{\phi\,S_w\,V_b}{t\,B_w}\right\} \quad \textbf{(5.108)}$$

$$q_w = \frac{1}{\alpha_c}\left\{(V_b\,S_w)\left[\frac{\phi}{B_w}\frac{1}{k}\frac{dk}{dP} - \phi\frac{dB_w}{dP}\right]\frac{dP}{dt} + \frac{V_b\,\phi}{B_w}\frac{dS_w}{dt} + \frac{\phi\,S_w\,V_b}{t\,B_w}\right\} \quad \textbf{(5.109)}$$

The equation for $q_g$ and $q_w$ can then be presented in a simplified format by grouping up the terms with respect to pressure and saturation:

$$q_g = C_{gP}\frac{dP}{dt} + C_{gS}\frac{dS_w}{dt} + \frac{V_b}{t}\left(\frac{\phi\,(1-S_w)}{B_g} + V_d\right) \quad \textbf{(5.110)}$$

$$q_w = C_{wP}\frac{dP}{dt} + C_{wS}\frac{dS_w}{dt} + \frac{\phi\, S_w\, V_b}{t\, B_w} \tag{5.111}$$

Where,

$$C_{gP} = \frac{V_b}{\alpha_c}\left[(1-S_w)\left\{\frac{\phi}{B_g}\frac{dk}{dP} - \phi\frac{dB_g}{dP}\right\} + \frac{dV_d}{dP} + V_d\left(\frac{1}{k}\frac{dk}{dP} - \frac{1}{\phi}\frac{d\phi}{dP}\right)\right] \tag{5.112}$$

$$C_{gS} = -\frac{V_b\,\phi}{\alpha_c\, B_g} \tag{5.113}$$

$$C_{wP} = \frac{V_b\, S_w}{\alpha_c}\left(\frac{\phi}{B_w}\frac{1}{k}\frac{dk}{dP} - \phi\frac{dB_w}{dP}\right) \tag{5.114}$$

$$C_{wS} = \frac{V_b\,\phi}{\alpha_c\, B_w} \tag{5.115}$$

Equations **(5.110)** and **(5.111)** can be solved simultaneously to derive the two ordinary differential equations of pressure and saturation in the time domain.

Multiply equation **(5.110)** by $C_{wS}$:

$$C_{wS}\, q_g = C_{wS}\, C_{gP}\frac{dP}{dt} + C_{wS}\, C_{gS}\frac{dS_w}{dt} + C_{wS}\,\frac{V_b}{t}\left(\frac{\phi\,(1-S_w)}{B_g} + V_d\right) \tag{5.116}$$

Multiply equation **(5.111)** by $C_{gS}$:

$$C_{gS}\, q_w = C_{gS}\, C_{wP}\frac{dP}{dt} + C_{gS}\, C_{wS}\frac{dS_w}{dt} + C_{gS}\frac{\phi\, S_w\, V_b}{t\, B_w} \tag{5.117}$$

Subtract equation **(5.116)** from **(5.117)**:

$$C_{gS}\, q_w - C_{wS}\, q_g = \left(C_{gS}\, C_{wP} - C_{wS}\, C_{gP}\right)\frac{dP}{dt} + C_{gS}\frac{\phi\, S_w\, V_b}{t\, B_w} - C_{wS}\,\frac{V_b}{t}\left(\frac{\phi\,(1-S_w)}{B_g} + V_d\right) \tag{5.118}$$

Therefore, the equation for pressure in the time domain is:

$$\frac{dP}{dt} = \frac{C_{gS}\, q_w - C_{wS}\, q_g - \frac{V_b}{t}\left[C_{gS}\frac{\phi\, S_w}{B_w} - C_{wS}\left(\frac{\phi\,(1-S_w)}{B_g} + V_d\right)\right]}{\left(C_{gS}\, C_{wP} - C_{wS}\, C_{gP}\right)} \tag{5.119}$$

Likewise, equations **(5.110)** and **(5.111)** can be solved to give saturation in the time domain:

Multiply equation **(5.110)** by $C_{wP}$:

$$C_{wP}\, q_g = C_{wP}\, C_{gP} \frac{dP}{dt} + C_{wP}\, C_{gS} \frac{dS_w}{dt} + C_{wP}\, \frac{V_b}{t} \left( \frac{\phi\, (1 - S_w)}{B_g} + V_d \right) \tag{5.120}$$

Multiply equation **(5.111)** by $C_{gP}$:

$$C_{gP}\, q_w = C_{gP}\, C_{wP} \frac{dP}{dt} + C_{gP}\, C_{wS} \frac{dS_w}{dt} + C_{gP}\, \frac{\phi\, S_w\, V_b}{t\, B_w} \tag{5.121}$$

Subtract equation **(5.121)** from **(5.120)**:

$$\begin{aligned} C_{wP}\, q_g - C_{gP}\, q_w & \\ &= \left( C_{gS}\, C_{wP} - C_{wS}\, C_{gP} \right) \frac{dS_w}{dt} + C_{wP}\, \frac{V_b}{t} \left( \frac{\phi\, (1 - S_w)}{B_g} + V_d \right) \\ &\quad - C_{gP}\, \frac{\phi\, S_w\, V_b}{t\, B_w} \end{aligned} \tag{5.122}$$

Therefore, the equation for pressure in the time domain is:

$$\frac{dS_w}{dt} = \frac{C_{gP}\, q_w - C_{wP}\, q_g - \frac{V_b}{t} \left[ C_{gP}\, \frac{\phi\, S_w}{B_w} - C_{wP}\, \left( \frac{\phi\, (1 - S_w)}{B_g} + V_d \right) \right]}{\left( C_{gS}\, C_{wP} - C_{wS}\, C_{gP} \right)} \tag{5.123}$$

The Muskat-type equation for “pseudo-transient” flow is then given by

$$\frac{dS_w}{dP} = \frac{\frac{dS_w}{dt}}{\frac{dP}{dt}} \tag{5.124}$$

## 5.4 Runge-Kutta Solution

Numerical methods have been previously developed for finding numerical approximations to solutions of ordinary differential equations (ODEs). These methods involve numerical computation of integrals in order to approximate a numerical solution to ordinary differential equations. Such methods include Euler's method. In this simple, yet least accurate method for integrating an ODE, an approximation of a nearby point on the curve can be found by moving a "step" along a line tangent to the curve (illustrated in **Figure 5-2**). The Euler method is expressed by the following equation.

$$y_{n+1} = y_n + hf(x_n, y_n) \qquad \textbf{(5.125)}$$

Where $h$ is the step size and the interval at which each new solution is evaluated. The Euler method is an example of an explicit method where $y_{n+1}$ is evaluated in terms of knowns such as $y_n$. Therefore, initial conditions are necessary.

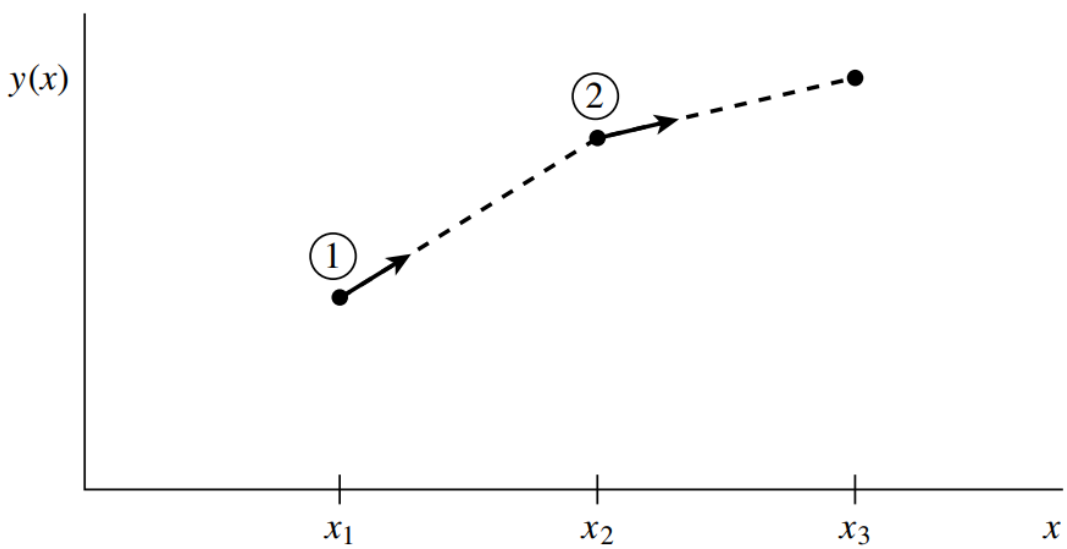


**Figure 5-2 -** Euler method. Showing the evaluation of an ODE from one interval to another. (Press, 2007)

However, a large disadvantage in using the Euler method is because it is a first-order method. This means that the error per step size is proportional to the square of the step size and the error at a given time is proportional to the step size (Press, 2007).

Carl Runge and Martin Kutta improved upon the Euler method. One of the methods that they have developed involved taking a "trial" step to the midpoint of the desired interval and then using the x and y evaluated at that midpoint to compute the total step across the whole interval. This midpoint method, also known as second-order Runge-Kutta, has a second-order degree of accuracy. **Figure 5-3** illustrates this idea.

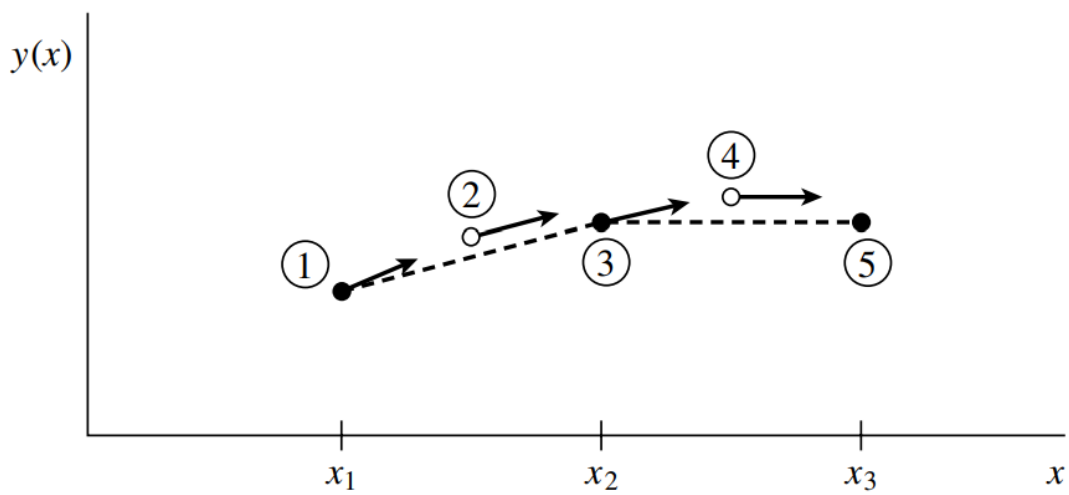


**Figure 5-3** - Midpoint method. Second-order accuracy is obtained by using the initial derivative at each step to find a point halfway across the interval, then using the midpoint derivative across the full width of the interval. (Press, 2007)

This method was further expanded upon to develop the classical fourth-order Runge-Kutta method where in each step, the derivative is evaluated four times: Once at the initial point ($y_n$), twice at two different midpoints, and finally, at the end point ($y_{n+1}$) (as shown in **Figure 5-4**) (Press, 2007). This results in a higher degree of accuracy.

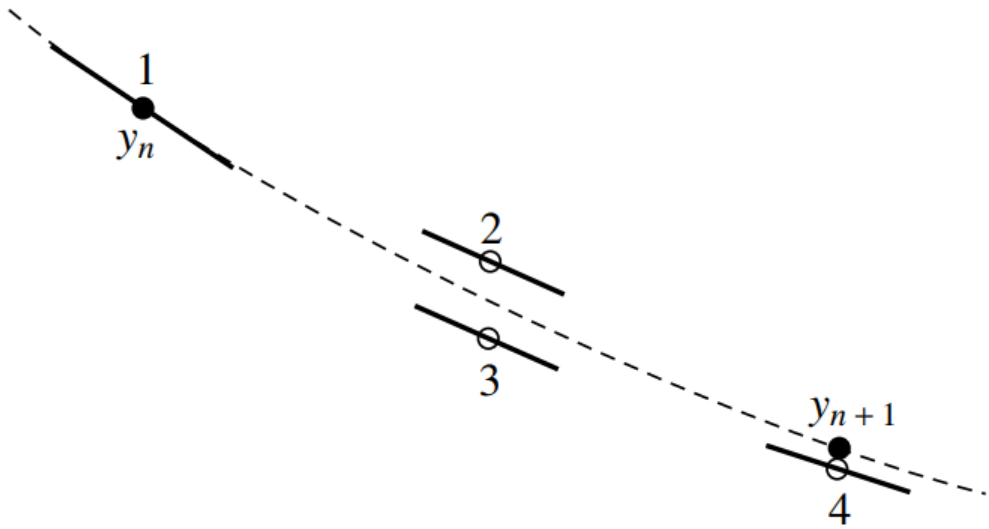


**Figure 5-4** - Fourth-order Runge-Kutta. (Press, 2007)

Fourth-order Runge-Kutta is evaluated using the following equations.

$$k_1 = hf(x_n, y_n) \tag{5.126}$$

$$k_2 = hf\left(x_n + \frac{1}{2}h, y_n + \frac{1}{2}k_1\right) \tag{5.127}$$

$$k_3 = hf\left(x_n + \frac{1}{2}h, y_n + \frac{1}{2}k_2\right) \tag{5.128}$$

$$k_4 = hf(x_n + h, y_n + k_3) \tag{5.129}$$

$$y_{n+1} = y_n + \frac{1}{6}k_1 + \frac{1}{3}k_2 + \frac{1}{3}k_3 + \frac{1}{6}k_4 + O(h^5) \tag{5.130}$$

Where $O$ is the error function given at every time step.

Fourth-order Runge-Kutta will be used to evaluate the developed Muskat-type equation in order to solve for water saturation as a function of pressure. This step-wise process can be modeled in MATLAB over a desired number of steps. The number of steps can be viewed as the time period for production. One step does not necessarily mean one day of production and can be modified as desired.

Runge-Kutta can also be used to solve the equations for saturation and pressure in the time domain (developed in 5.2.1). The two differential equations must be solved simultaneously while also including time in the Runge-Kutta formulation. The formulation for this problem is as follows.

$$k_{1P} = hf_P(t, P_n, S_n) \tag{5.131}$$

$$k_{1S} = hf_S(t, P_n, S_n) \tag{5.132}$$

$$k_{2P} = hf_P\left(t + \frac{1}{2}h\,, P_n + \frac{1}{2}k_{1P}h\,, S_n + \frac{1}{2}k_{1P}h\right) \tag{5.133}$$

$$k_{2S} = hf_S\left(t + \frac{1}{2}h\,, P_n + \frac{1}{2}k_{1S}h\,, S_n + \frac{1}{2}k_{1S}h\right) \tag{5.134}$$

$$k_{3P} = hf_P\left(t + \frac{1}{2}h\,, P_n + \frac{1}{2}k_{2P}h\,, S_n + \frac{1}{2}k_{2P}h\right) \tag{5.135}$$

$$k_{3S} = hf_S\left(t + \frac{1}{2}h\,, P_n + \frac{1}{2}k_{2S}h\,, S_n + \frac{1}{2}k_{2S}h\right) \tag{5.136}$$

$$k_{4P} = hf_P(t + h\,, P_n + k_{3P}h\,, S_n + k_{3P}h) \tag{5.137}$$

$$k_{4S} = hf_S(t + h\,, P_n + k_{3S}h\,, S_n + k_{3S}h) \tag{5.138}$$

$$P_{n+1} = P_n + \frac{1}{6}k_{1P} + \frac{1}{3}k_{2P} + \frac{1}{3}k_{3P} + \frac{1}{6}k_{4P} + O(h^5) \tag{5.139}$$

$$S_{n+1} = S_n + \frac{1}{6}k_{1S} + \frac{1}{3}k_{2S} + \frac{1}{3}k_{3S} + \frac{1}{6}k_{4S} + O(h^5) \tag{5.140}$$

Where $f_P$ and $f_S$ are $\frac{dP}{dt}$ and $\frac{dS}{dt}$, respectively.

The result is the saturation and pressure at every time period. Saturation as a function of pressure can be back calculated using the following equation:

$$\frac{dS_w}{dP} = \frac{\frac{dS_w}{dt}}{\frac{dP}{dt}} \tag{5.141}$$

# Chapter 6

# Results and Discussion

Using the equations developed in Chapter 5, a MATLAB code was developed that solves the ordinary differential equations (ODEs) using Runge-Kutta. Even though the equations developed are fully analytical, the use of Runge-Kutta is not. Thus, this is a semi-analytical model and will be referred to as such throughout this thesis. This chapter presents the results of this model including the discussion of the results and the observations made. Additional results for the base case are presented in Appendix A.

## 6.1 Model Validation

### 6.1.1 Model Validation Using Analytical Equations and Finite Difference

Through MATLAB, three functions have been developed using the derived equations in chapter 5: water saturation as a function of pressure ($\frac{dS_w}{dP}$), water saturation as a function of time ($\frac{dS_w}{dt}$), and pressure as a function of time ($\frac{dP}{dt}$). Runge-Kutta is then coded and utilized as described in section 5.4. Water saturation as a function of pressure ($\frac{dS_w}{dP}$) can be solved independently unlike pressure and water saturation as a function of time (they have to be solved simultaneously), however, pressure values are required to be fed into the Runge-Kutta algorithm. On the other hand, for water saturation and pressure as a function of time, time is varied linearly and the results are pressure and saturation values for each given time step.

Using the properties of the base case developed in chapter 4, water saturation and pressure in the time domain have been evaluated as discussed earlier. The total time period selected was 10

years in intervals of 1-day time steps. The resulting water saturation and pressure plots are presented in **Figure 6-1** and **Figure 6-2** respectively.

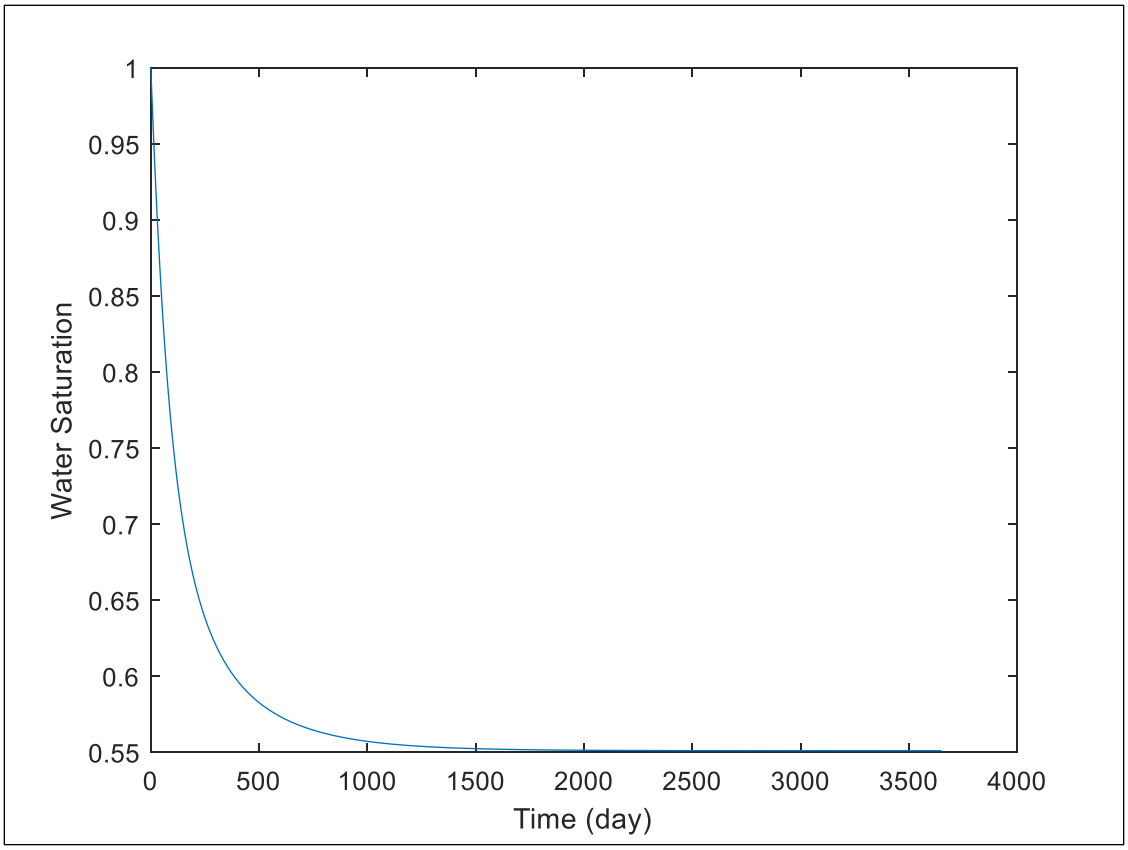


**Figure 6-1** - Water saturation vs time using base case properties.

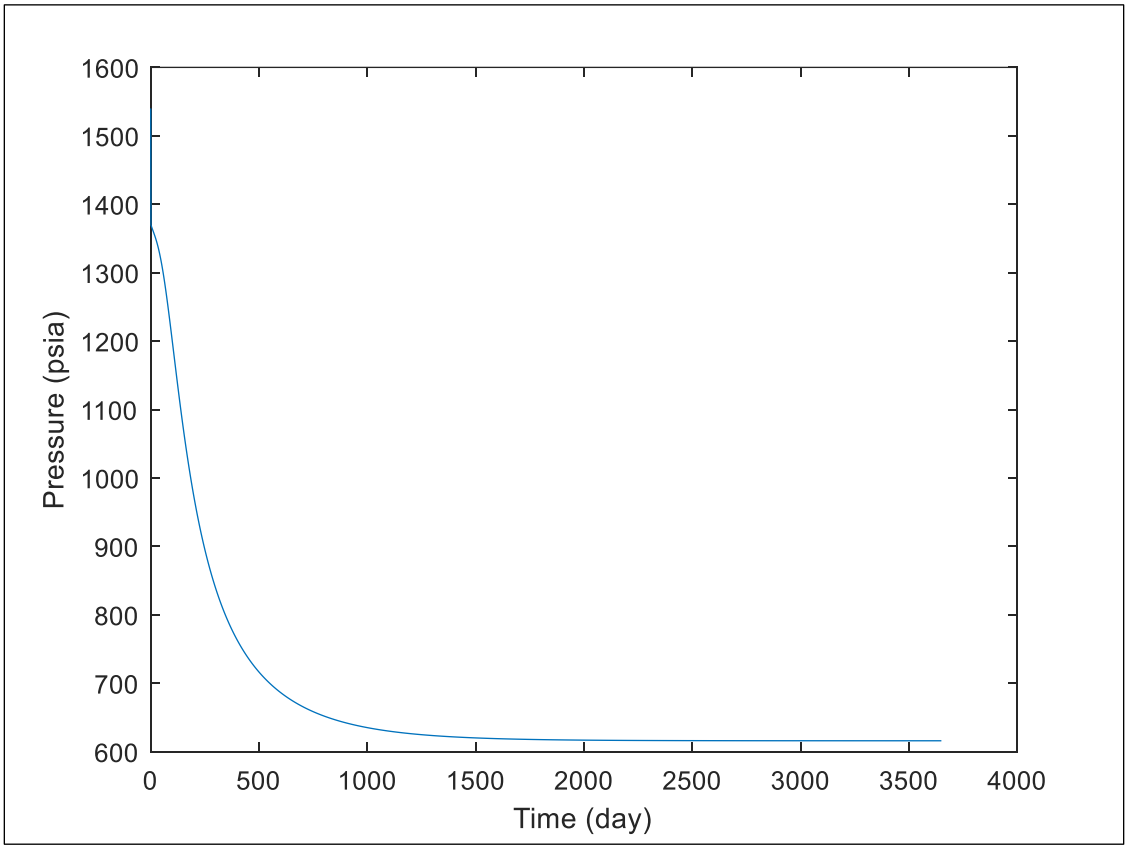


**Figure 6-2** - Pressure vs time using base case properties.

In order to validate the developed model and ensure that the code is bug-free, finite difference and MATLAB's gradient function (which essentially performs finite difference) are applied on the results. Finite difference is measured by evaluating the y-axis difference between the data point of interest and the data points above and below it, and then dividing it by the x-axis difference between the two points. It is essentially the derivative or the slope measured at every single point on any given plot. However, it is important to note that the first and last data points are skipped as they cannot be evaluated due to the unavailability of a data point above or below them. Thus, by applying these two methods on the calculated water saturation and pressure values presented in **Figure 6-3** and **Figure 6-4** respectively, the result should give the derivative in terms

of time ($\frac{dS_w}{dt}$ and $\frac{dP}{dt}$). A plot comparing the two methods with the original derivative evaluated using Runge-Kutta is generated.

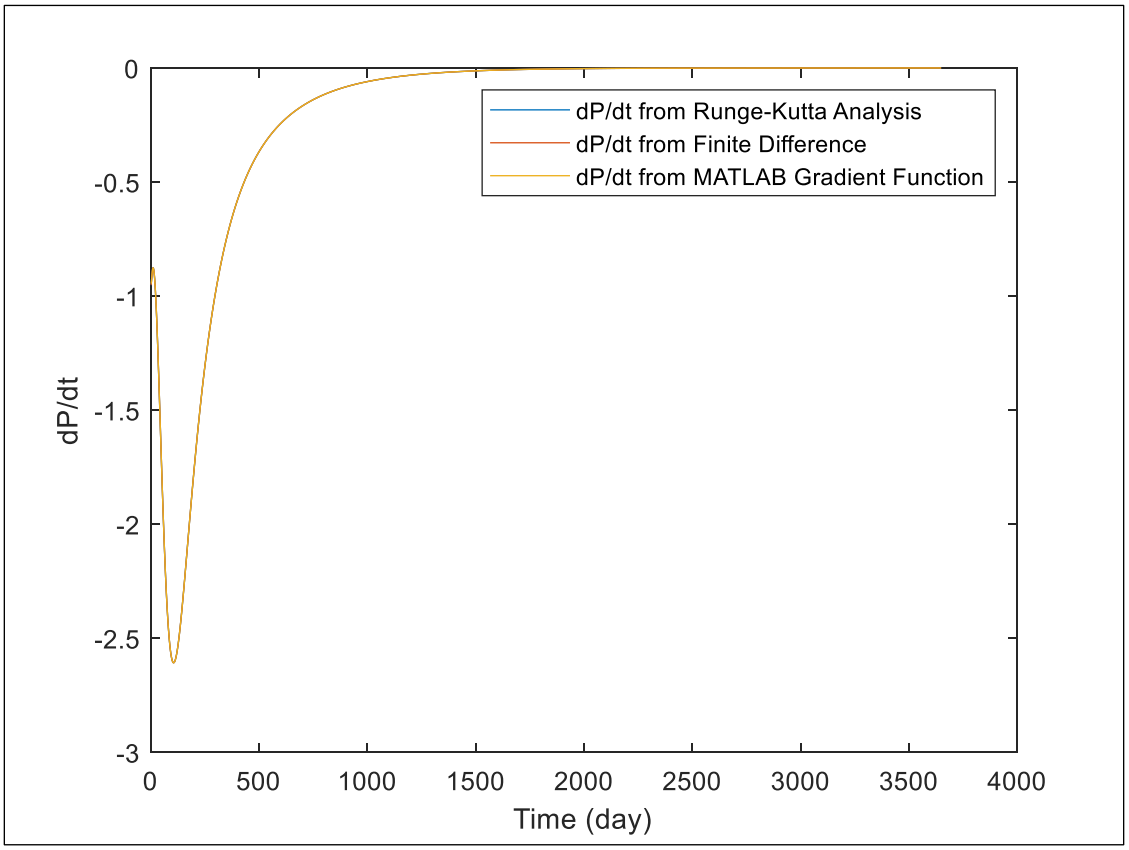


**Figure 6-3** - Plot comparing dP/dt calculated from finite diffrence and MATLAB gradient function with dP/dt generated from Muskat's equation using Runge-Kutta.

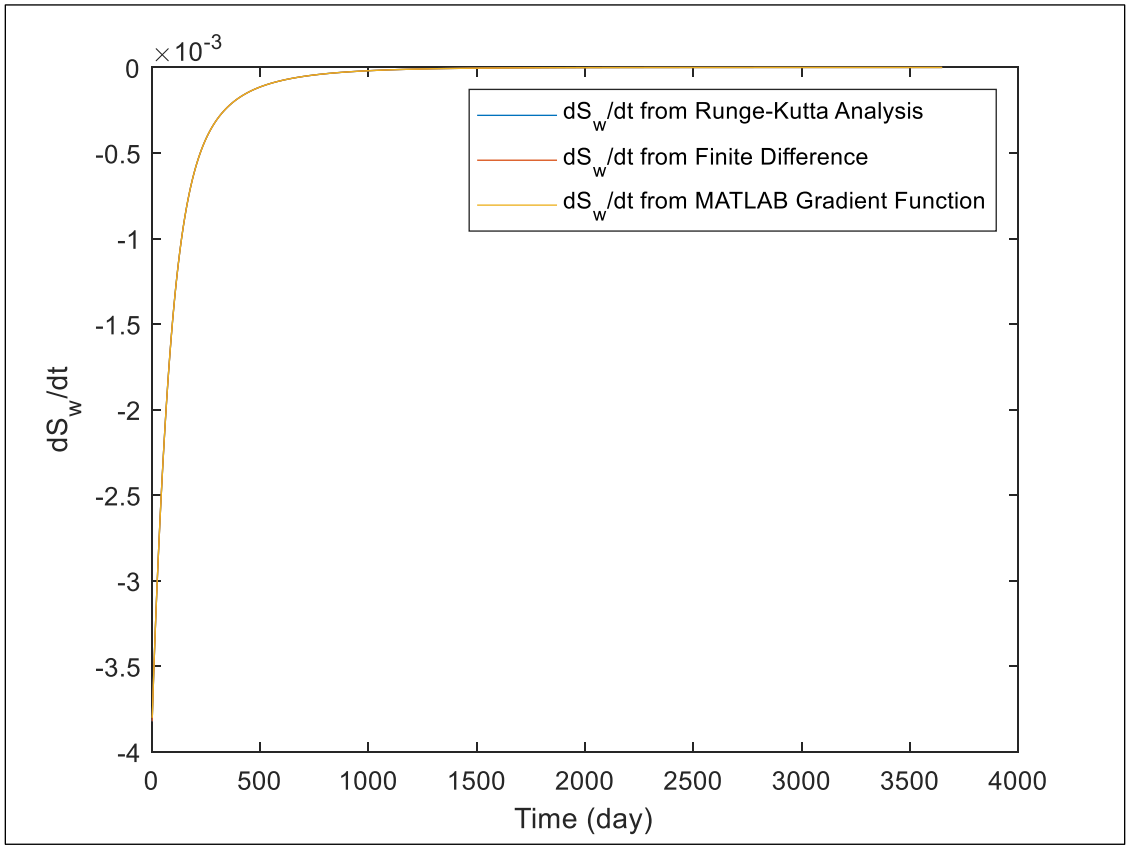


**Figure 6-4** - Plot comparing dSw/dt calculated from finite diffrence and MATLAB gradient function with dSw/dt generated from Muskat's equation using Runge-Kutta.

As seen from **Figure 6-3** and **Figure 6-4**, the results are almost identical as all the plots overlap. This means that the calculated water saturation and pressure values from Runge-Kutta are consistent and that there are no bugs in the code performing the analysis. However, it is important to note that the first two points were skipped in the $\frac{dP}{dt}$ comparison due to the large pressure drop that occurs initially as seen in **Figure 6-2**. Including these two points would result in the plot having a very large scale that cannot be analyzed. One of the reasons for the large pressure drop is the compressibility of the reservoir rock. As soon as production starts, the reservoir is shocked with a high-pressure differential between the reservoir pressure and the wellbore pressure. Therefore, since the reservoir rock is compressible, it shrinks the pores causing some of the fluid in the reservoir pores to be ejected and produced. To visualize, it is the same effect as when a wet sponge is squeezed. Also, at the beginning of production, all of the gas in the reservoir is adsorbed on the

reservoir rock in this case and will not desorb until the pressure reaches desorption pressure and the saturation of gas reaches its critical value. Thus, water is ejected from the pores at a higher rate which causes the large drop in the average reservoir pressure.

Another validation that could be performed is to see if the division of $\frac{dS_w}{dt}$ by $\frac{dP}{dt}$ yields the same results as that achieved by the Muskat-type equation $(\frac{dS_w}{dP})$ function developed and analyzed using Runge-Kutta independently.

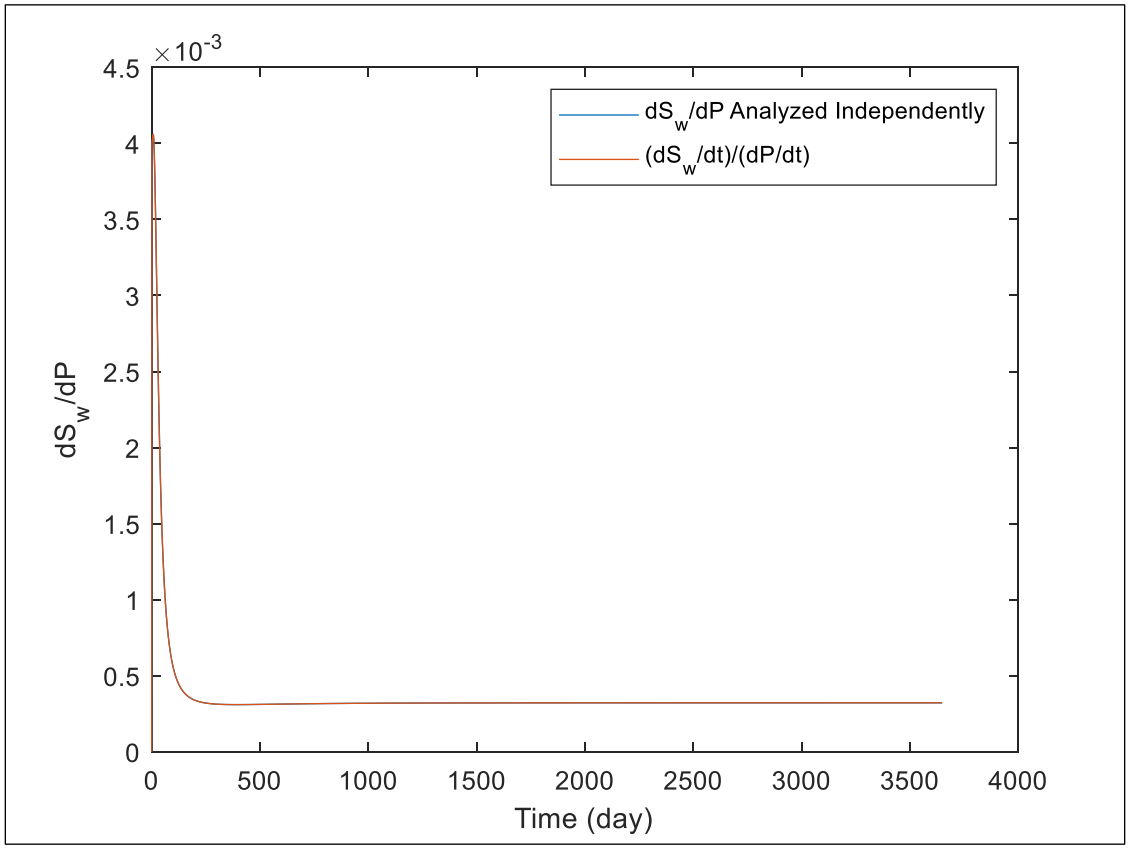


**Figure 6-5** - dSw/dt analyzed independently with Runge-Kutta compared with the division of water saturation and pressure in the time domain.

**Figure 6-5** confirms that all functions are working as intended with no bugs in the code.

Moving on, it is also important to validate the production profile. This can be done analytically using the results of the aforementioned functions. **Figure 6-6** presents the gas production over time for the base case.

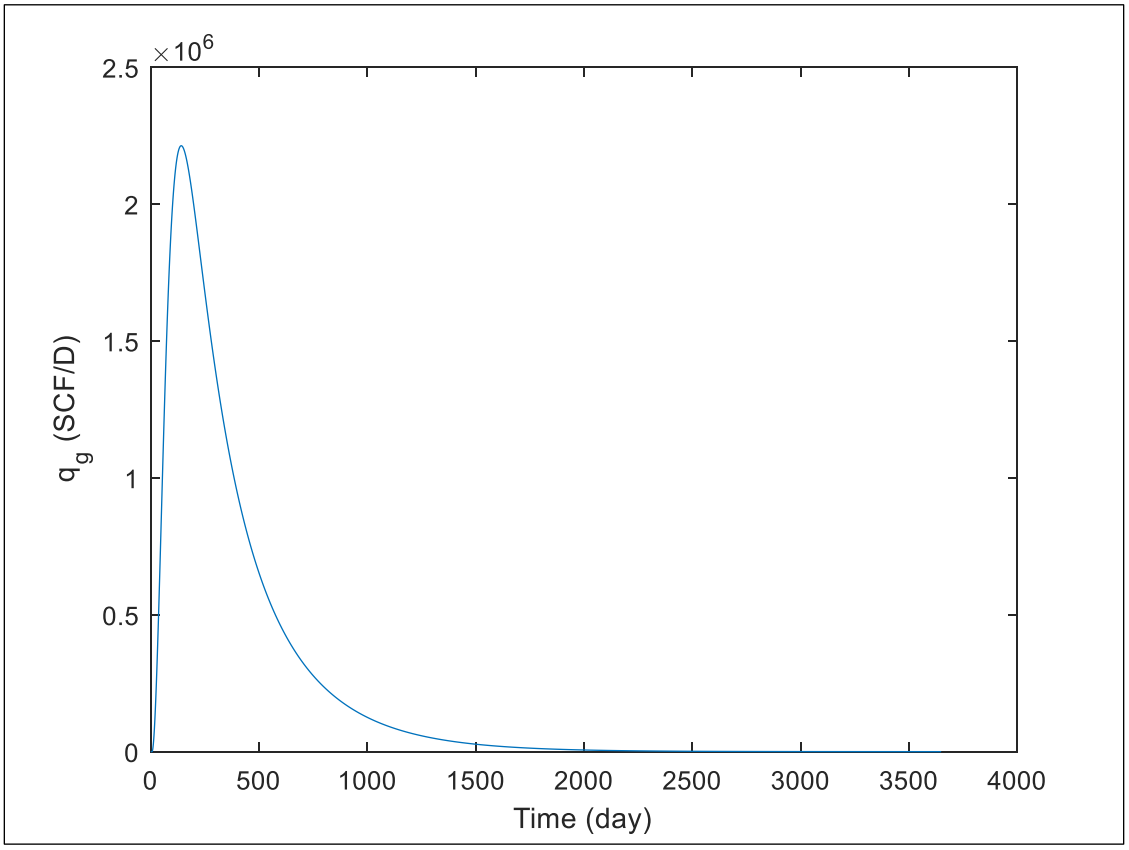


**Figure 6-6** - Gas production over a period of 10 years for the base case.

As done previously, finite difference and MATLAB's gradient function provides the derivative of the plot. In this case, it will provide $\frac{dq_g}{dt}$. Also, mathematically, $\frac{dq_g}{dt}$ can also be calculated from the following equation:

$$\frac{dq_g}{dt} = \frac{dq_g}{dP}\frac{dP}{dt} + \frac{dq_g}{dS_w}\frac{dS_w}{dt} \tag{6.1}$$

Water saturation and reservoir pressure in the time domain ($\frac{dS_w}{dt}$ and $\frac{dP}{dt}$) are available from the Runge-Kutta analysis. What remains is gas rate in the pressure domain and in the water saturation domain. This can be evaluated by deriving Darcy's law for gas rate in each of the two domains. Given that Darcy's law for gas rate in $[\frac{SCF}{day}]$ is:

$$q_g = \frac{\alpha_c\, k_{rg}\, k\, h\, (\bar{P} - P_{wf})}{141.2\, \mu_g\, B_g\, \left(\ln\left(\frac{r_e}{r_w}\right) - 0.5 + S\right)} \tag{6.2}$$

Where

$h = thickness\ of\ the\ reservoir, ft$
$\bar{P} = average\ reservoir\ pressure, psia$
$r_e = drainage\ radius, ft$
$r_w = wellbore\ radius, ft$
$S = skin\ factor, dimensionless$

Therefore, the derivative of the gas rate with respect to pressure is:

$$\frac{dq_g}{dP} = \frac{\alpha_c\, h\, k_{rg}}{141.2\, \left(\ln\left(\frac{r_e}{r_w}\right) - 0.5 + S\right)} \left(\frac{k\, (\bar{P} - P_{wf})}{\mu_g\, B_g}\right) \left(\frac{k'}{k} + \frac{(\bar{P} - P_{wf})'}{(\bar{P} - P_{wf})} - \frac{\mu_g{}'}{\mu_g} - \frac{B_g{}'}{B_g}\right) \tag{6.3}$$

$$\frac{dq_g}{dP} = \frac{\alpha_c\, h\, k_{rg}}{141.2\, \left(\ln\left(\frac{r_e}{r_w}\right) - 0.5 + S\right)} \left(\frac{k\, (\bar{P} - P_{wf})}{\mu_g\, B_g}\right) \left(\frac{1}{k}\frac{dk}{dP} + \frac{1}{(\bar{P} - P_{wf})} - \frac{1}{\mu_g}\frac{d\mu_g}{dP} - \frac{1}{B_g}\frac{dB_g}{dP}\right) \tag{6.4}$$

$$\frac{dq_g}{dP} = \frac{\alpha_c\, h\, k_{rg}}{141.2\, \left(\ln\left(\frac{r_e}{r_w}\right) - 0.5 + S\right)} \left(\frac{(\bar{P} - P_{wf})}{\mu_g\, B_g}\frac{dk}{dP} + \frac{k}{\mu_g\, B_g} - \frac{k\, (\bar{P} - P_{wf})}{\mu_g^2\, B_g}\frac{d\mu_g}{dP} - \frac{k\, (\bar{P} - P_{wf})}{\mu_g\, B_g^2}\frac{dB_g}{dP}\right) \tag{6.5}$$

This was done by isolating the pressure dependent terms and then deriving them. To find the derivative of permeability, gas viscosity and gas formation volume factor with respect to pressure, the equations used to evaluate these terms (presented in Chapter 4) will have to be derived. The same could be done for the derivative of the gas rate with respect to water saturation, however, since there is only one saturation dependent term, it is a fairly simple one.

$$\frac{dq_g}{dS_w} = \frac{\alpha_c\, k\, h\, (\bar{P} - P_{wf})}{141.2\, \mu_g\, B_g\, \left(\ln\left(\frac{r_e}{r_w}\right) - 0.5 + S\right)} \frac{dk_{rg}}{dS_w} \tag{6.6}$$

Now, it is possible to evaluate equation **(6.1)**. The result could be compared to that from finite difference and MATLAB's gradient function to validate the analytical approach.

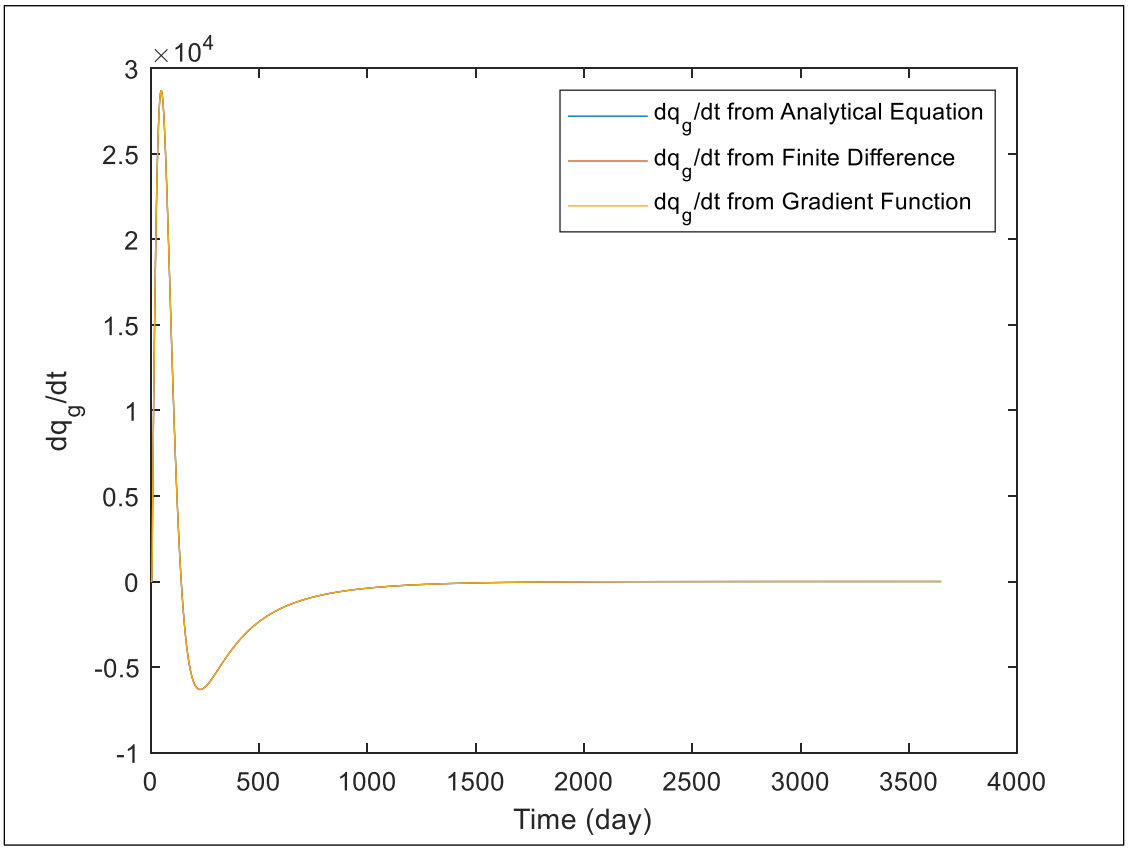


**Figure 6-7** - dqg/dt from analytical equation compared to finite difference and MATLAB's gradient function.

**Figure 6-7** confirms the validity of the analytical equation. Further use of this equation will be discussed later in this thesis.

### 6.1.2 Model Validation Using Numerical Simulator

Since the developed model is a semi-analytical model, it is not expected to outperform numerical simulation in terms of accuracy. This is because numerical simulation is a rigorous computational method that performs calculations at every discrete location of a modeled reservoir, each giving a different output (Ertekin et al., 2001). Numerical simulation is computationally expensive and requires a lot of inputs in order for it to perform its analysis. In contrast, the developed semi-analytical model assumes every part of the reservoir to have the same value and output while requiring less inputs.

For reasons that will be discussed later in this thesis, the model developed based on the derived "pseudo-transient" equations in Chapter 5 did not perform as intended. Therefore, the available, working model assumes pseudo-steady state flow only. This gives numerical simulation the edge since it is able to model transient-state flow which occurs at the beginning of production. Nevertheless, the developed semi-analytical model for pseudo-steady state flow will be benchmarked against a numerical simulator.

A numerical simulator developed by Dr. Gregory King will be used for this comparison. The model is a homogenous, isotropic, CBM reservoir which uses the same correlations used in the semi-analytical model in order to calculate parameters such as z factors, gas viscosities and relative permeabilities. The developed base case will be used to compare the results of both models. However, there is a limitation within the numerical simulator as it does not incorporate a desorption pressure. Thus, both models will desorb gas at initial pressure.

Initially, the base case had a rock compressibility of $6 * 10^{-4}\, psia^{-1}$ derived from literature for San Juan basin (Palmer & Mansoori, 1996). However, the numerical simulator did not accept this rock compressibility since it was out of its operating range. Thus, it was tuned to a number that falls within the range that is acceptable by the numerical simulator. Through multiple

runs with different rock compressibility, it was concluded that rock compressibility was a main factor affecting the accuracy of the developed semi-analytical model when compared to the numerical simulator. Therefore, five cases with different rock compressibility were conducted and compared. **Table 6-1** summarizes the cases with their different rock compressibility value.

**Table 6-1 - Summary of cases used to compare the developed model against numerical simulation**

| Case Number | Rock compressibility, $psia^{-1}$ |
|---|---|
| 1 | $2 * 10^{-4}$ |
| 2 | $5 * 10^{-5}$ |
| 3 | $1 * 10^{-5}$ |
| 4 | $5 * 10^{-6}$ |
| 5 | $1 * 10^{-6}$ |

Additionally, two more cases were developed for different permeabilities for reasons that will be discussed later on in this thesis.

**Table 6-2 - Cases with modified permeability.**

| Case Number | Permeability, $md$ |
|---|---|
| 6 | 5 |
| 7 | 60 |

The main comparison will be based upon the rate of gas produced in $[MSCF/D]$ and the cumulative gas produced over 10 years of production in $[MMSCF]$. The following figures show the results of each case for the two models.

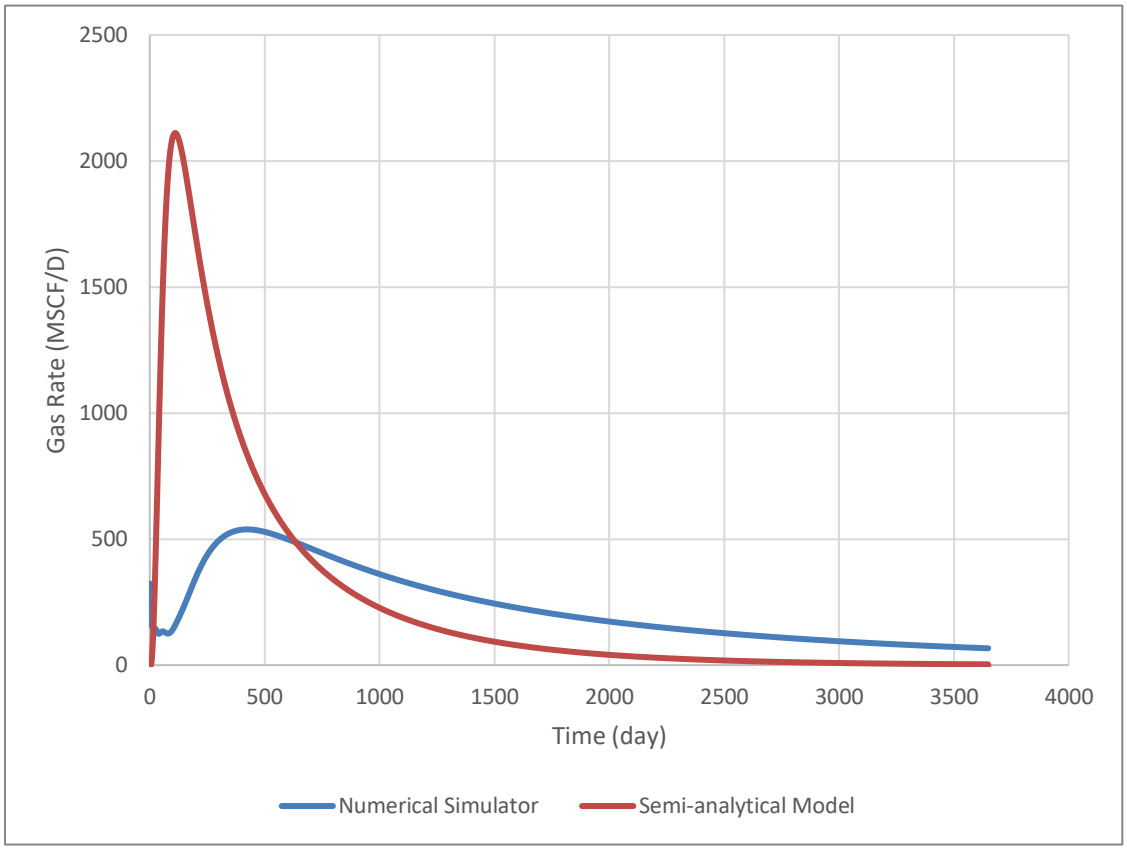


**Figure 6-8** - Case 1 gas rate comparison.

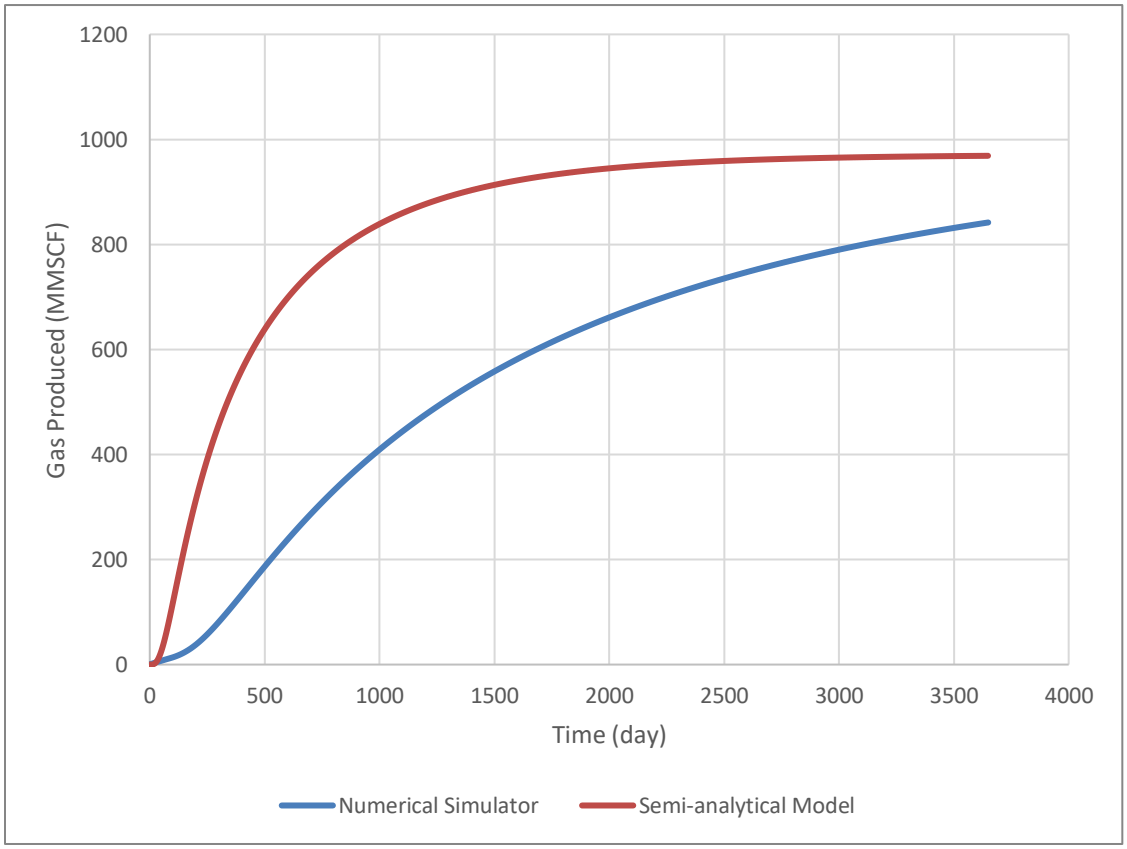


**Figure 6-9** - Case 1 gas produced comparison.

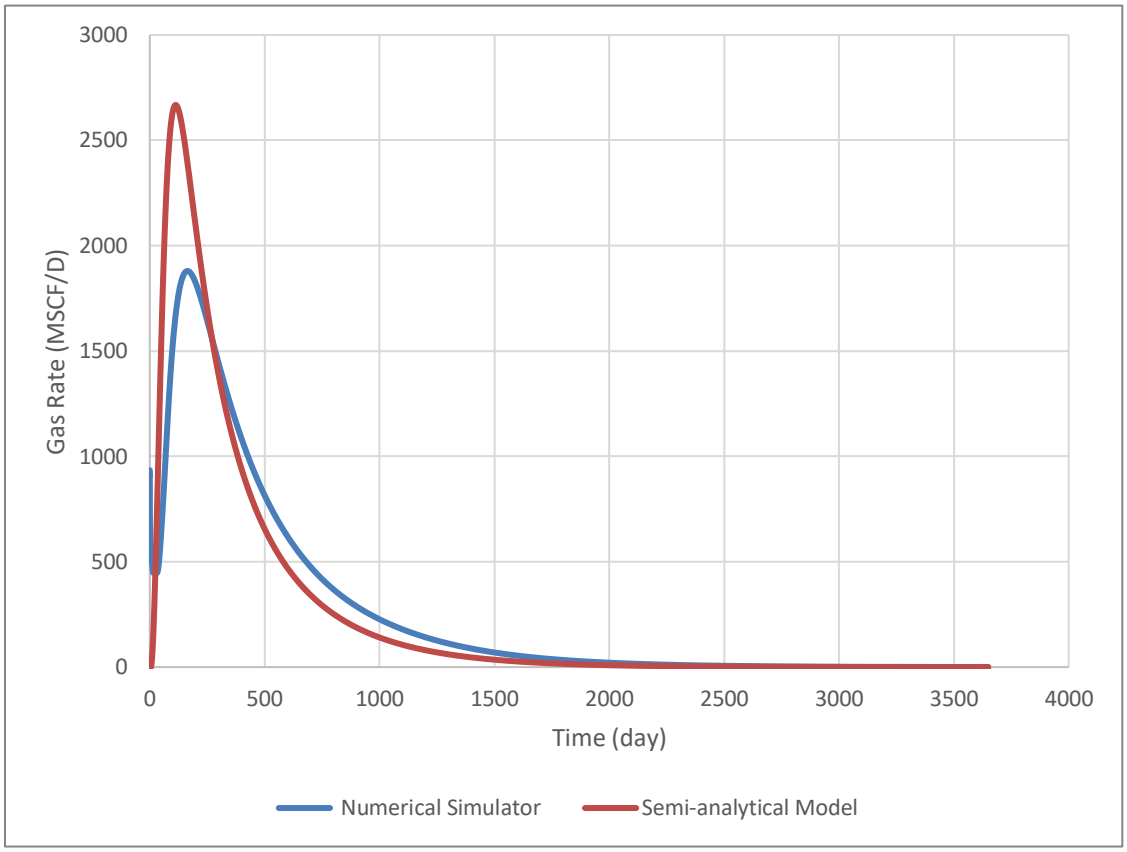


**Figure 6-10** - Case 2 gas rate comparison.

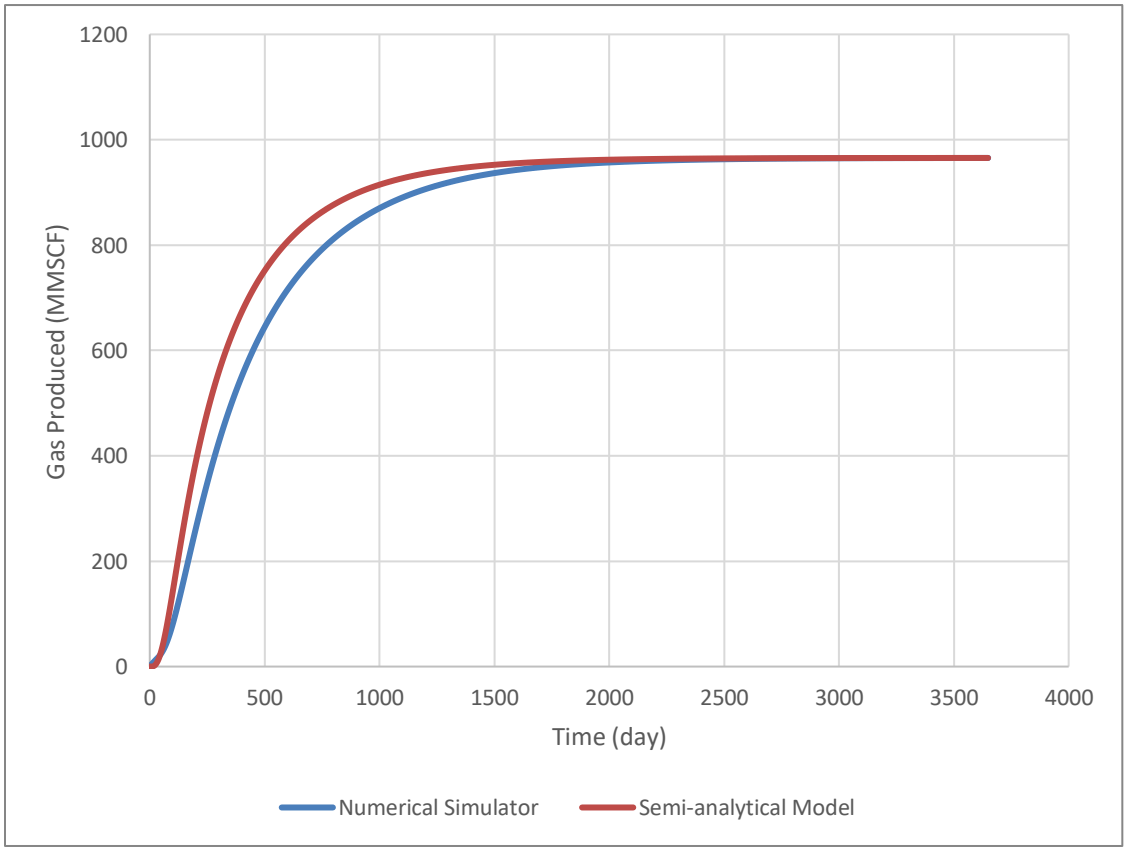


**Figure 6-11** - Case 2 gas produced comparison.

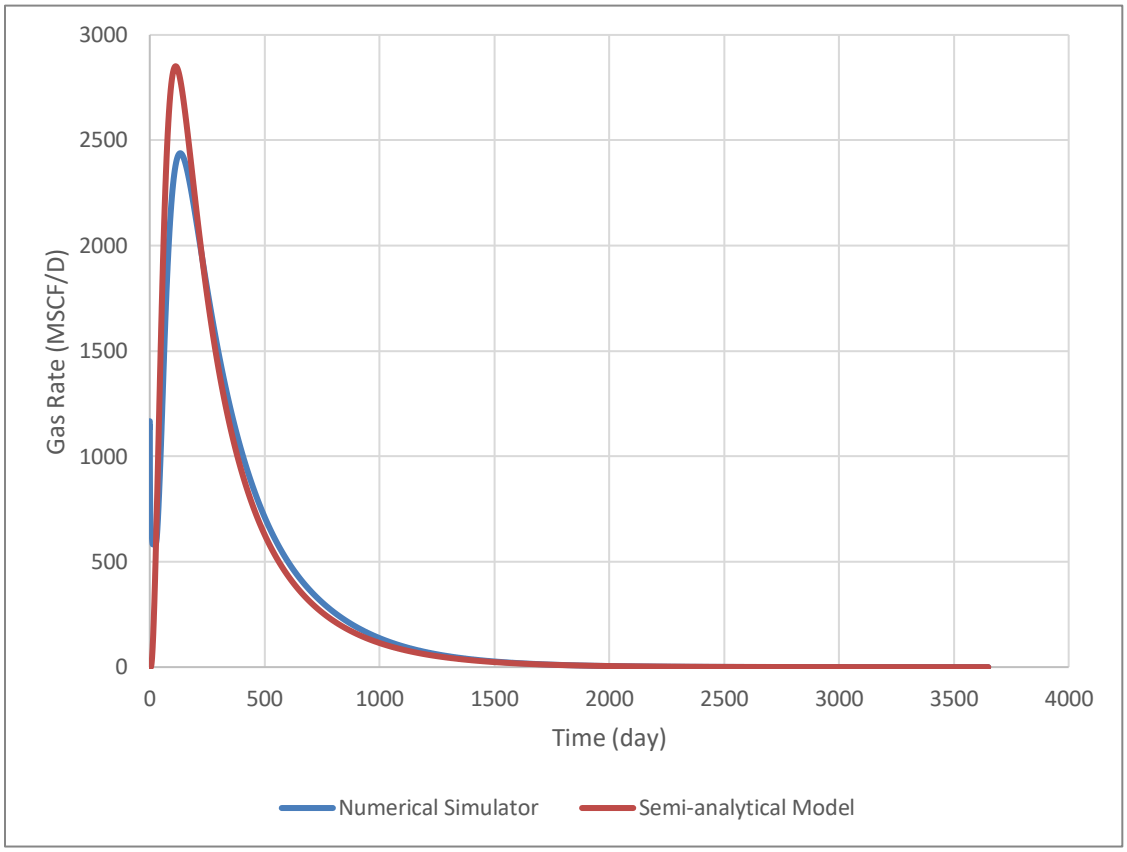


**Figure 6-12** - Case 3 gas rate comparison.

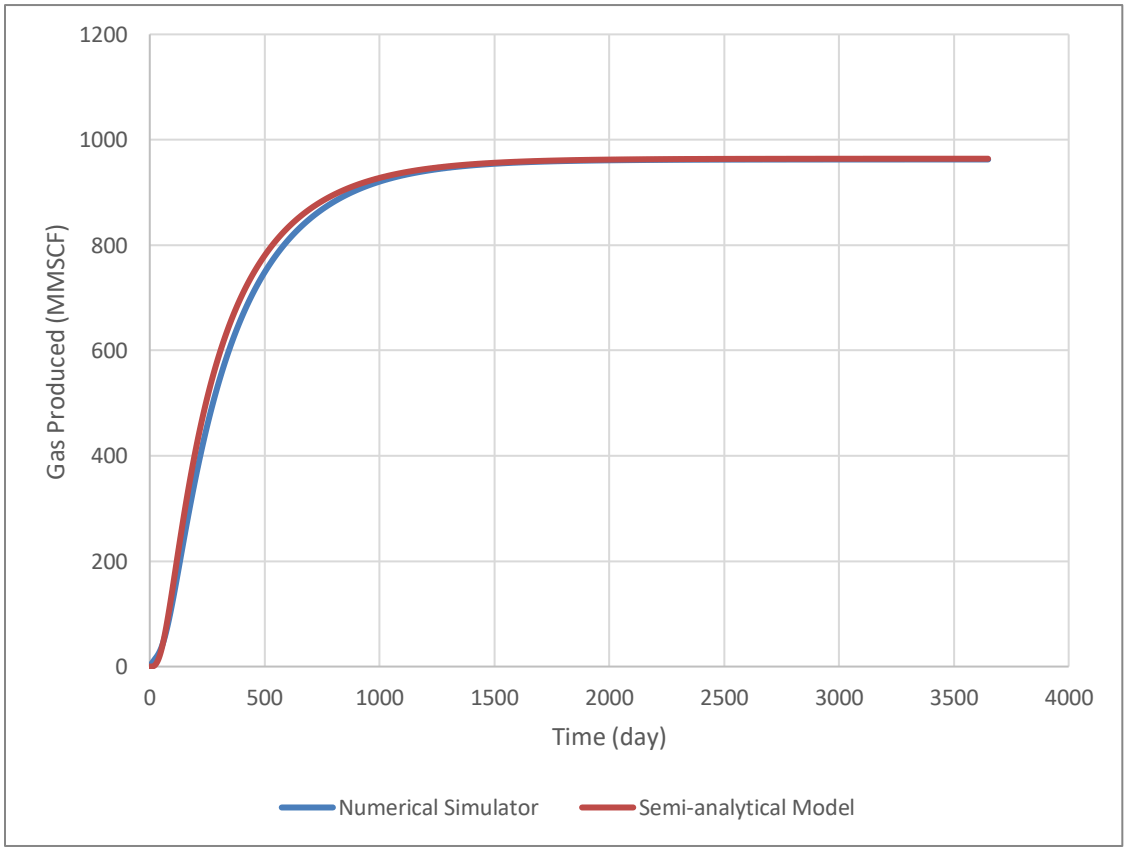


**Figure 6-13** - Case 3 gas produced comparison.

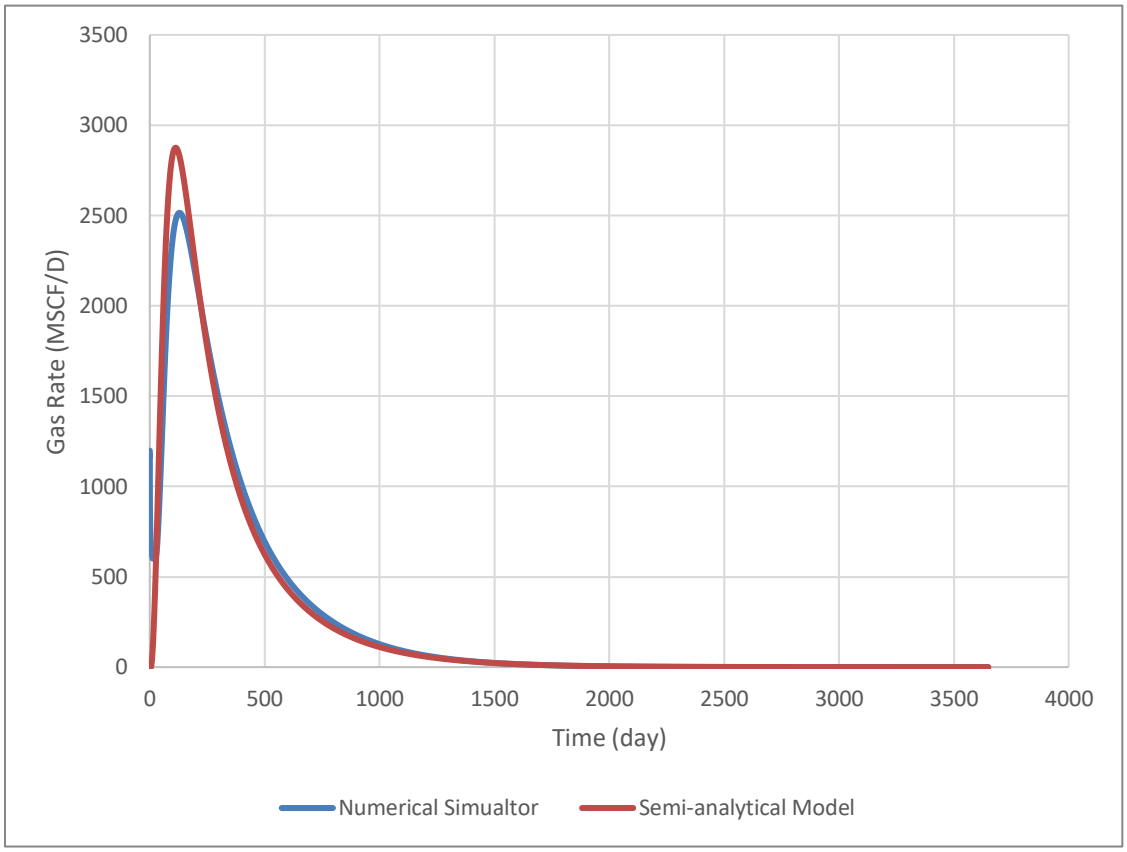


**Figure 6-14** - Case 4 gas rate comparison.

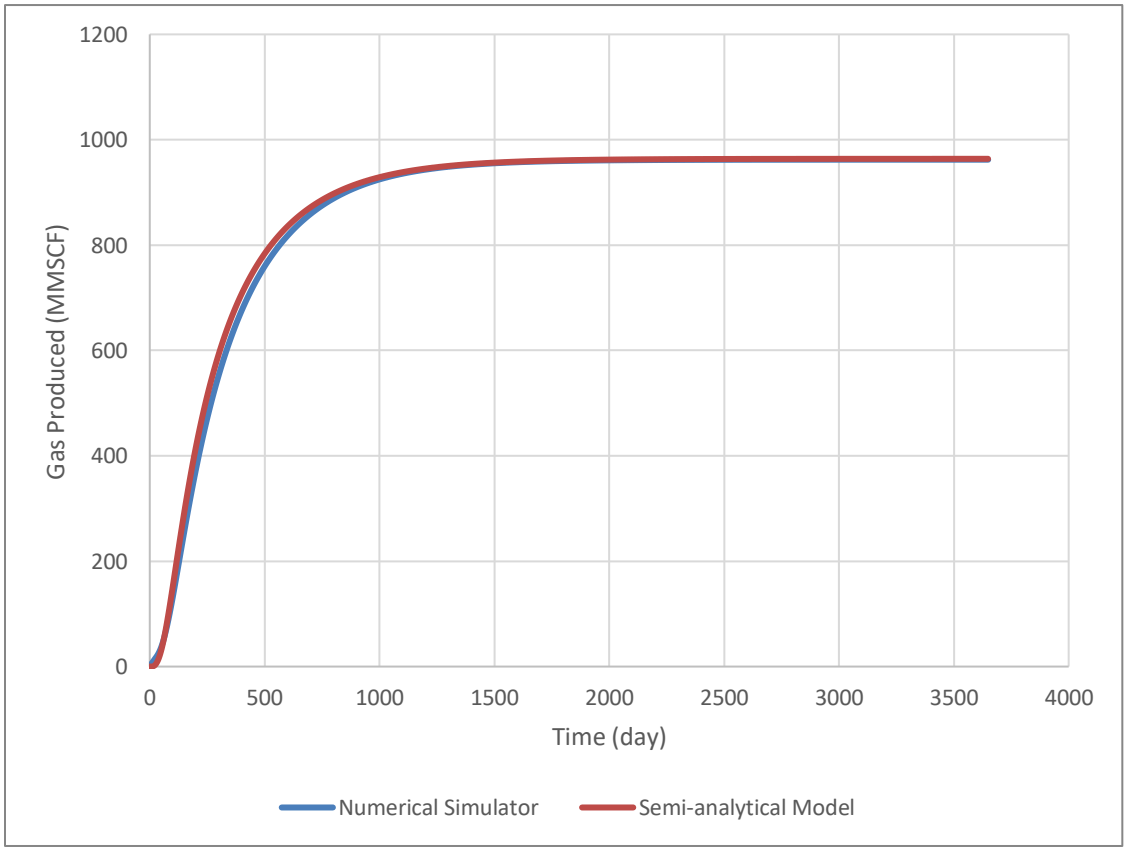


**Figure 6-15** - Case 4 gas produced comparison.

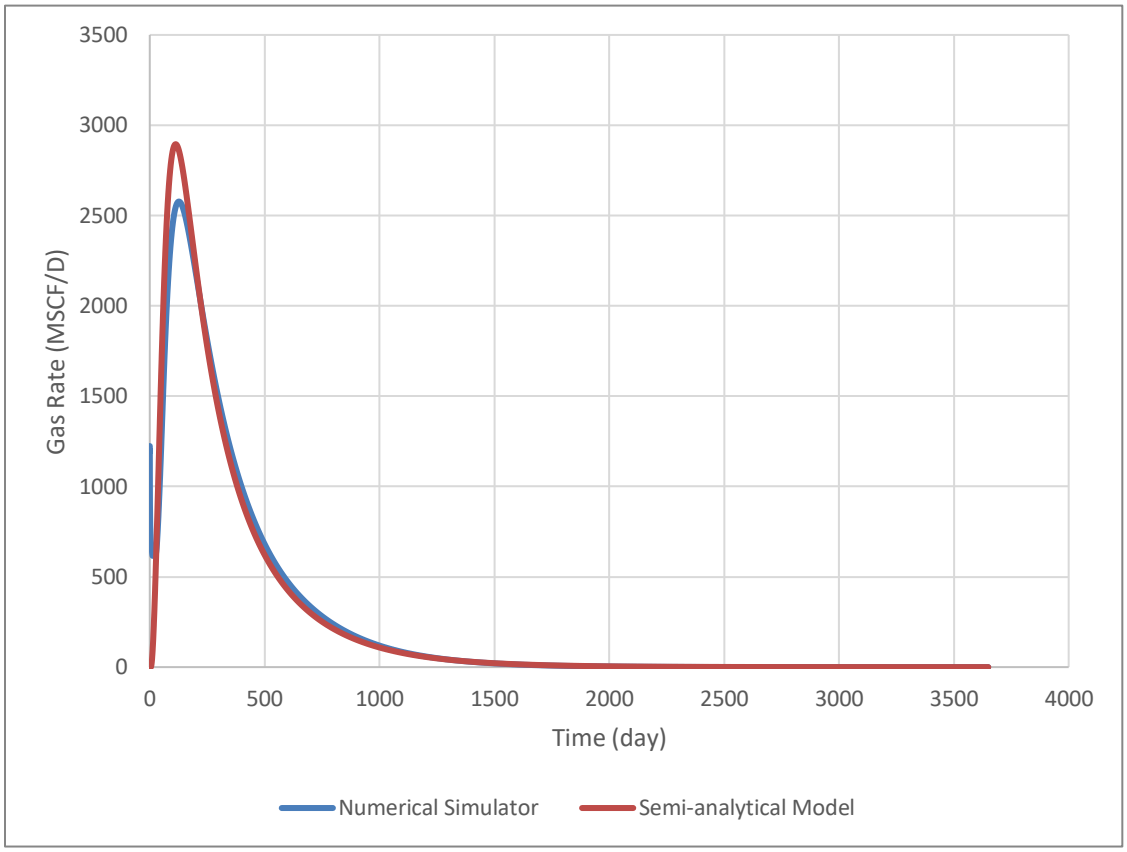


**Figure 6-16** - Case 5 gas rate comparison.

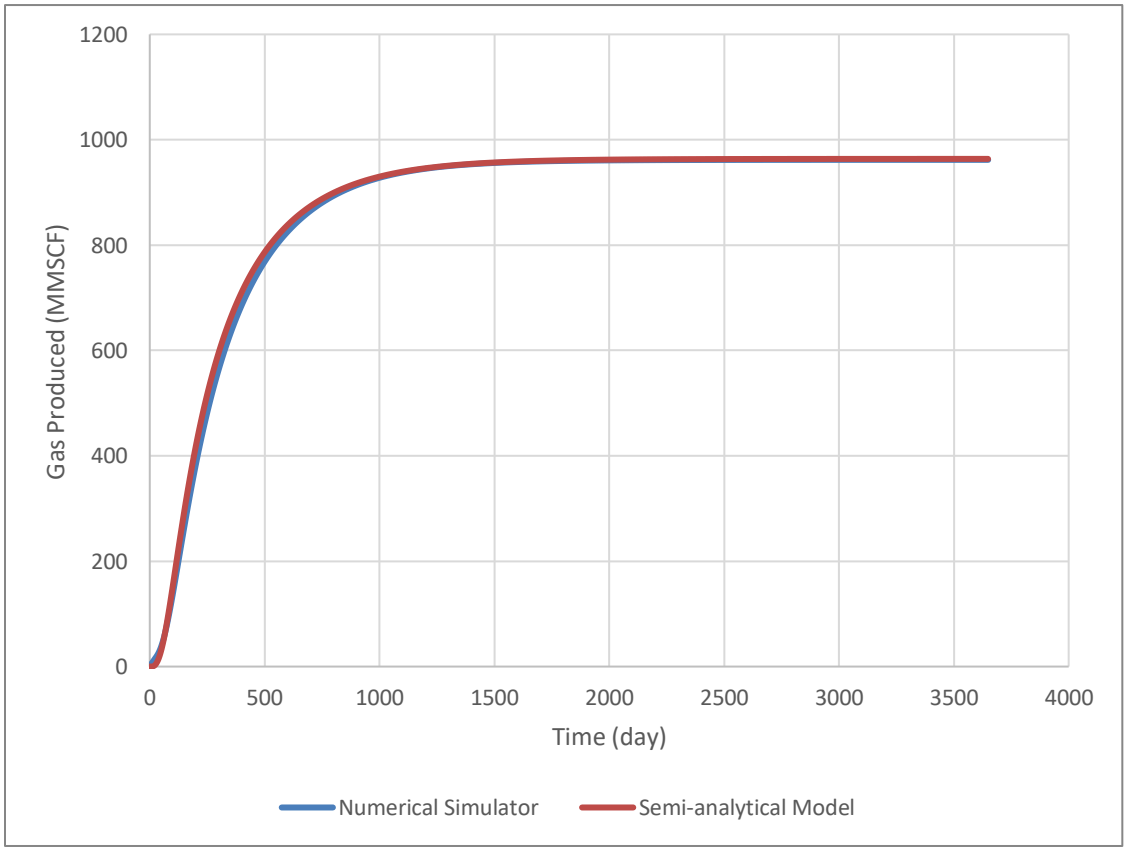


**Figure 6-17** - Case 5 gas produced comparison.

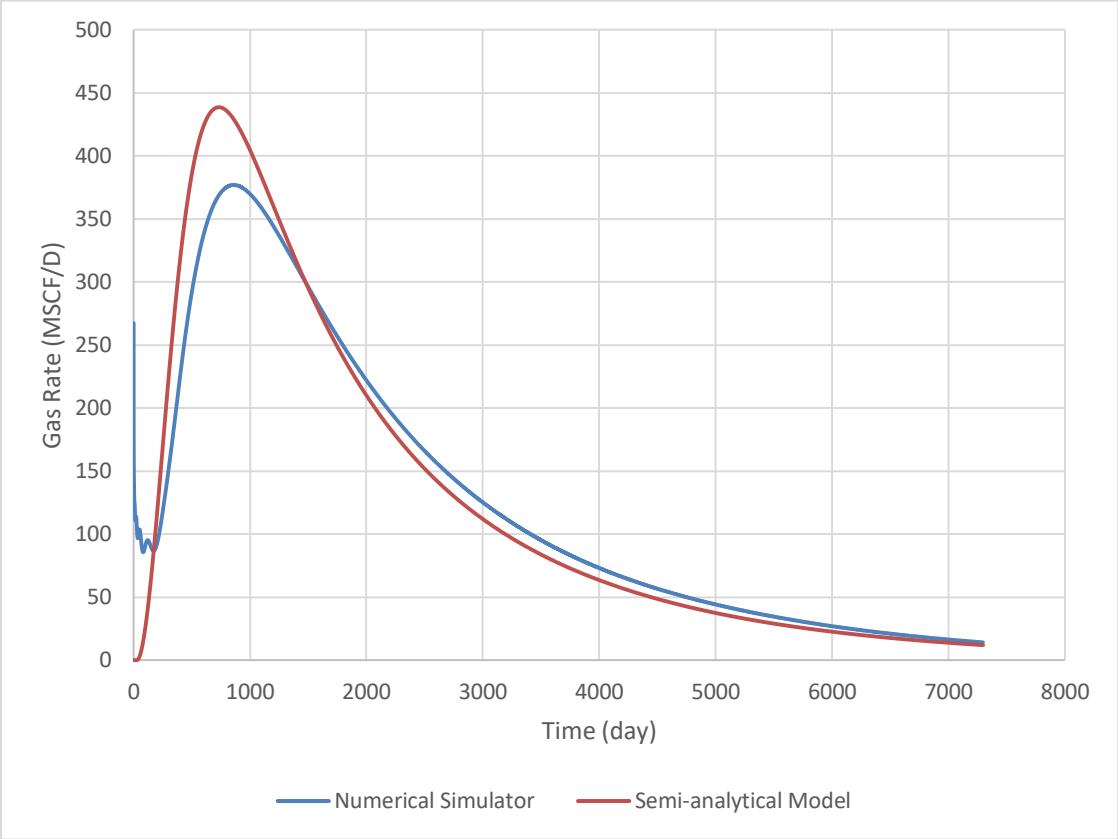


**Figure 6-18** - Case 6 gas rate comparison.

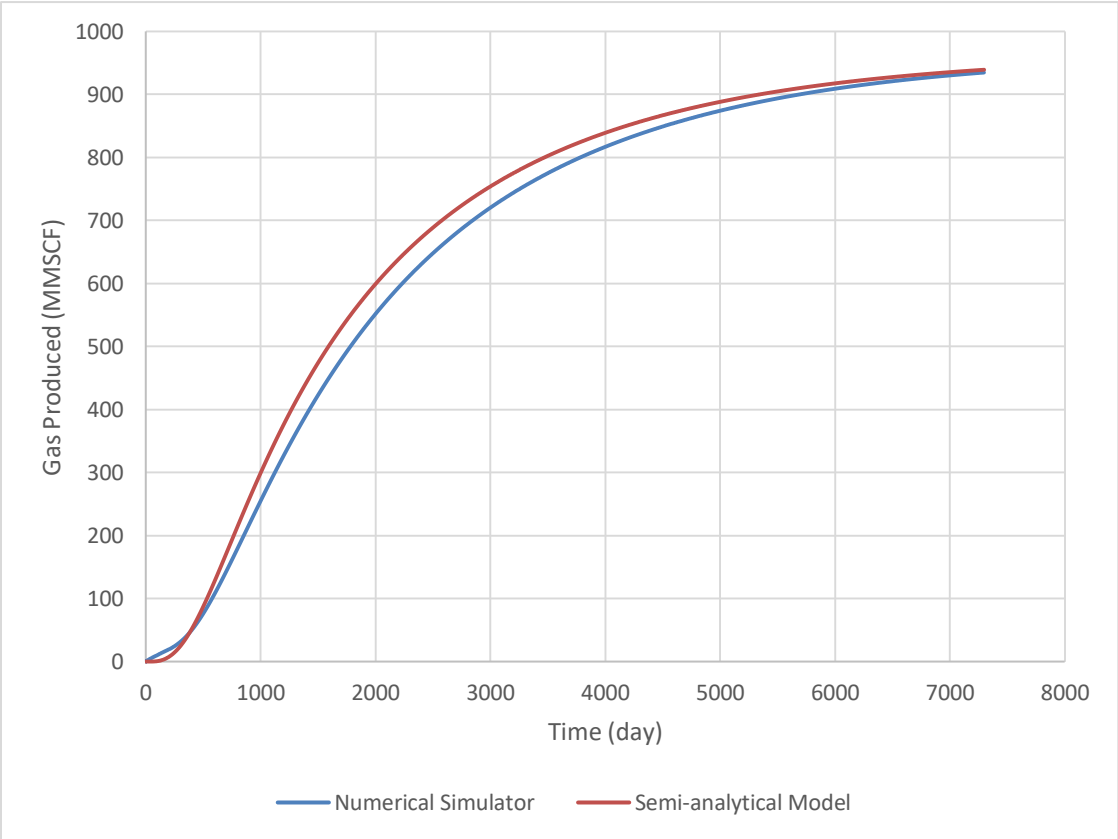


**Figure 6-19** - Case 6 gas produced comparison.

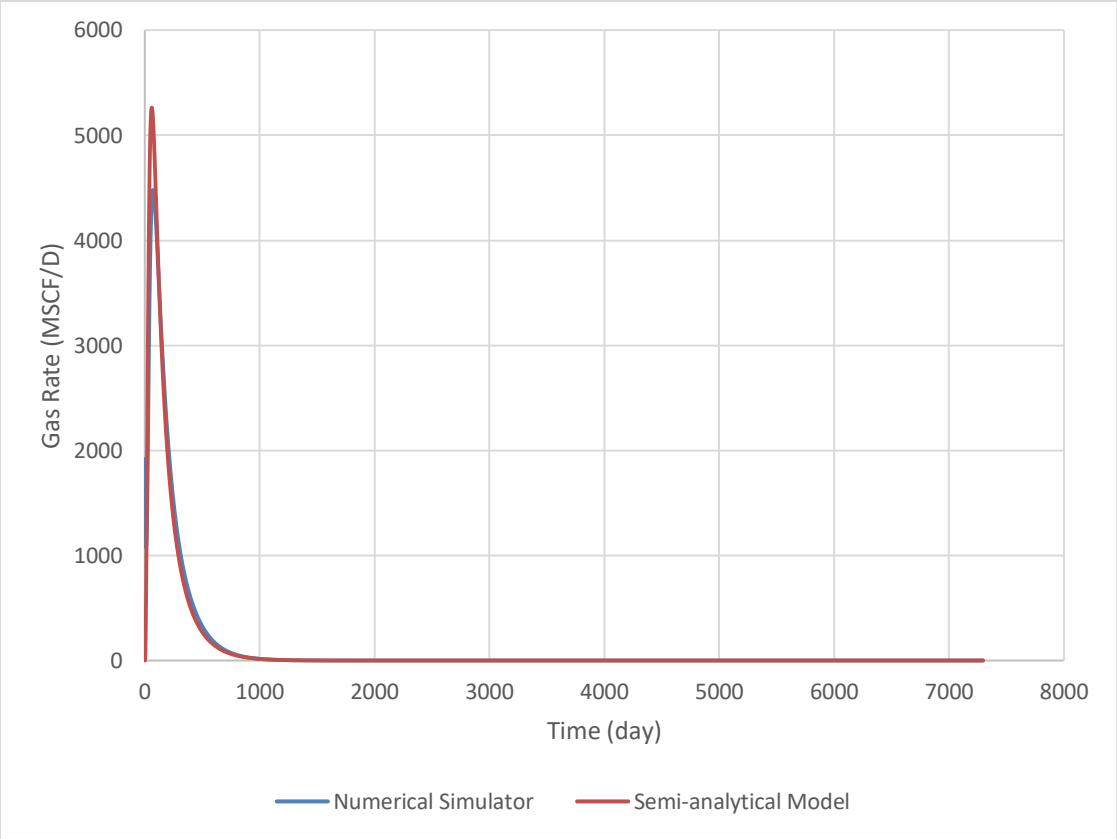


**Figure 6-20** - Case 7 gas rate comparison.

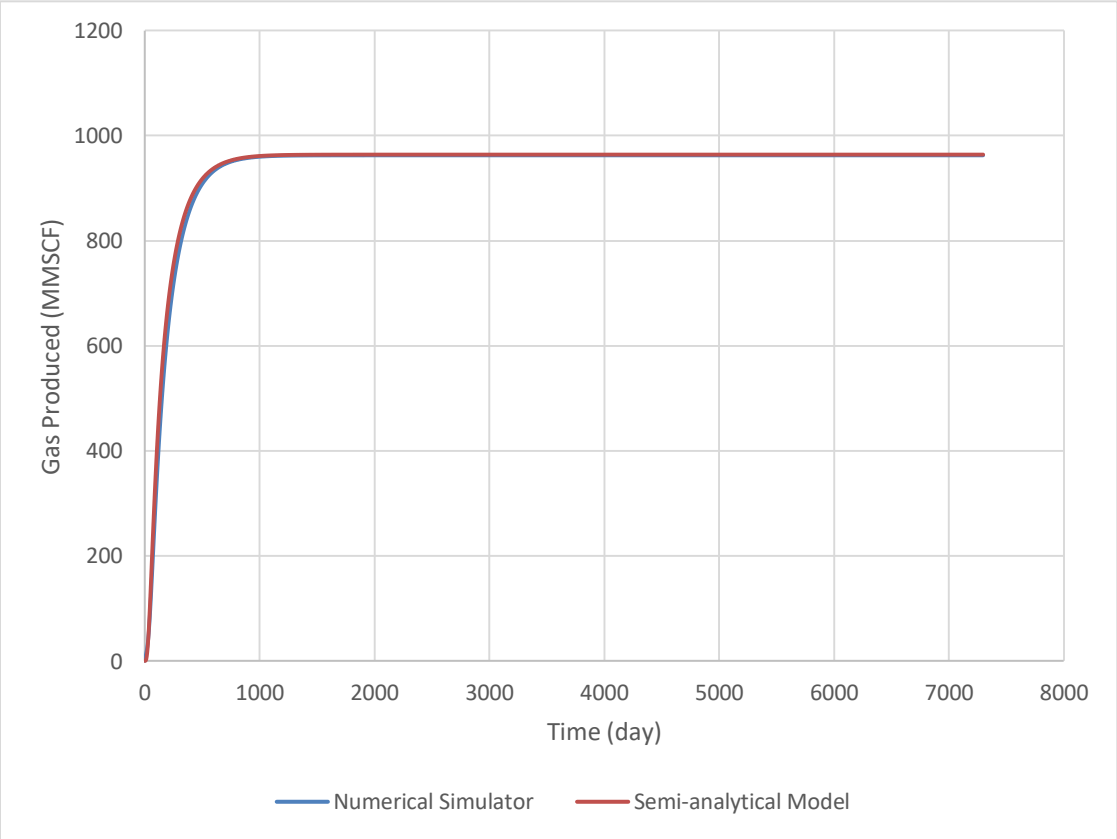


**Figure 6-21** - Case 7 gas produced comparison.

The results of the comparison show a substantial, positive difference in accuracy as rock compressibility is reduced. The reason behind this could mainly be due to the transient-state flow that is not considered within the semi-analytical model. It could be possible that in Case 1, where the error is very large, the pressure wave does not reach the boundary (to achieve pseudo-steady state) as fast as it does in the other cases. On the other hand, the semi-analytical model assumes pseudo-steady state from the first day of production. This disparity could be the reason for the large error. Fortunately, the time it takes to reach pseudo-steady state can be quantified using the equation for the radius of investigation.

$$t_{pss} = \frac{39.5\ \phi\ \mu_w\ c_t\ r_e^2}{k} \tag{6.7}$$

Where $t_{pss}$ is the time to pseudo-steady state given in $[days]$ (Dake, 1978). The reason water viscosity is used in the equation is because at the beginning, the reservoir is fully saturated with water. **Table 6-3** summarizes the time to pseudo-steady state calculated for every case.

**Table 6-3 - Time to pseudo-steady state for each case.**

| Case Number | Time to Pseudo-Steady State, $days$ |
|---|---|
| 1 | 2.738 |
| 2 | 0.717 |
| 3 | 0.178 |
| 4 | 0.111 |
| 5 | 0.057 |
| 6 | 1.156 |
| 7 | 0.096 |

This further validates that for lower times to pseudo-steady state, the semi-analytical model provided results comparable to a numerical simulator. The advantages of using the semi-analytical model over the simulator is the low input and computational power required to characterize a homogenous, isotropic, gas reservoir. In addition, Equation **(6.7)** can be used appropriately to determine whether the pseudo-steady state model is valid for a given reservoir.

## 6.2 Semi-Analytical Analysis of the Production Profile

### 6.2.1 Analysis of Peak Production ($q_g$ max)

One of the main tasks for a production engineer is to analyze and be able to forecast production profiles for a well or a field. In a well's life, production will reach a peak at some point. After that, it will begin to decline until it plateaus. It is not easy to identify the exact pressure, saturation or time that the peak production will occur at. However, through our observations, it is possible to analytically solve for the peak production using the developed model. It is then possible to identify the rock and fluid properties that have control on the peak production. As defined earlier:

$$\frac{dq_g}{dt} = \frac{dq_g}{dP}\frac{dP}{dt} + \frac{dq_g}{dS_w}\frac{dS_w}{dt} \qquad \textbf{(6.8)}$$

Mathematically, it is known that a maximum or a minimum on a curve has a derivative equal to zero. Therefore, at peak production, $\frac{dq_g}{dt} = 0$.

$$0 = \frac{dq_g}{dP}\frac{dP}{dt} + \frac{dq_g}{dS_w}\frac{dS_w}{dt} \qquad \textbf{(6.9)}$$

Now, it is possible to factor out $\frac{dP}{dt}$ from the equation.

$$0 = \left(\frac{dq_g}{dP} + \frac{dq_g}{dS_w}\frac{dS_w}{dP}\right)\frac{dP}{dt} \qquad \textbf{(6.10)}$$

For any fluid withdrawal from a reservoir, there needs to be a pressure differential to support it. Thus, it is known that $\frac{dP}{dt} \neq 0$ and can be eliminated from the equation. The resulting equation for the peak is:

$$0 = \frac{dq_g}{dP} + \frac{dq_g}{dS_w}\frac{dS_w}{dP} \tag{6.11}$$

At this point, it is still necessary to solve this equation analytically since $\frac{dS_w}{dP}$ needs to be evaluated. However, this form of the equation can be further expanded upon to make it in terms of fluid and rock properties using equations **(6.5)** and **(6.6)** defined earlier.

$$\frac{dS_w}{dP} = -\frac{\frac{dq_g}{dP}}{\frac{dq_g}{dS_w}} \tag{6.12}$$

Substituting in equations **(6.5)** and **(6.6)** for $\frac{dq_g}{dP}$ and $\frac{dq_g}{dS_w}$.

$$\frac{dS_w}{dP} = -\frac{\frac{\alpha_c\, h\, k_{rg}}{141.2\left(\ln\left(\frac{r_e}{r_w}\right) - 0.5 + S\right)}\left(\frac{\left(\bar{P} - P_{wf}\right)}{\mu_g\, B_g}\frac{dk}{dP} + \frac{k}{\mu_g\, B_g} - \frac{k\left(\bar{P} - P_{wf}\right)}{\mu_g^2\, B_g}\frac{d\mu_g}{dP} - \frac{k\left(\bar{P} - P_{wf}\right)}{\mu_g\, B_g^2}\frac{dB_g}{dP}\right)}{\frac{\alpha_c\, k\, h\left(\bar{P} - P_{wf}\right)}{141.2\,\mu_g\, B_g\left(\ln\left(\frac{r_e}{r_w}\right) - 0.5 + S\right)}\frac{dk_{rg}}{dS_w}} \tag{6.13}$$

$$\frac{dS_w}{dP} = -\frac{k_{rg}}{k_{rg}'}\left[\frac{\mu_g\, B_g}{k\left(\bar{P} - P_{wf}\right)}\right]\left(\frac{\left(\bar{P} - P_{wf}\right)}{\mu_g\, B_g}\frac{dk}{dP} + \frac{k}{\mu_g\, B_g} - \frac{k\left(\bar{P} - P_{wf}\right)}{\mu_g^2\, B_g}\frac{d\mu_g}{dP} - \frac{k\left(\bar{P} - P_{wf}\right)}{\mu_g\, B_g^2}\frac{dB_g}{dP}\right) \tag{6.14}$$

$$\frac{dS_w}{dP} = -\frac{k_{rg}}{k_{rg}'}\left(\frac{1}{k}\frac{dk}{dP} + \frac{1}{\left(\bar{P} - P_{wf}\right)} - \frac{1}{\mu_g}\frac{d\mu_g}{dP} - \frac{1}{B_g}\frac{dB_g}{dP}\right) \tag{6.15}$$

The equation can be rearranged to be given in terms of the average reservoir pressure $\bar{P}$.

$$\bar{P} = \left(\frac{1}{B_g}\frac{dB_g}{dP} + \frac{1}{\mu_g}\frac{d\mu_g}{dP} - \frac{1}{k}\frac{dk}{dP} - \frac{k_{rg}'}{k_{rg}}\frac{dS_w}{dP}\right)^{-1} + P_{wf} \tag{6.16}$$

Where $\frac{dS_w}{dP}$ and the pressure dependent terms are evaluated at the average reservoir pressure $\bar{P}$. Thus, the pressure at which maximum (or minimum) production will occur are the roots of equation **(6.16)**.

This equation is only valid at the peak (or minimum) or production. By using this equation on the base case of the developed model, it yielded an answer with 0.2% error from the $\frac{dS_w}{dP}$ value (at the peak) calculated from the Muskat-type equation and Runge-Kutta. This proves the validity of this equation. Now, if history matching is done, it is possible to adjust the properties in this equation in order to identify which property is causing the peak.

Furthermore, an investigation was conducted using the developed model to explore certain production conditions effect on the peak production. These conditions are:

1. Specified (constant) well pressure, $P_{wf}$.
2. Specified (constant) water production, $q_w$.
3. Specified (constant) pressure drawdown, $(\bar{P} - P_{wf})$.

Since the base case involves using a constant well pressure ($P_{wf}$), it is known that a peak will always be present under this condition. This can be seen in **Figure 6-6**. On the other hand, using a constant water production of 10 $bbl/day$, 50 $bbl/day$, and 500 $bbl/day$, a peak was not produced in any of the cases. In fact, the production rate kept rising until the well reached abandonment pressure. The results are presented in **Figure 6-22**, **Figure 6-23**, and **Figure 6-24**.

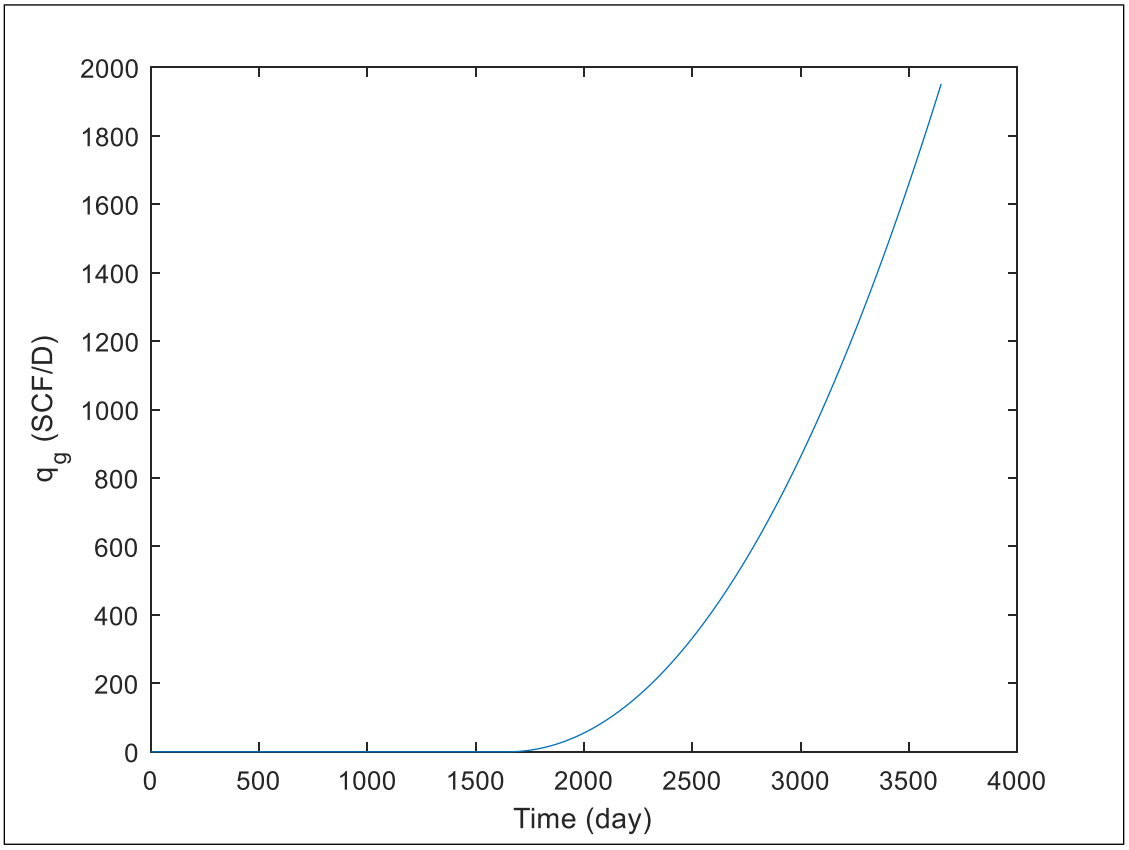


**Figure 6-22** - Gas production profile using a constant water production rate of 10 bbl/day.

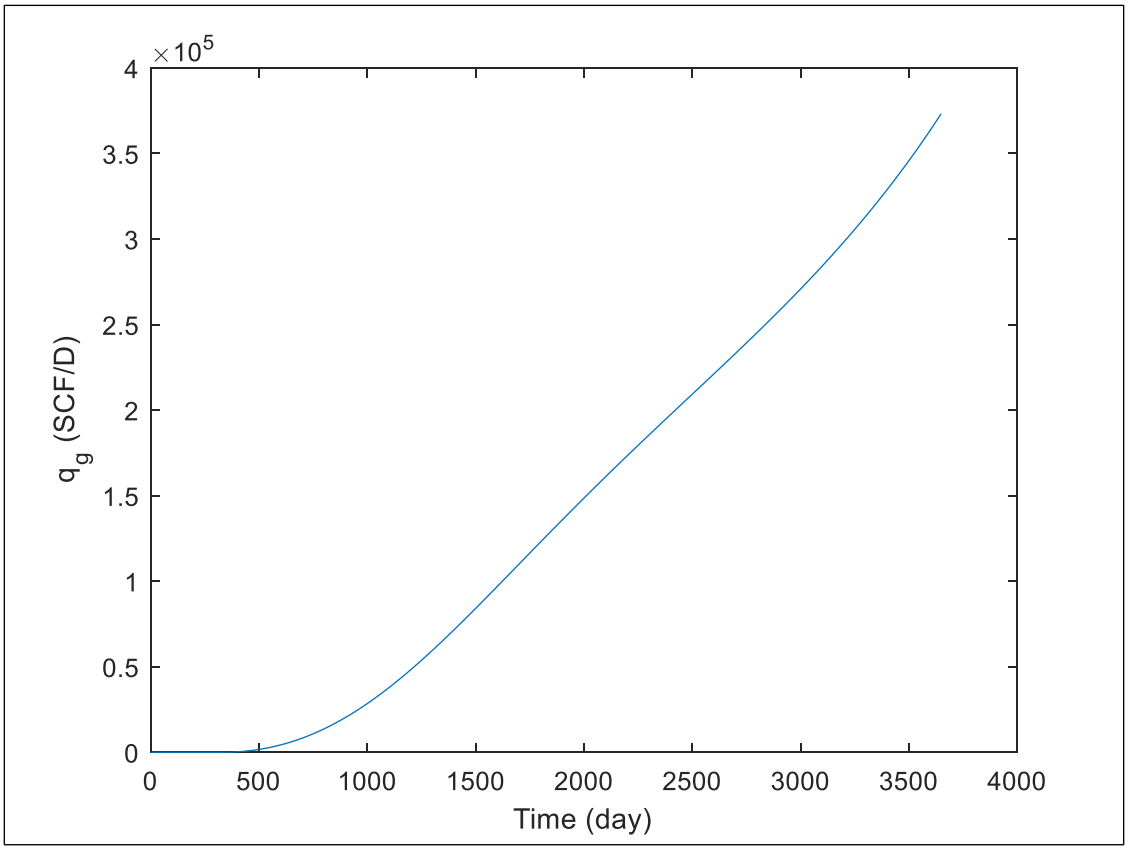


**Figure 6-23** - Gas production profile using a constant water production rate of 50 bbl/day.

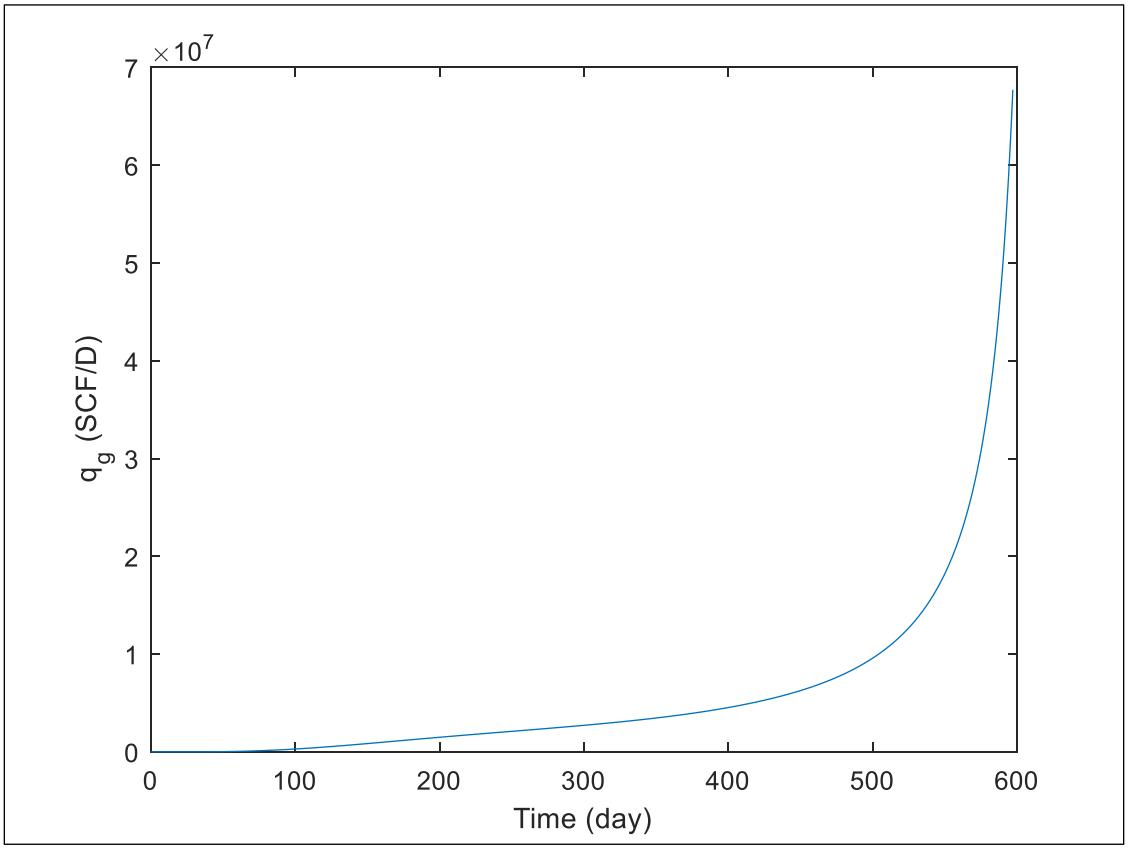


**Figure 6-24** - Gas production profile using a constant water production rate of 500 bbl/day.

It seems that if the well has a constant water production during the dewatering phase, a peak production will not be achieved as the gas rate will continue to increase until abandonment pressure is reached.

Finally, for a constant pressure drawdown $(\bar{P} - P_{wf})$, the drawdown pressure was set to be the average of the initial reservoir pressure and the well flowing pressure using base case values. **Figure 6-25** shows the results of this case.

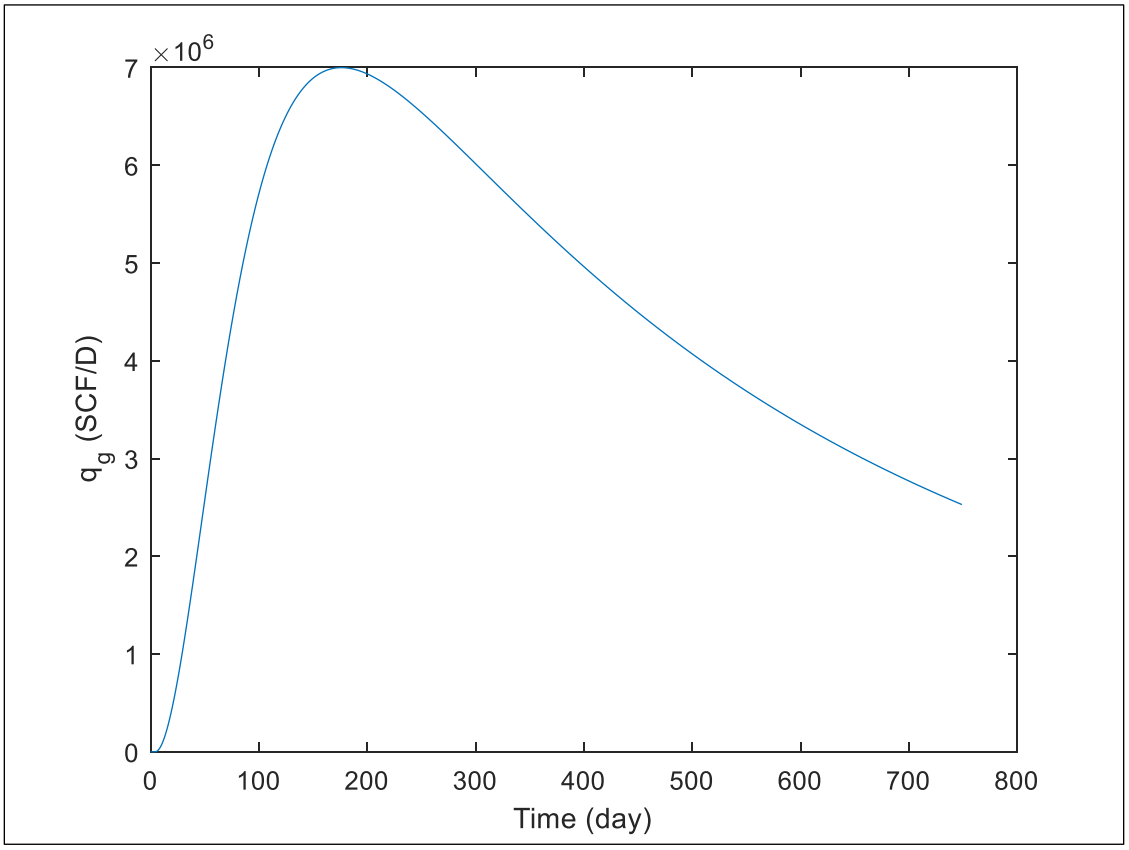


**Figure 6-25** - Gas production profile using a constant pressure drawdown.

In this case, a peak is present. However, it is broader and peaks at a higher rate than the original base case. It also reaches abandonment pressure since it is not restricted by a well flowing pressure. Looking further into the cause of the peak, it seems that the pressure drawdown is not the dominant term controlling the peak. To further investigate this, the effect of the pressure dependent and saturation dependent terms in the gas rate equation needs to be evaluated. The pressure dependent terms include the absolute permeability, gas viscosity and gas formation volume factor. On the other hand, the only saturation dependent term is the relative permeability of gas. **Figure 6-26** and **Figure 6-27** show the value of these terms.

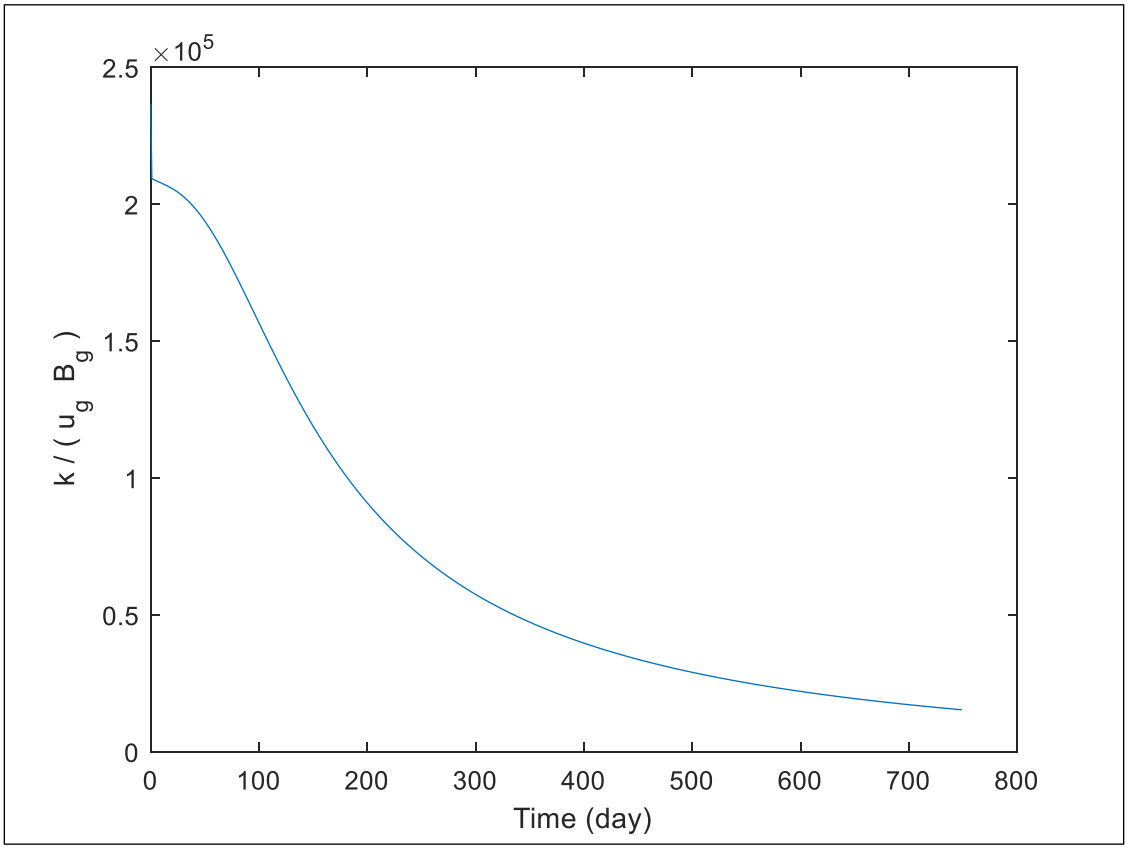


**Figure 6-26** - Pressure dependent terms change over time for the constant pressure drawdown case.

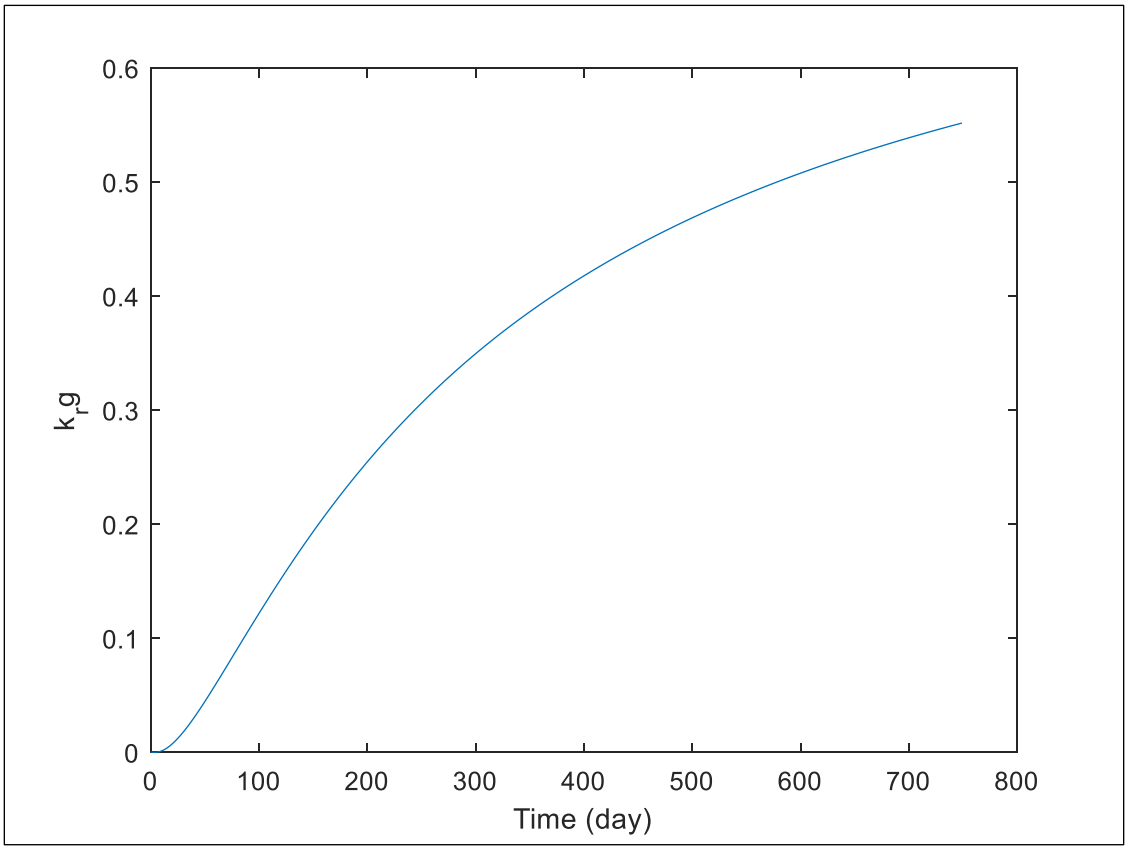


**Figure 6-27** - Relative permeability of gas for the constant pressure drawdown case.

Multiplying both pressure and saturation dependent term.

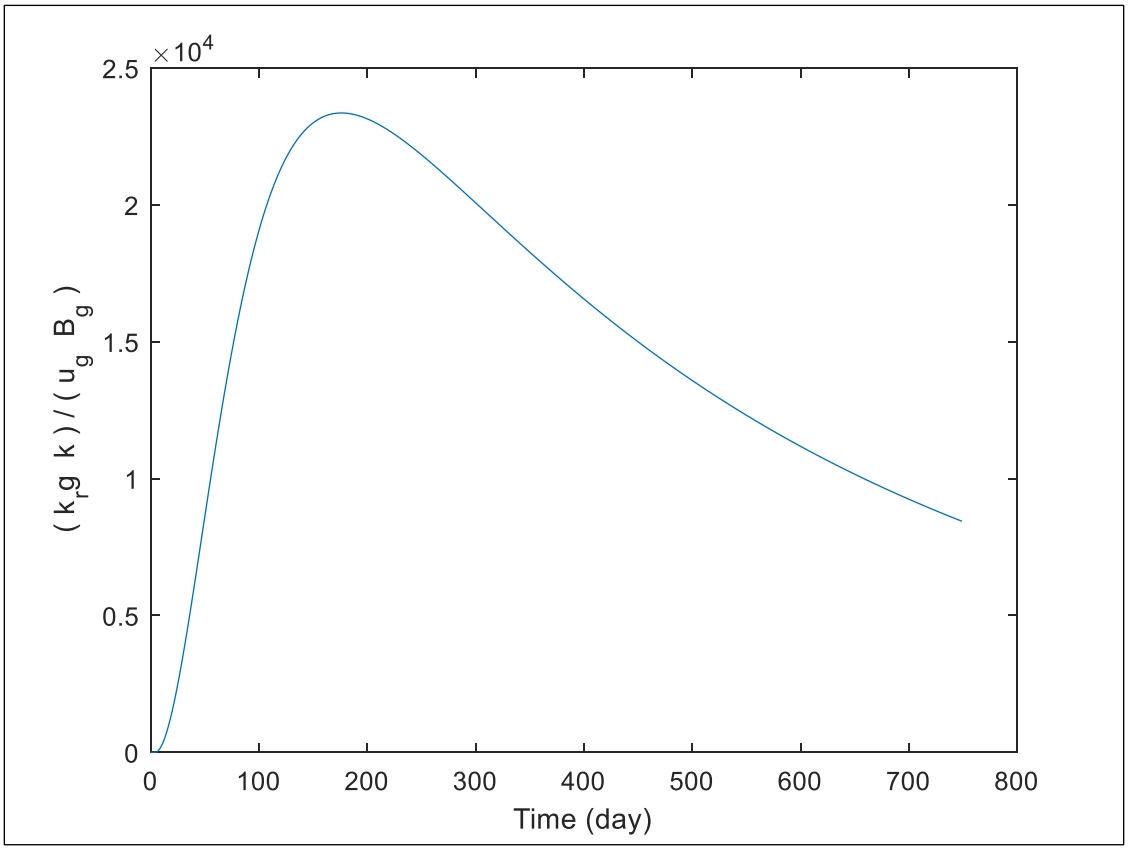


**Figure 6-28** - Pressure dependent terms multiplied by the saturation dependent term for the constant pressure drawdown case.

The trend in **Figure 6-28** is almost identical as to that shown in **Figure 6-25**. This shows that indeed, the pressure drawdown is not the most dominant term controlling the peak rate.

### 6.2.2 Analysis of Inflection Points

An inflection point is a point on a curve at which there is a change in the direction of curvature. Through the analysis of the production profile resulting from the developed model, there are two inflection points present in the gas rate plot against time. The first inflection point occurs as the gas rate begins to peak, this is when the slope changes sign from positive to negative. The other inflection point occurs when the decline after peaking reaches its most negative value and starts becoming less negative. These inflection points can be easily identified as they are the maximum and minimum of the derivative of gas rate with respect to time (**Figure 6-29**). Therefore, it is possible to find the time at which they occur. For the base case, **Figure 6-30** shows the location of the inflection points on the gas rate plot.

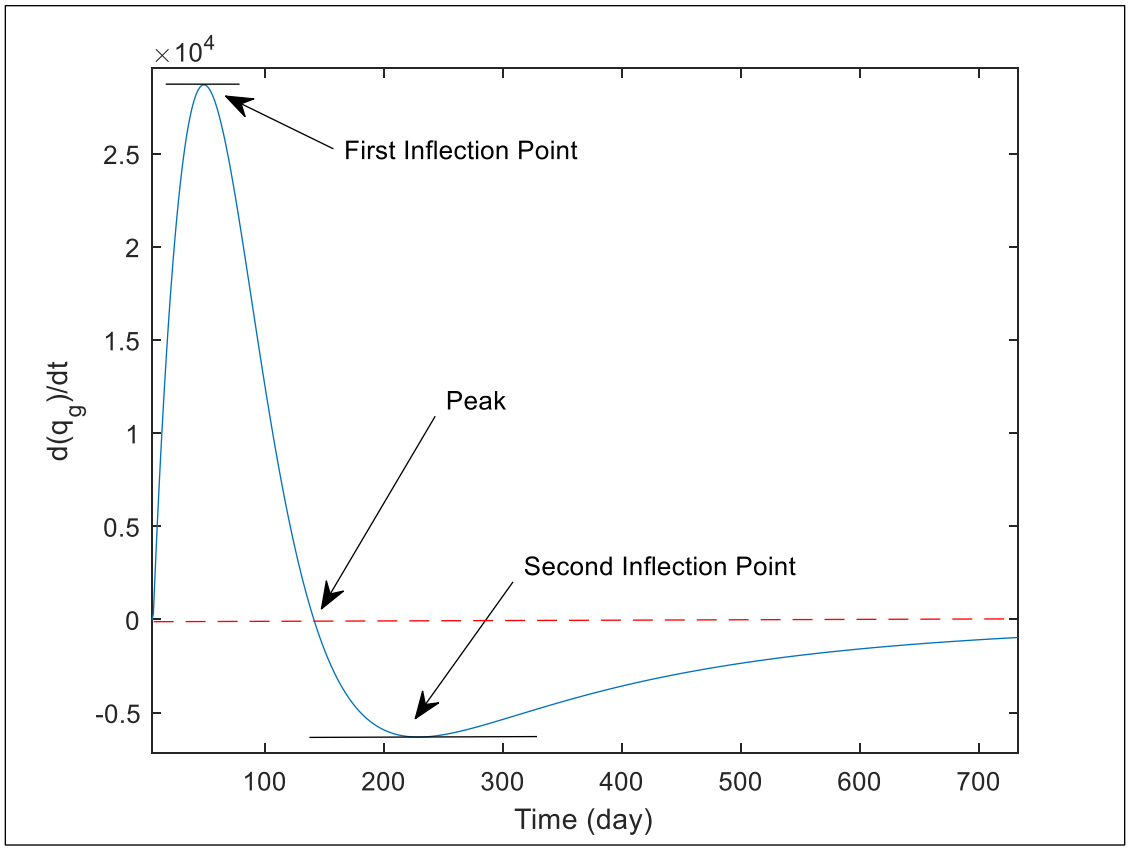


**Figure 6-29 -** Inflection points identified on the derivative of gas rate with respect to time plot (d(qg)/dt).

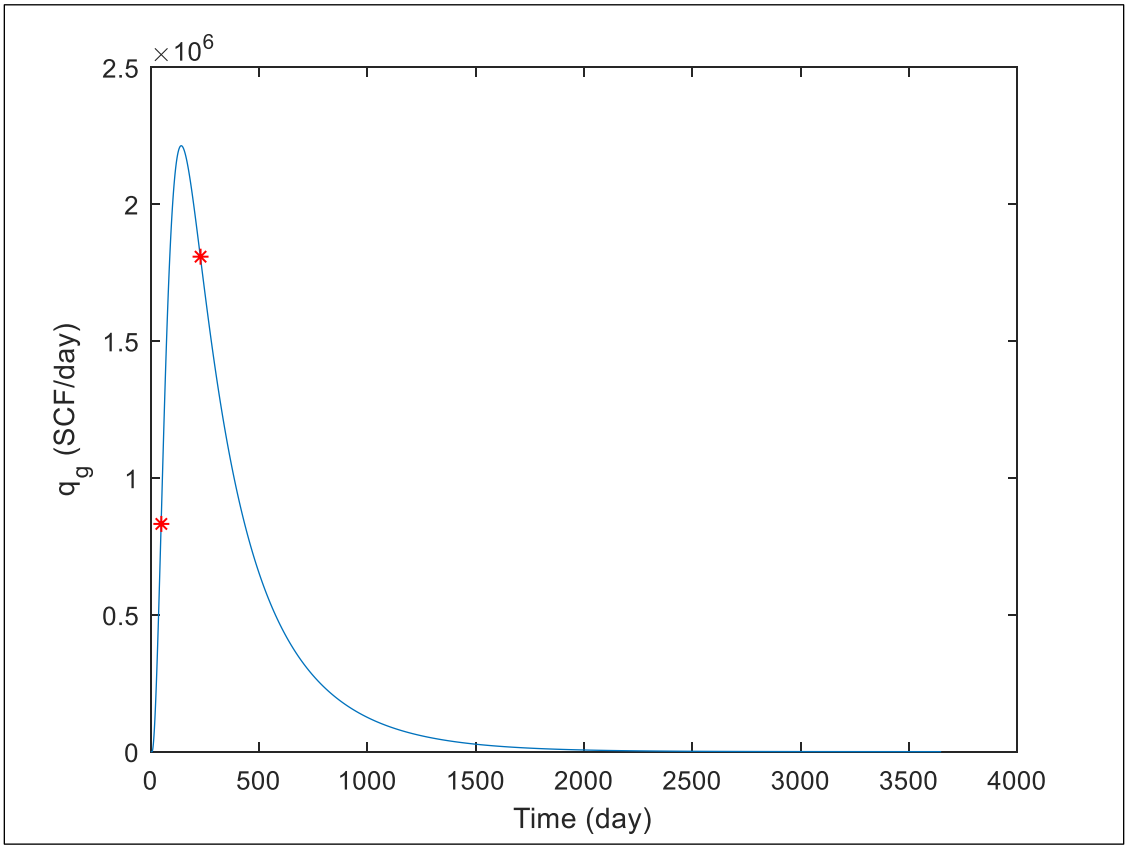


**Figure 6-30** - Inflection points identified on a gas rate vs time plot.

The significance of this observation is that we can study the effect of certain parameters on the location of the inflection points. This will be useful when doing history matching to see which parameters need to be adjusted in order to get a better history match. In this case, relative permeability exponents and Langmuir properties will be adjusted according to the minimum and maximum range values identified in **Table 4-1**. The following figures show the difference between each case and their base case value.

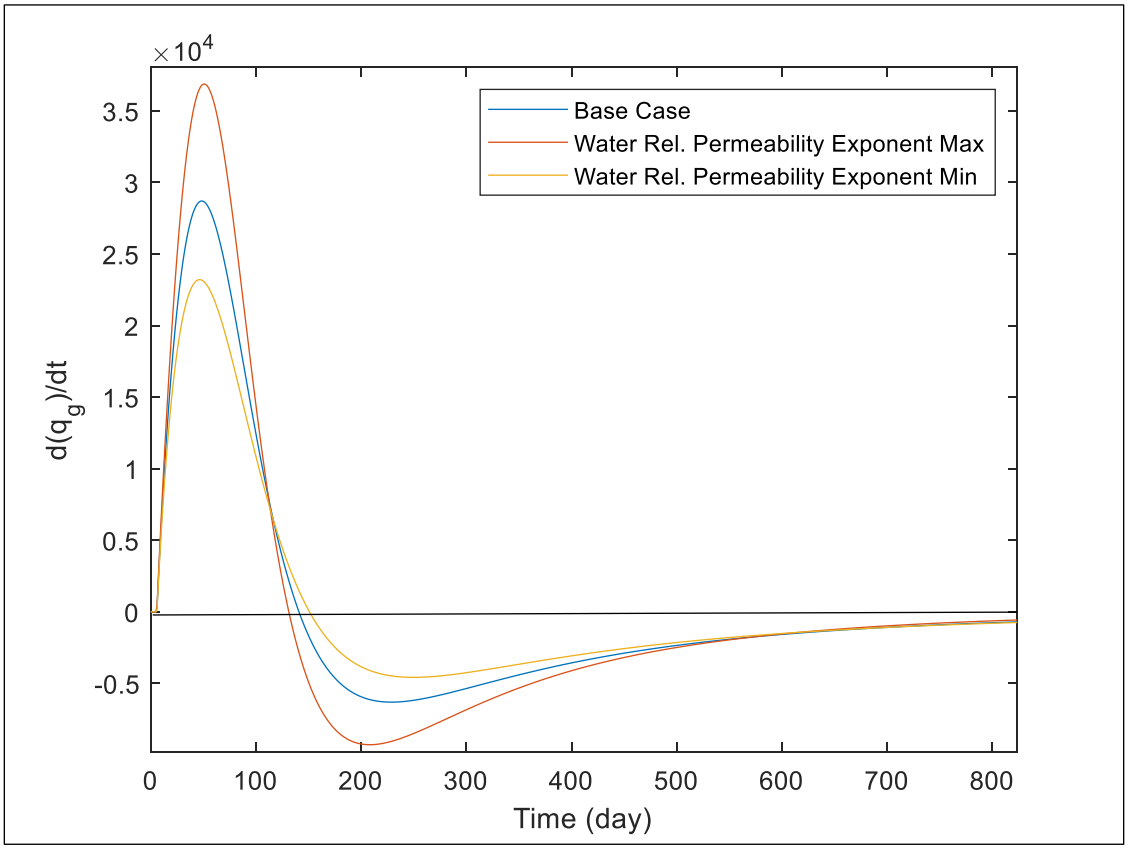


**Figure 6-31** - Derivative of gas rate with respect to time (d(qg)/dt) using different water relative permeability exponents.

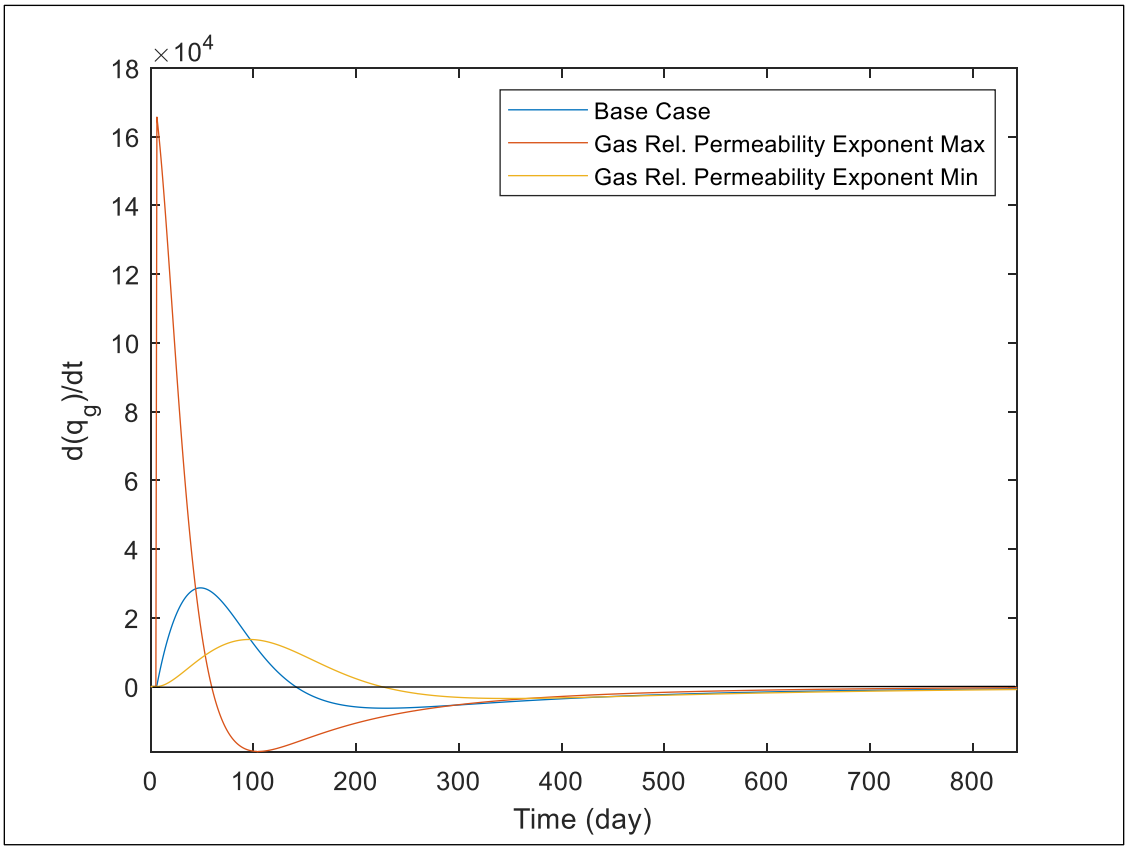


**Figure 6-32** - Derivative of gas rate with respect to time (d(qg)/dt) using different gas relative permeability exponents.

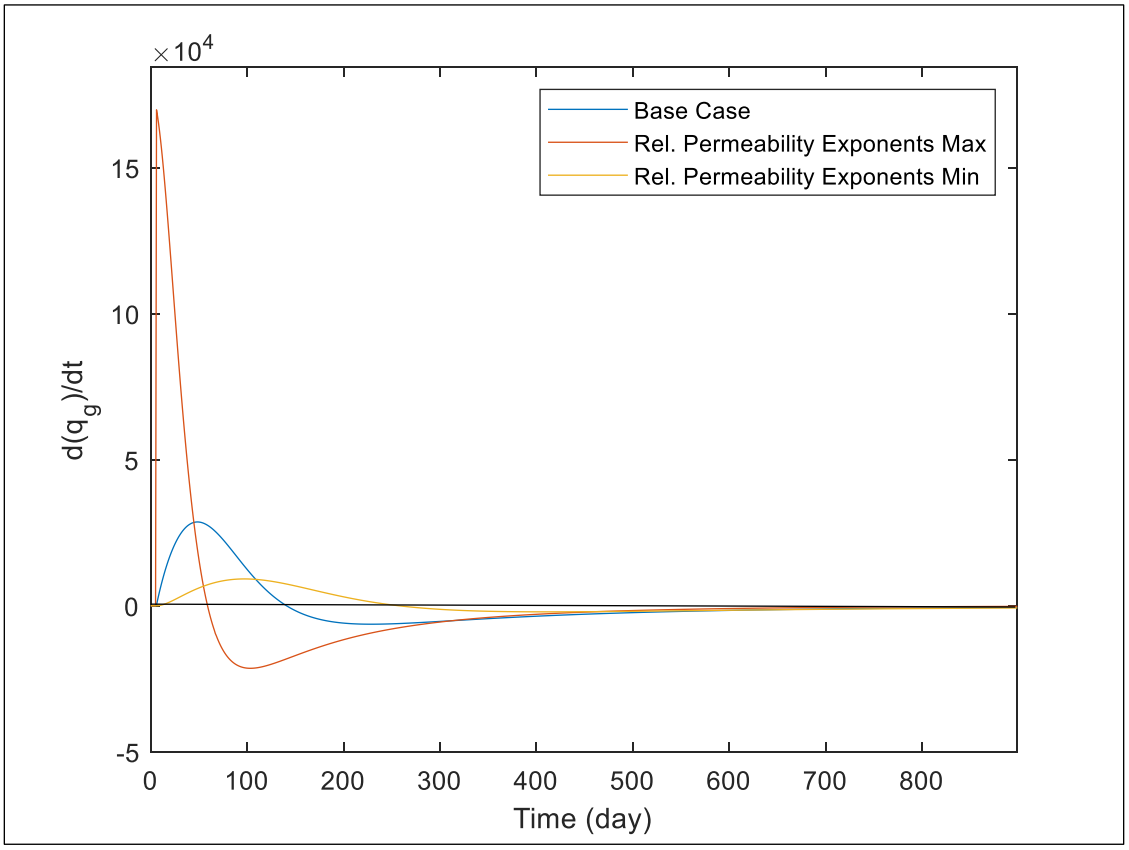


**Figure 6-33** - Derivative of gas rate with respect to time (d(qg)/dt) using different gas and water (equal) relative permeability exponents.

There is a large difference on the time to the inflection point observed when the permeability exponent is changed. Even the peaks ($\frac{dq_g}{dt} = 0$) have shifted accordingly. Since this is a fitting parameter, it should be selected carefully and can be very effective when doing history matching. The gas relative permeability exponent has a more significant effect since it is directly involved in the gas production rate equation. In the case of the relative permeability of water exponent, the water production has a direct impact on $\frac{dS_w}{dP}$ which in return affects the gas production slightly as can be seen in **Figure 6-31**.

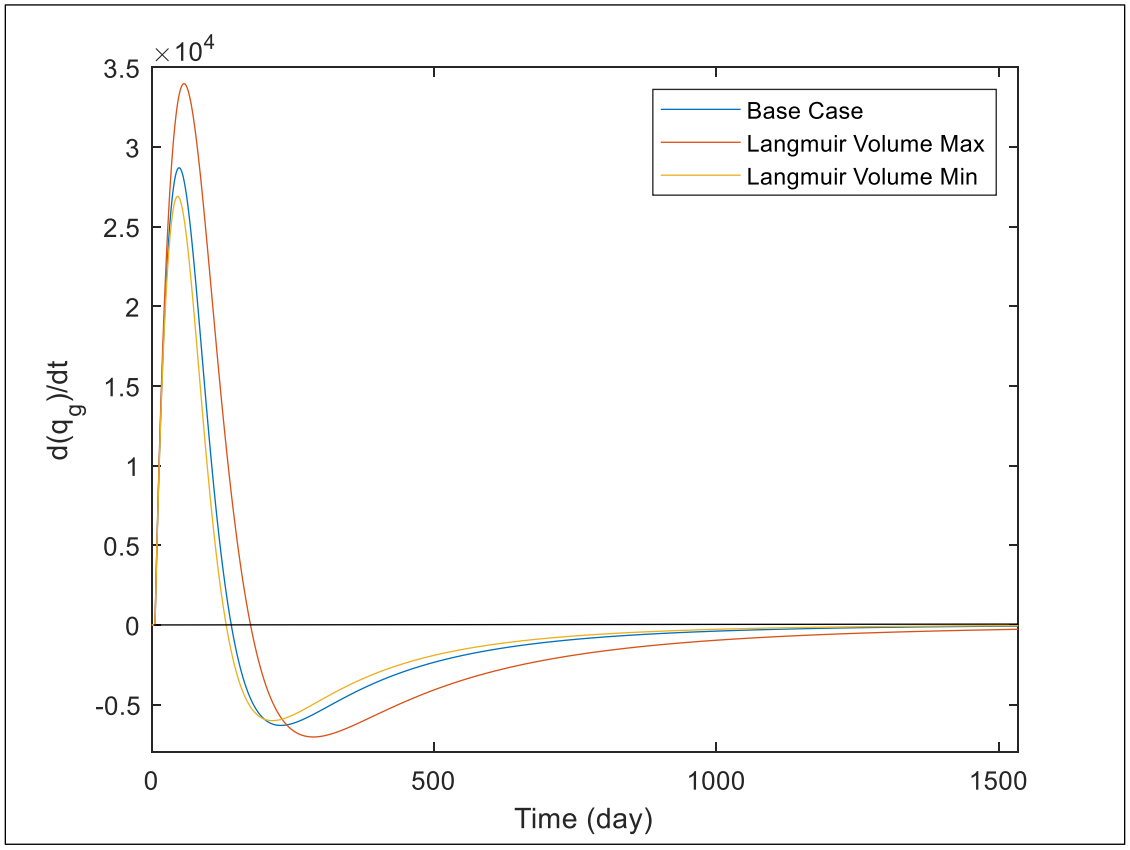


**Figure 6-34** - Derivative of gas rate with respect to time (d(qg)/dt) using different Langmuir volumes.

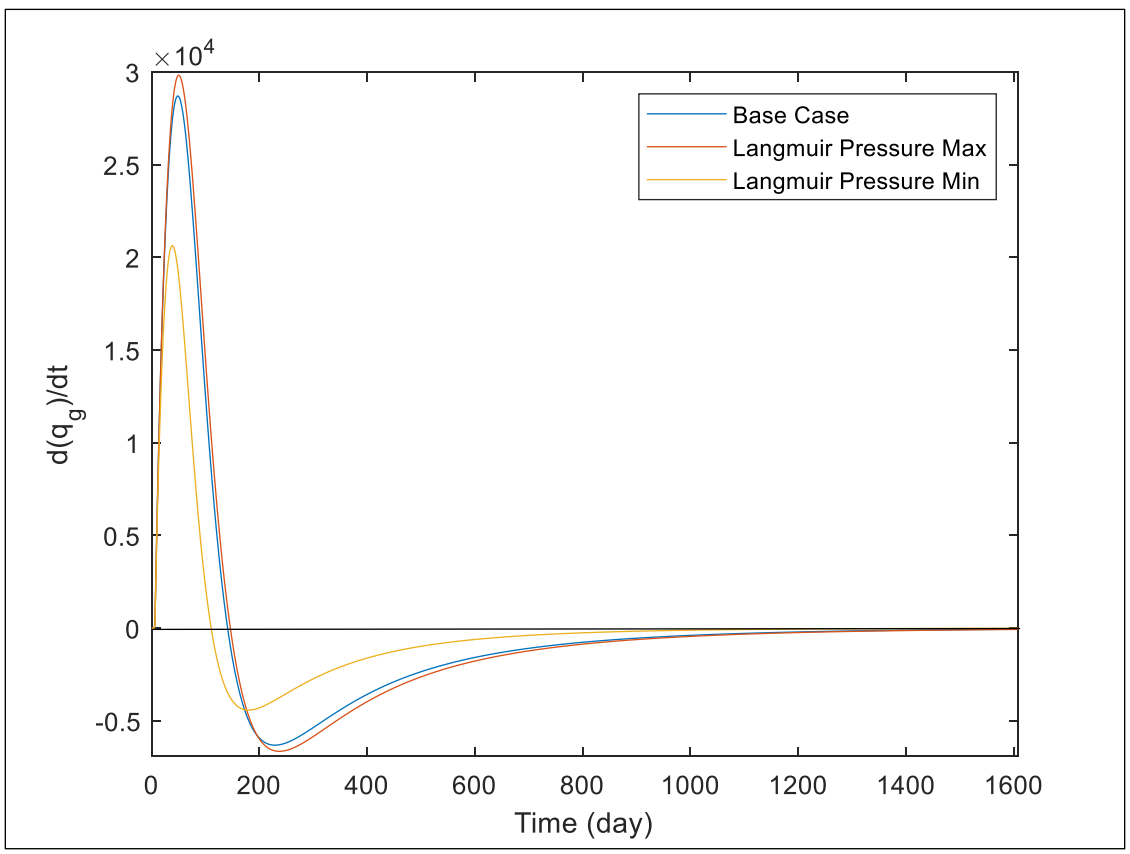


**Figure 6-35** - Derivative of gas rate with respect to time (d(qg)/dt) using different Langmuir pressures.

Both Langmuir properties had the same effect on the inflection points. The Langmuir values used were data driven, meaning they were extracted from literatures. Therefore, the base case was not symmetrically placed between both the minimum and maximum values. However, the general trend shows a proportional relationship between the properties and the time it takes to reach an inflection point.

## 6.3 Decline Curve Analysis

Decline curve analysis is used widely to predict the future performance of a producing well. It is done by fitting a line to a historical production decline curve and then manipulating this equation in order to solve for the production rate and cumulative production for future times. The advantages of this analysis are that production data is widely available and the method is easy to apply with little cost. However, with all that being said, it is still a mathematical relationship that does not take into consideration the realistic nature of reservoirs. Production curves can change shape due to changes in operating conditions and unforeseen events. Basically, there a lot of uncertainties that have to be considered (Poston & Poe, 2007).

### 6.3.1 Relationship Between Material Balance and Decline Constant D (Arps)

Arps developed empirical relations that can be used to express rate-time-cumulative production characteristics of production decline curves (Poston & Poe, 2007). One of the constants developed expresses the rate of change of the flow rate in terms of the decline rate. The decline rate, D, is defined through the following equation:

$$D = -\frac{1}{q_g}\frac{dq_g}{dt} \tag{6.17}$$

In order to relate this to material balance and investigate the use of the developed semi-analytical model as an alternative to decline curves, equation **(6.17)** can be solved using the results of the semi-analytical model. It can also be rewritten and expressed in terms of physical properties.

$$D = -\frac{1}{q}\left(\frac{dq_g}{dP}\frac{dP}{dt} + \frac{dq_g}{dS_w}\frac{dS_w}{dt}\right) \tag{6.18}$$

Where equations **(6.5)** and **(6.6)** can be substituted for $\frac{dq_g}{dP}$ and $\frac{dq_g}{dS_w}$ and equation **(5.68)** and **(5.72)** for $\frac{dP}{dt}$ and $\frac{dS_w}{dt}$.

The beauty of the semi-analytical model is that it provides production rate readings for future times as well. Therefore, it is possible to evaluate the decline rate constant at every time. However, it is important to note that decline rate analysis is only valid after the second inflection point that was discussed earlier in this thesis. This is one of the advantages of the semi-analytical model as it provides indication for when the decline starts.

**Figure 6-36** shows the constant D at every time step after the second inflection point. Interestingly enough, the shape of the curve mimics that of the gas production curve.

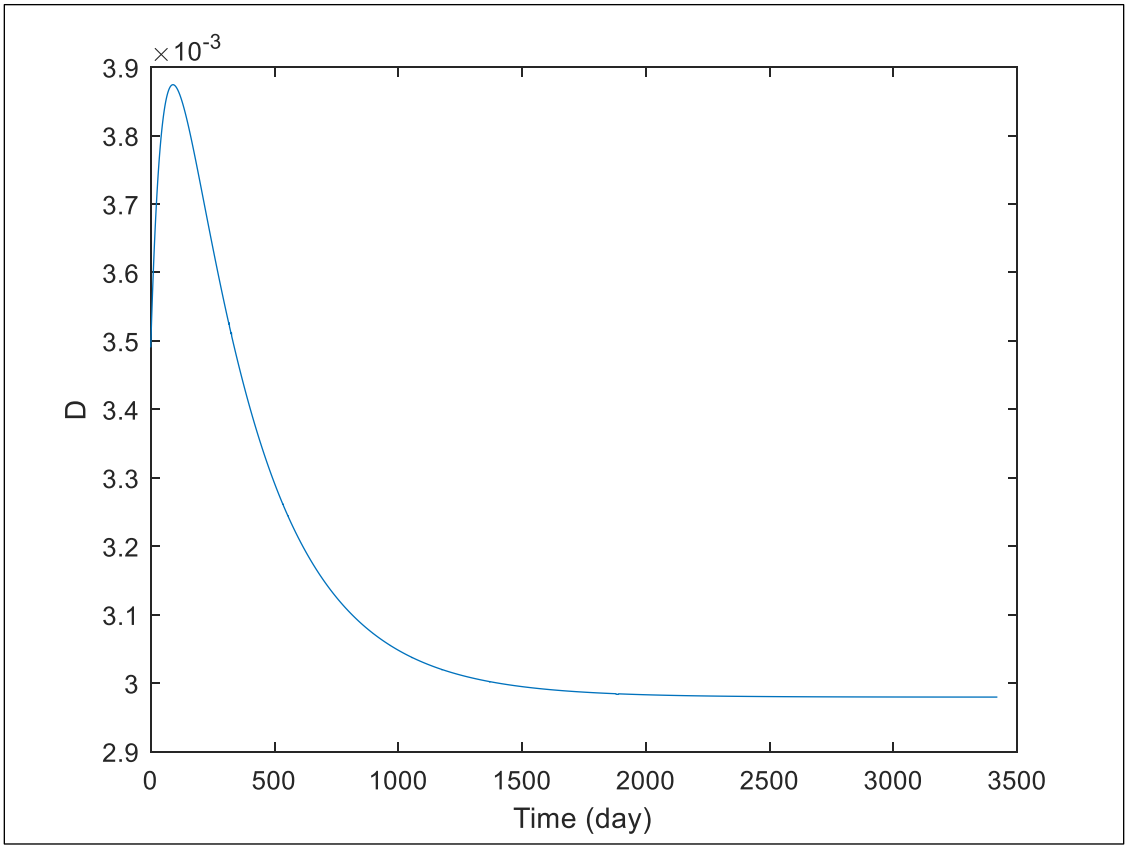


**Figure 6-36** - Decline constant D (Arps) change with respect to time evaluated using the developed semi-analytical model and base case values.

### 6.3.2 Relationship Between Material Balance and Decline Constant b (Arps)

Arps empirical relationship involves the use of another decline constant. This constant is called the b-exponent and is defined as follows (Poston & Poe, 2007):

$$b = -\frac{d}{dt}\left(\frac{q}{\frac{dq}{dt}}\right) \tag{6.19}$$

It is also related to the D constant using the following relationship:

$$b = \frac{d}{dt}\left(\frac{1}{D}\right) \tag{6.20}$$

**Figure 6-37** shows the value of this constant at every time step after the second inflection point.

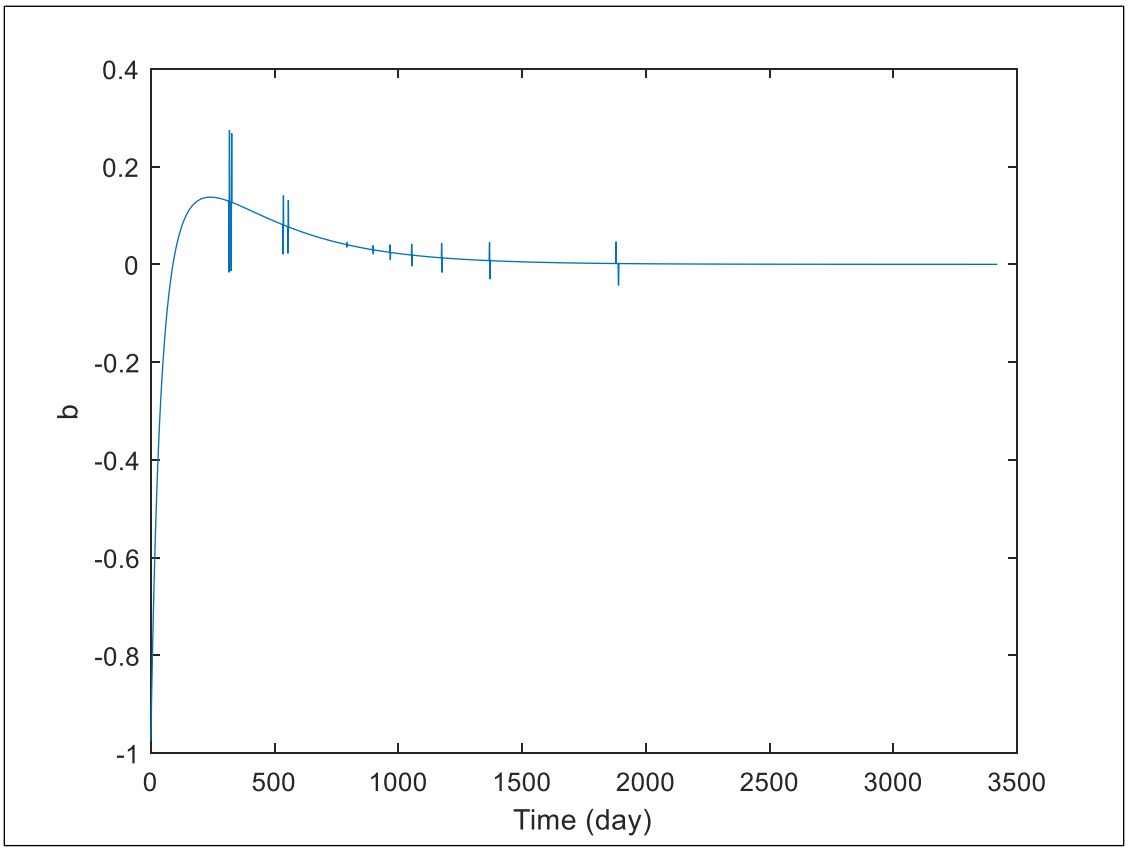


**Figure 6-37** - Decline constant b (Arps) change with respect to time evaluated using the developed semi-analytical model and base case values.

There are fluctuations present in the data that are not understood. However, they seem to be at single data points and can be ignored. The b-exponent seems to be at a higher value at the start of the decline (which is at the inflection point) but at the end (around 1750 days) it declines to a value very close to zero. This implies that the decline is exponential since the value of the b-exponent is very close to zero. The average of all the data points is 0.0142.

### 6.3.3 Use of Material Balance as an Alternative to Decline Curve Analysis

One of the goals of this thesis is to explore the use of differential material balance as an alternative to decline curve analysis. This is can be investigated by seeing if the empirical equations developed by Arps can be used to fit the decline curve to the production predicted by the developed semi-analytical model. The Arps predicted production rate equation is expressed in terms of the two constants mentioned earlier.

$$q_{g2} = \frac{q_i}{(1 + bD_i t)^{\frac{1}{b}}} \qquad \textbf{(6.21)}$$

Where $q_i$ and $D_i$ are the initial values at the inflection point. Using this equation, a predicted production rate is calculated. **Figure 6-38** shows the actual production rate from the developed semi-analytical model versus the predicted production rate calculated from equation **(6.21)**.

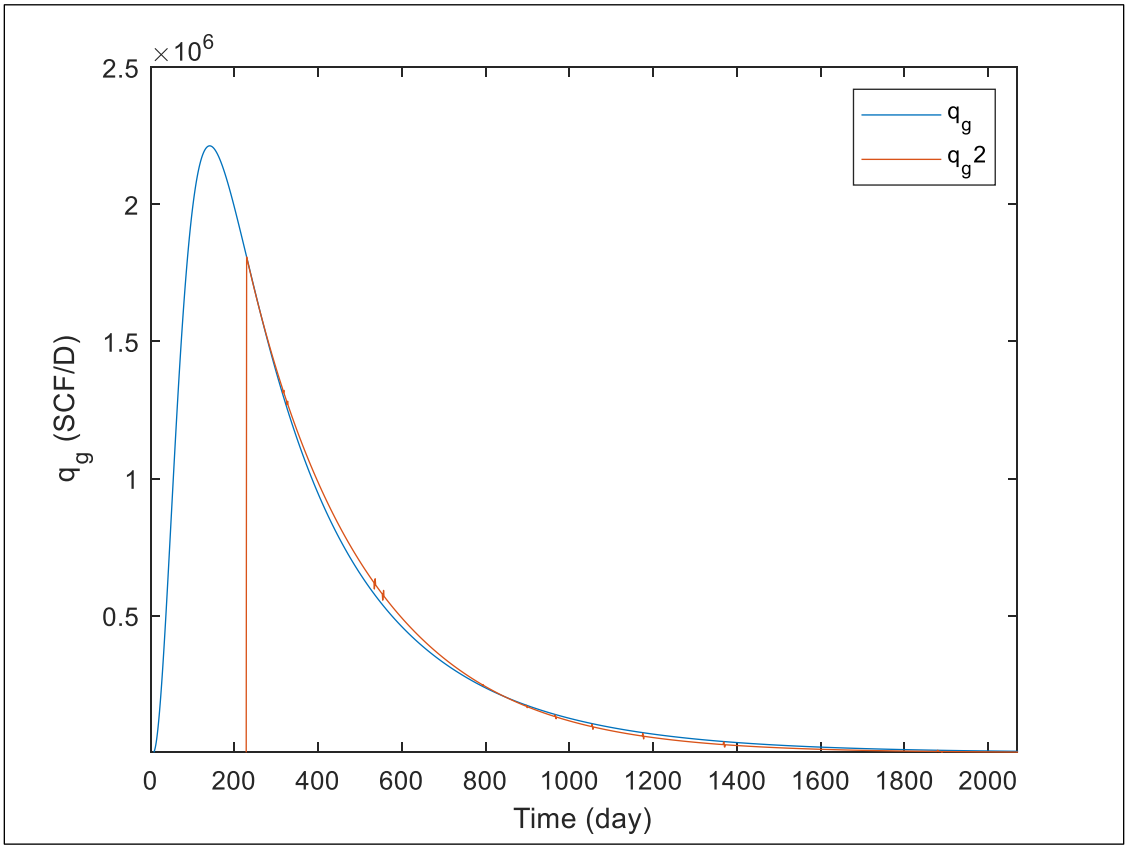


**Figure 6-38** - Decline curve analysis rate prediction versus the semi-analytical model with b-exponent varied at every time step.

The predicted model seems to present a good fit that is comparable to the one generated by material balance. However, in this case the b-exponent was varied at every time step. Arps assumes that it is a constant. Therefore, another attempt was made by using the average b-exponent for all time steps. **Figure 6-39** shows the results.

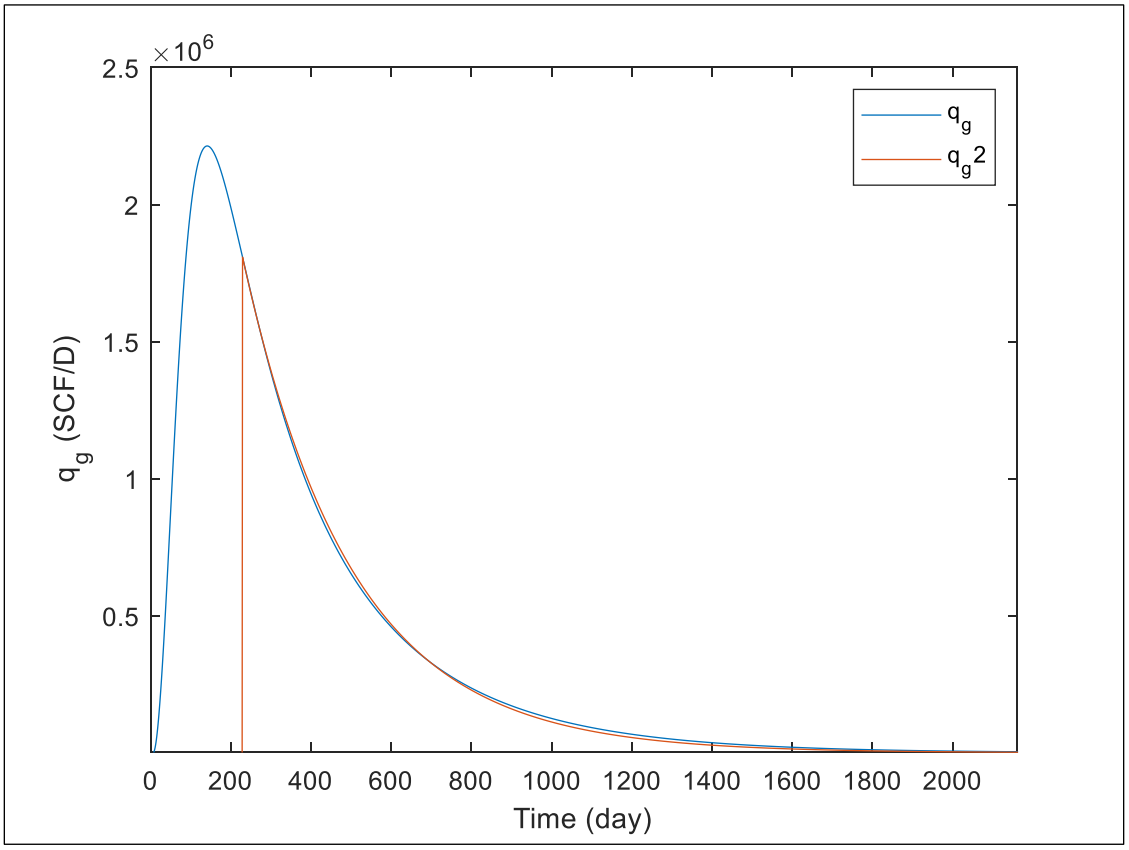


**Figure 6-39** - Decline curve analysis rate prediction versus the semi-analytical model with b-exponent average.

By averaging the b-exponent and using it as a constant, a better fit was achieved. It was also attempted at lower rock compressibility of $1 * 10^{-6}\ psia^{-1}$ to see if this prediction holds.

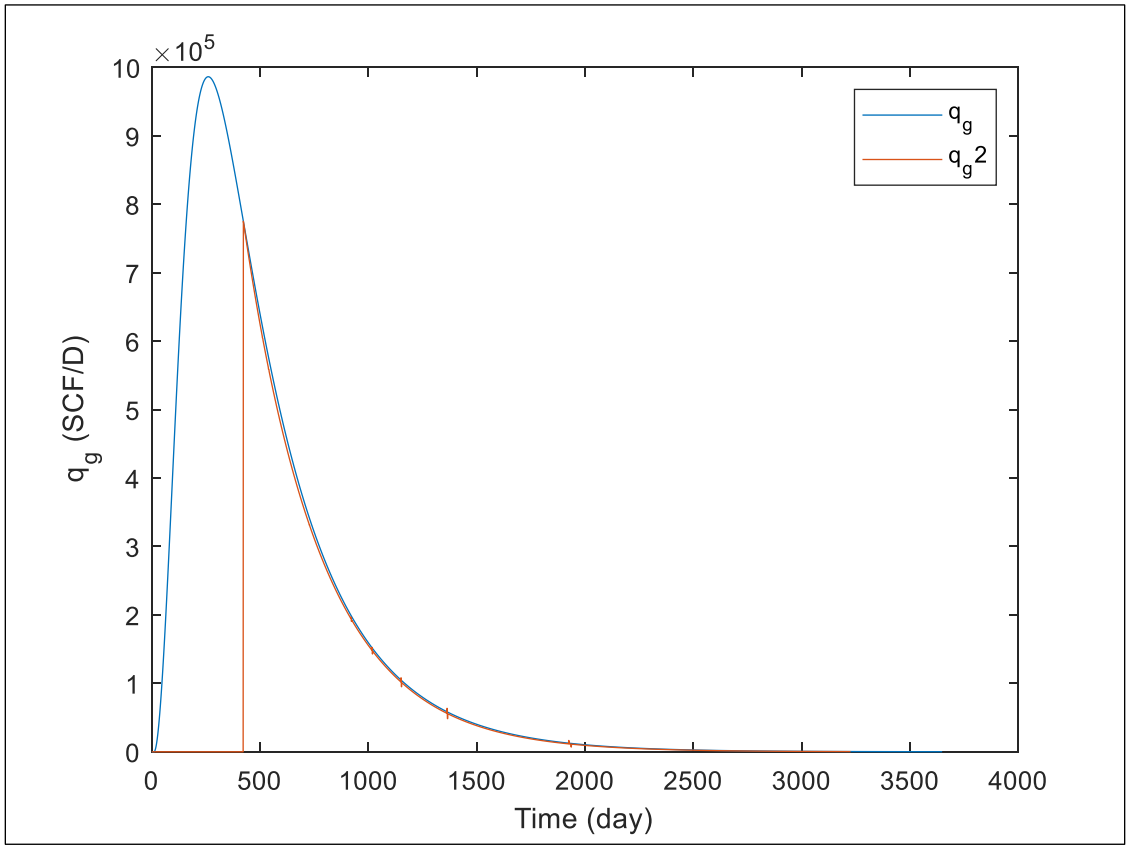


**Figure 6-40** - Decline curve analysis rate prediction versus the semi-analytical model with rock compressibility of 1*10^-6 psia^-1.

As expected, this provided a better fit than the base case which had a rock compressibility of $1 * 10^{-5}\ psia^{-1}$. The cause of this can again tie up with the fact that a low rock compressibility makes the semi-analytical model more accurate due to the less time it takes for it to achieve pseudo-steady state. As observed previously, the semi-analytical model provided results comparable to that of a numerical simulator when the reservoir had a low rock compressibility. However, it is also important to observe the late time production and how both the semi-analytical model and the numerical simulator compare. To perform this analysis, a plot of the gas rate in the cumulative gas produced domain will be generated for the case that provided the best results (case 5).

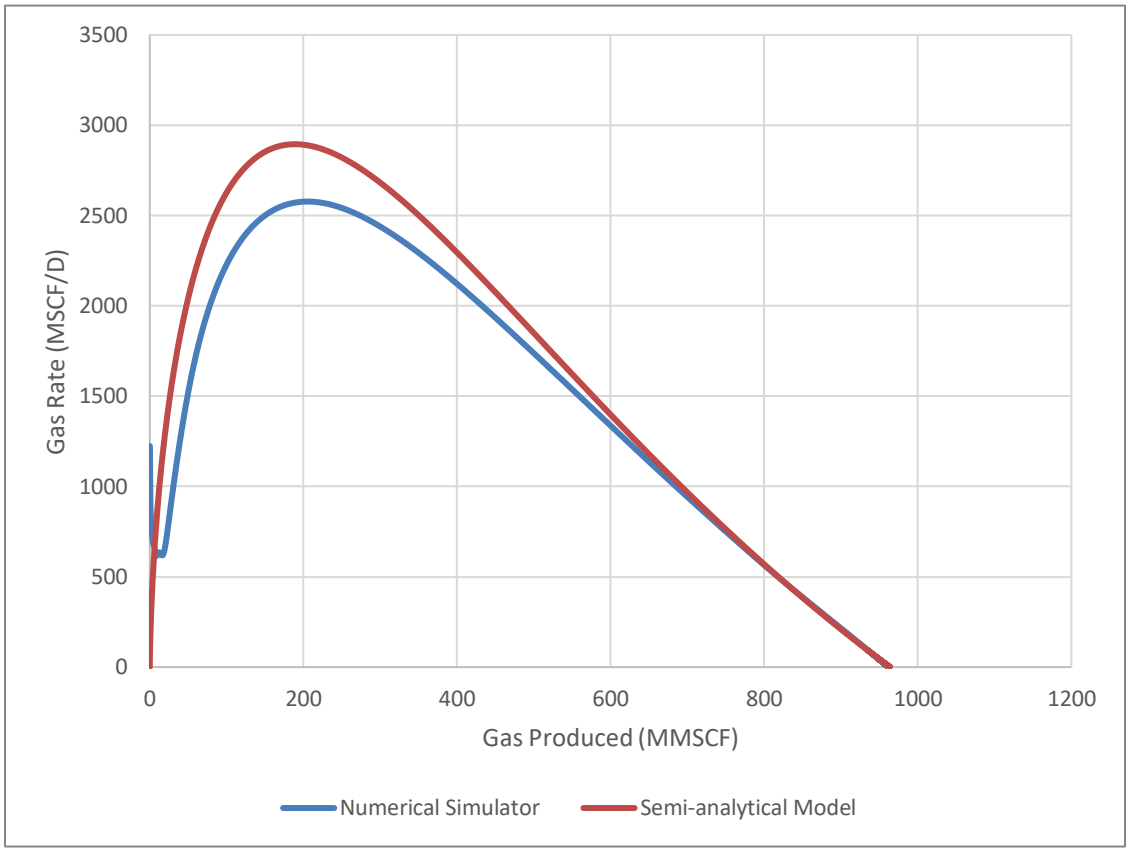


**Figure 6-41** - Gas rate vs gas produced comparison for case 5.

**Figure 6-41** shows that the semi-analytical model can be used to predict the late time production as both rates and gas produced curves line up. This also shows that the derived equations in Chapter 5 for the Muskat-type equation in the gas domain can be used to forecast the late time production region.

### 6.4 Comparison of Pseudo-Steady-State vs "Pseudo-Transient" State Analysis

Unfortunately, the "pseudo-transient" model developed from the equations derived in section 5.3 of this thesis did not work as intended. The hypothesis is that the equations developed were considered to be stiff equations. This means that the equation is unstable due to the solution sought varying very slowly which requires the step size to be reduced to an extremely small value. In an attempt to solve this problem, MATLAB's built-in ODE solvers such as ODE15s and ODE23s (which are specifically designed for stiff equations) were used. However, they have also failed to solve the developed differential equations.

One iteration was possible but it produced a solution with a pressure value of $-1 * 10^9\ psia$. This led to the hypothesis that the equations developed did not honor mass balance. The reason for this is because a highly negative pressure value could mean that the amount of fluid being drained from the reservoir is more than what is available within the bulk volume calculated at that time step. Therefore, resulting in a highly negative pressure value. To test this theory, we have attempted to inject fluids every time step until the pressure wave reaches the boundary and pseudo-steady state is achieved. Using a constant volume change and uniform time steps, the following equations were used to define the amount of gas and water that needs to be injected in order to mimic the expanding bulk volume in transient-state as the pressure wave travels to the boundary. For $\Delta t = 1$:

$$r_1 = \sqrt{\frac{24\ k\ (1)}{(948)\mu_w\ \phi\ c_t}} \tag{6.22}$$

$$\Delta volume = (r_1^2 - r_w^2)\pi\ h \tag{6.23}$$

$$q_{w,inj} = \frac{\Delta volume\ S_{wi}\ \phi_i}{\alpha_c\ B_{wi}\ \Delta t} \tag{6.24}$$

$$q_{g,inj} = \frac{\Delta volume}{\Delta t}\left(\frac{S_{gi}\,\phi_i}{B_{gi}} + V_d(P_i)\right) \quad \textbf{(6.25)}$$

The time step that was used was one day intervals. Also, the amount of gas and water injected at every time step is constant since the new bulk volume is considered to be at initial reservoir conditions. This is in line with the aforementioned divergence theorem (section 5.1.4) since the boundary is considered to be open and allows for mass entering the system.

By applying this method, the results were no longer negative. In fact, they were increasing away from the initial pressure after every time step. The model worked for a few time steps before crashing. No more attempts were made.

## 6.5 Use of Differential Material Balance Equation to Improve Integral Material Balance, P/z*

Due to the unique dual-porosity nature of unconventional gas reservoirs impacted by adsorption, the conventional material balance equations cannot be used to appropriately estimate original gas in place. However, King (G. R. King, 1993) modified and improved upon the conventional material balance equation in order to have it include the effects of having a dual-porosity system (free and adsorbed gas). This new equation utilizes a modified z-factor (gas compressibility factor) denoted by $z^*$ and is expressed through the following:

$$z^* = \frac{z}{\left\{\left[1 - c_\phi (P_i - P)\right](1 - \overline{S_w}) + \left(\frac{z\,R\,T\,V_d}{\phi_i\,P}\right)\right\}} \qquad \textbf{(6.26)}$$

The produced gas can then be estimated using the following equation:

$$G_p = \frac{V_{b2}\,\phi_i\,z_{sc}\,T_{sc}}{P_{sc}\,T}\left(\frac{P}{z_i^*} - \frac{P}{z^*}\right) \qquad \textbf{(6.27)}$$

Where

$G_P = produced\ gas, SCF$
$V_{b2} = bulk\ volume\ of\ secondary - porosity\ system, ft^3$
$z_{sc} = gas\ compressibility\ factor\ at\ standard\ conditions, dimensionless$
$z_i^* = initial\ gas\ factor\ for\ unconventional\ reservoirs, dimensionless$

Just as it is in conventional material balance, $P/z^*$ should be a straight line when plotted against the produced gas $G_p$. The intercept of the plot will provide the original gas in place. However, the bulk volume of the secondary-porosity system $V_{b2}$ is unknown in equation **(6.27)**. The average water saturation $\overline{S_w}$ in equation **(6.26)** is also unknown since it is dependent on $V_{b2}$. King provides an iterative graphical method to calculate $V_{b2}$ and $\overline{S_w}$. This iterative method can be tedious as it requires multiple steps until a converged solution is reached.

Meanwhile, the differential (Muskat-type) material balance equation that is solved through Runge-Kutta provides an estimation for the average water saturation as a function of average

reservoir pressure. These are the exact missing ingredients required to solve King's integral material balance equation without the need of an iterative method to calculate $V_{b2}$ and $\overline{S_w}$. Since the average reservoir pressure is also available from the differential material balance solution, the gas produced can be calculated by simply using Darcy's law. Thus, eliminates the need to evaluate $G_p$ using equation **(6.27)**.

To validate this observation, using the base case developed, the original-gas-in-place (OGIP) was calculated through King's material balance equation coupled with differential material balance and Runge-Kutta. **Figure 6-42** shows the resulting $P/z^*$ plot.

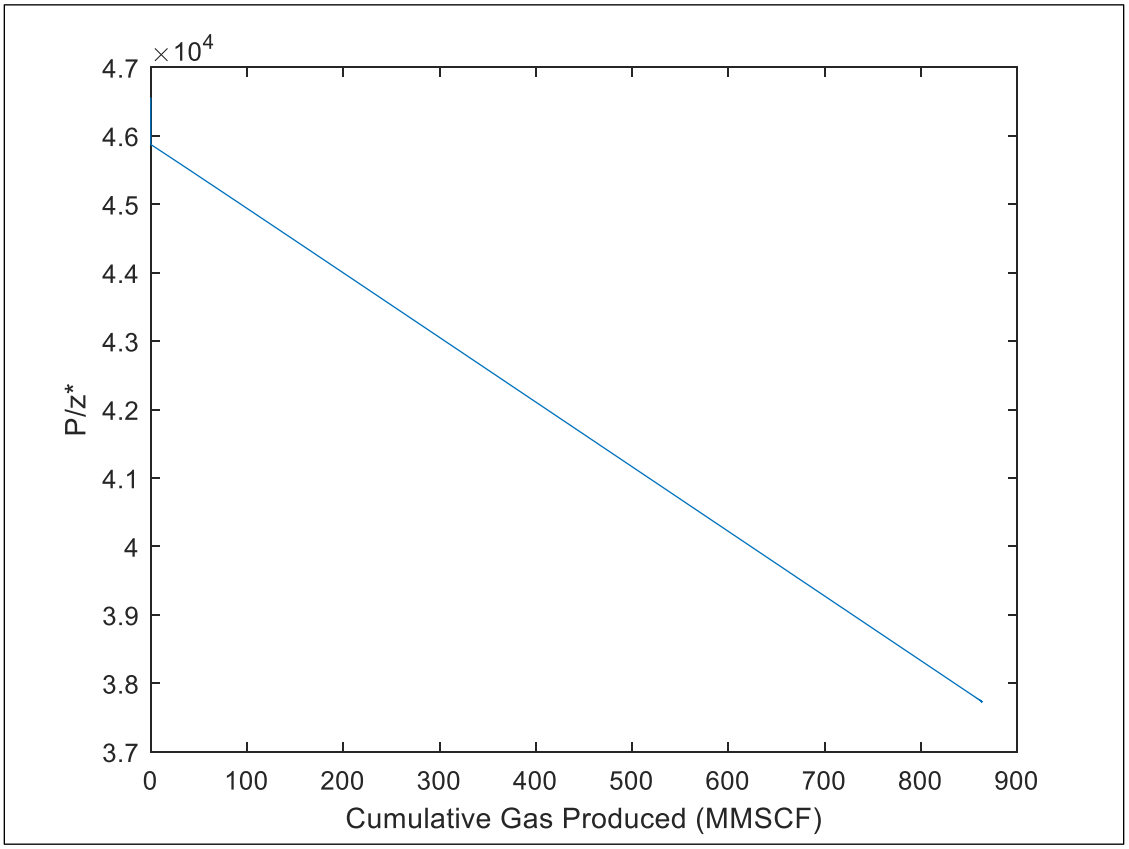


**Figure 6-42** - P/z* vs gas produced using base case values.

Using the generated plot, there are two ways to calculate the original-gas-in-place (OGIP). The first is the traditional way through the value at the intercept of the gas produced axis when $P/z^* = 0$. Note that it is possible to plot $P/z^*$ on the x-axis and the gas produced on the y-axis. In

fact, this would be easier to evaluate since the known format of the equation of the line would give the intercept value. The second way to calculate the original gas in place (OGIP) is through the slope of the line. King uses this method since it does not require any extrapolations in order to estimate the value at the intercept. The procedure involves calculating the slope of the $P/z^*$ plot and then using an analytical equation to estimate the bulk volume of the secondary-porosity system.

$$V_{b2} = -\frac{mP_{sc}T}{\phi_i\, z_{sc}\, T_{sc}} \tag{6.28}$$

Where $m$ is the slope of the $P/z^*$ plot. This equation assumes that $P/z^*$ is on the x-axis. After that, the original-gas-in-place (OGIP) can be calculated volumetrically using equation **(5.1)** defined previously in Chapter 5. In this case, since there is no free gas and only adsorbed gas, then the equation for the original-gas-in-place (OGIP) is:

$$G = V_{b2}\, V_d \tag{6.29}$$

Therefore, to validate the results of the plot (**Figure 6-42**), both methods will be used and compared to the volumetric original-gas-in-place (OGIP) calculated through the known bulk volume of the reservoir from the base case. The results of all methods are summarized in **Table 6-4**.

**Table 6-4 – Table summarizing results of original gas in place (OGIP) calculated through different methods.**

| Method | Original Gas in Place (OGIP), MMscf |
|---|---|
| Intercept approach | 485.87 |
| Slope approach | 495.92 |
| Volumetric determination | 496.56 |

The calculation through the intercept of the $P/z^*$ plot produced a larger error of 2.15% compared to the slope approach which had an error of 0.13% only. Thus, it is suggested to use the slope approach for a better estimation of the original-gas-in-place (OGIP).

Moghadam et. al further improved upon the known gas material balance equations by combining them into one equation that can be used for all gas reservoirs including conventional, overpressured and CBM/shale. This was done by introducing a new variable: $z^{**}$. When it is plotted as $P/z^{**}$ vs. $G_p$, it yields a straight line which can be extrapolated to identify the original gas in place (Moghadam, Jeje, & Mattar, 2011). It is related to King's $z^*$ through the following relationship:

$$z^{**} = z^* \left( \frac{z_i}{z_i^*} \right) \tag{6.30}$$

Where

$z_i = gas\ compressibility\ factor\ at\ initial\ pressure, dimensionless$

The difference between $z^*$ and $z^{**}$ is that $z^{**}$ is in the same magnitude as the conventional gas compressibility factor $z$. Therefore, when $P/z^{**}$ is plotted on the same plot with $P/z$, it does not dwarf the other as $P/z^*$ would. This can be seen in **Figure 6-43**.

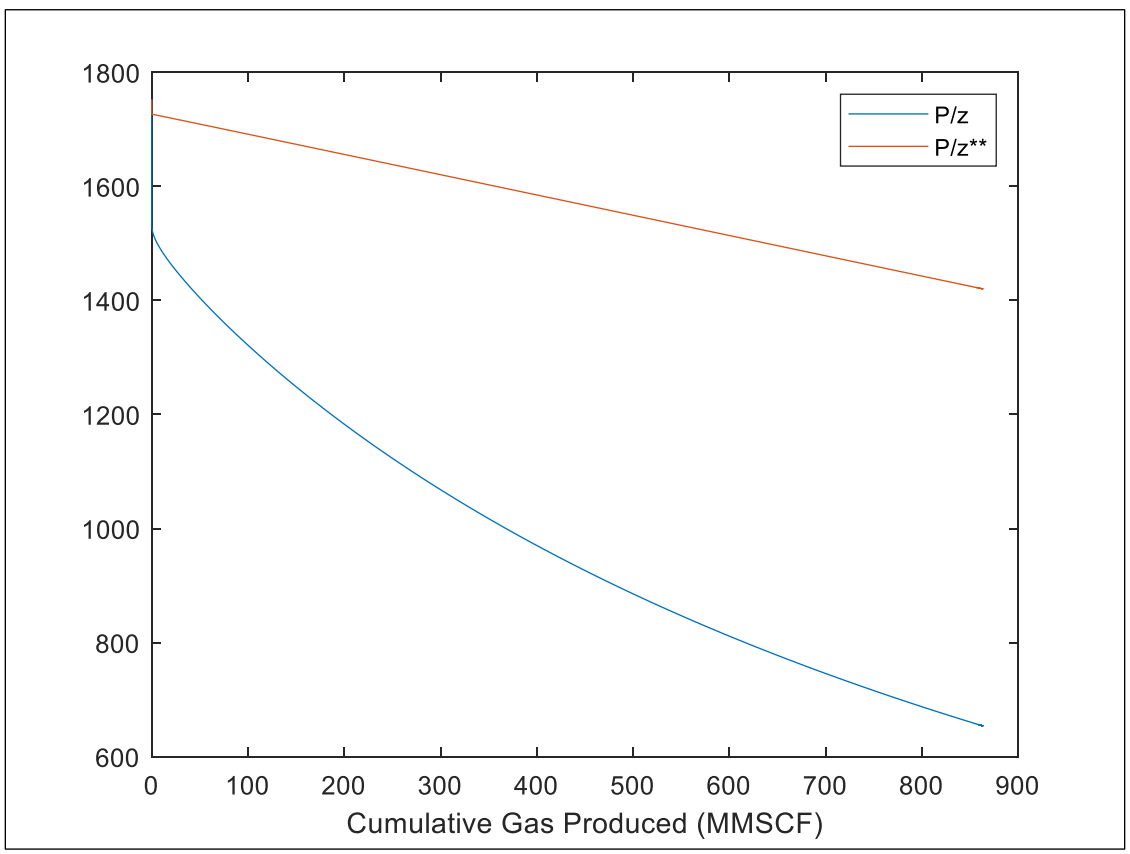


**Figure 6-43** - P/z** and P/z on the same plot.

## 6.6 Observations

### 6.6.1 Range of Properties Effect

A range of all the reservoir parameters have been previously developed and recorded in **Table 4-1**. To investigate the effect of certain parameters on the results of the developed semi-analytical model, each parameter was changed to their maximum and minimum value independently while keeping the other parameters at their base case value. This type of analysis is also known as an OVAT (one variable at a time). Four different results were specifically evaluated: time to peak rate, maximum gas rate, cumulative gas produced, and cumulative water produced. The results were then recorded and represented as a tornado chart to display the difference from the base case value. All results are based on the constant flowing pressure, $P_{wf}$, for the well specification.

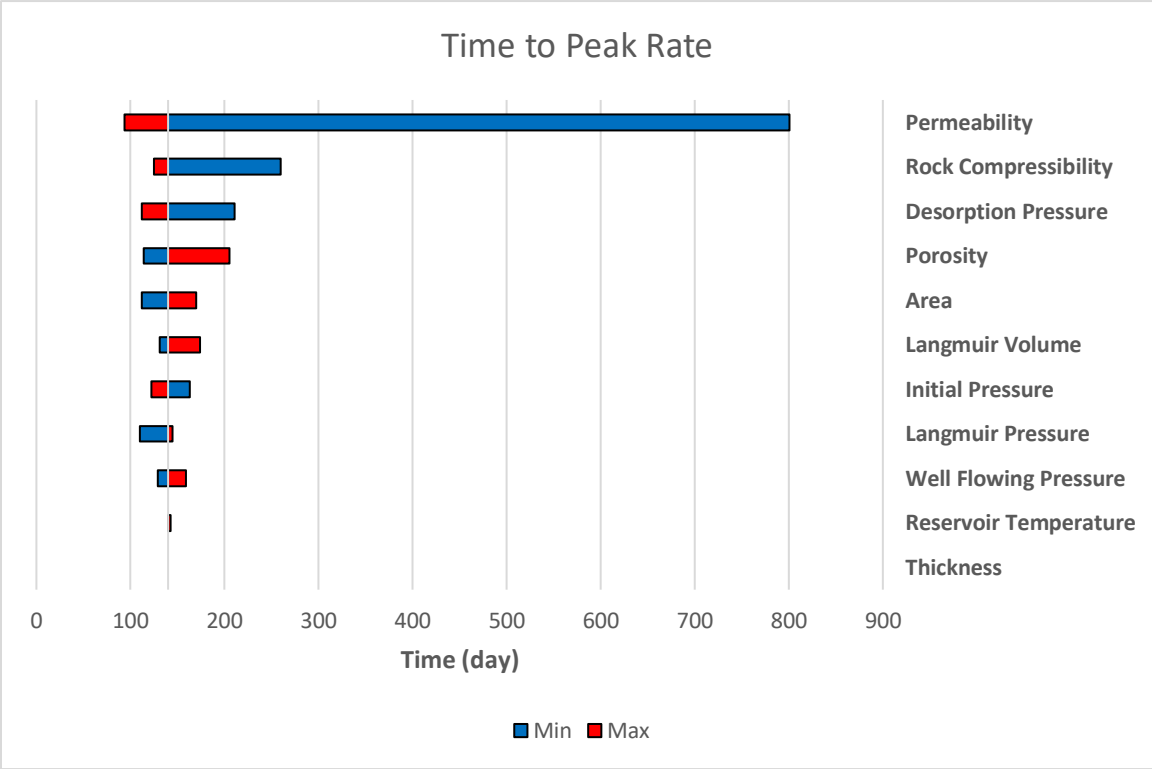


**Figure 6-44** - Tornado chart showing the effect of each parameter on the time to peak gas rate in days.

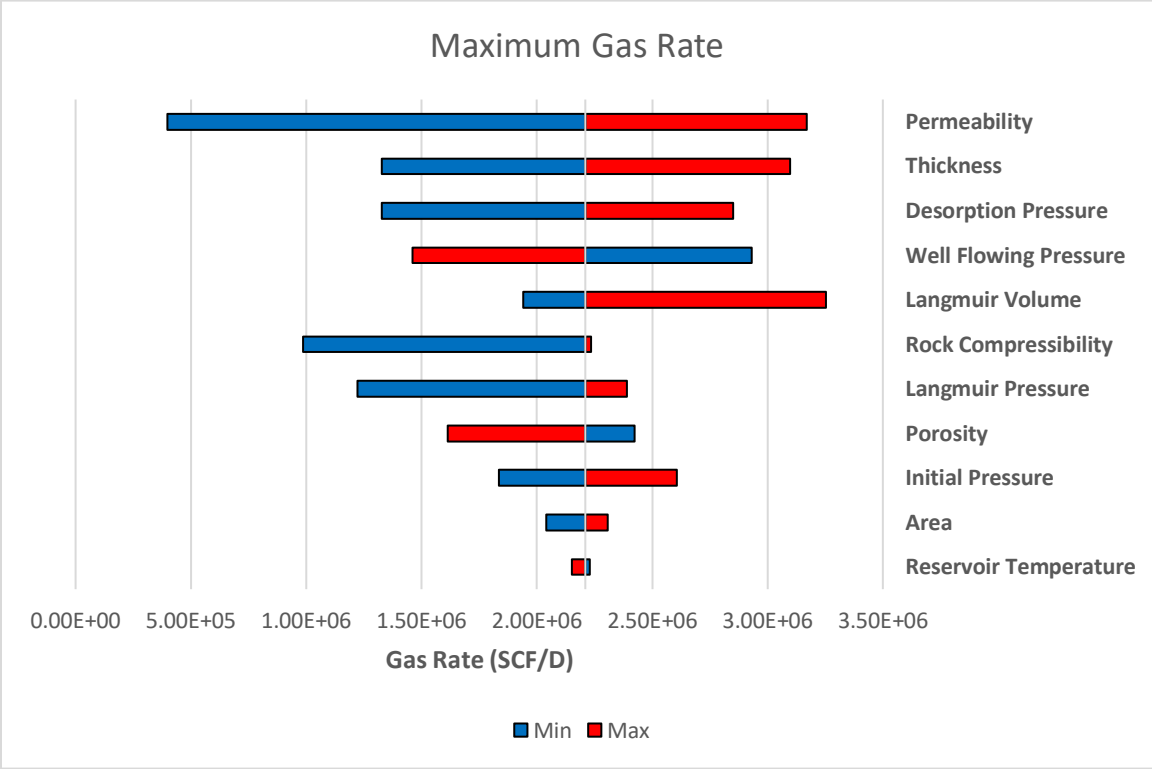


**Figure 6-45** - Tornado chart showing the effect of each parameter on the maximum gas rate in SCF/D.

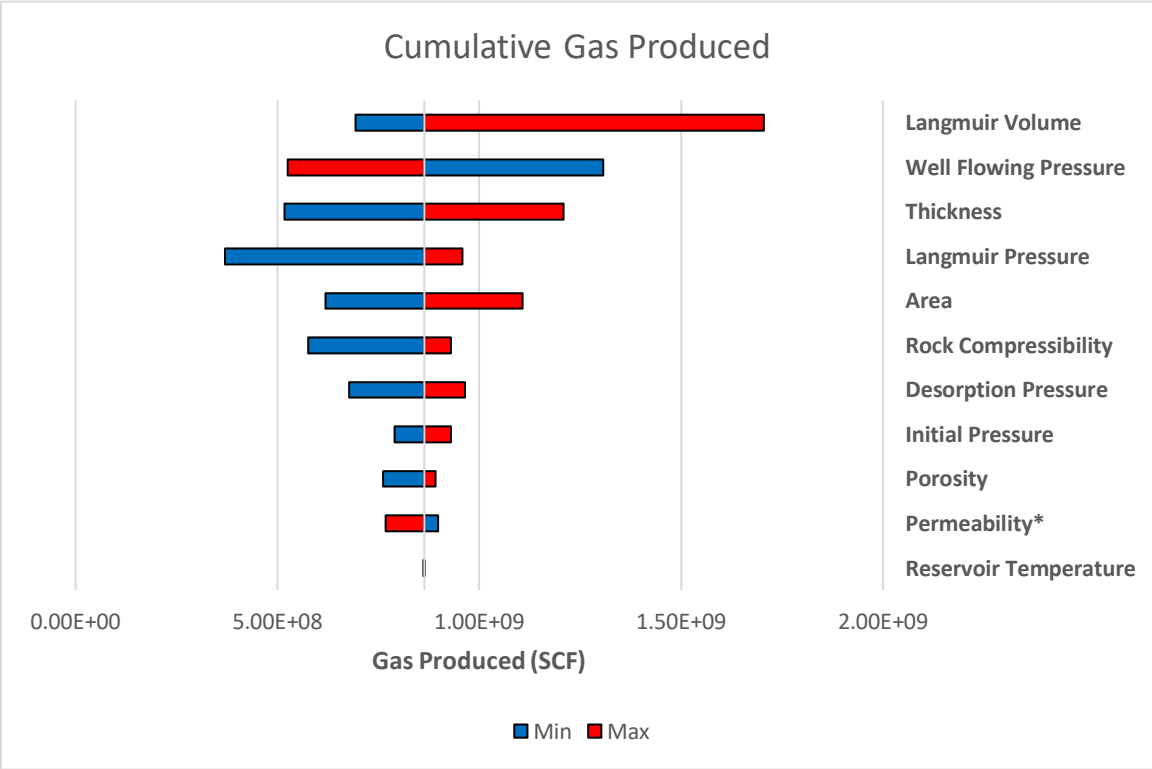


**Figure 6-46** - Tornado chart showing the effect of each parameter on the cumulative gas produced in SCF.

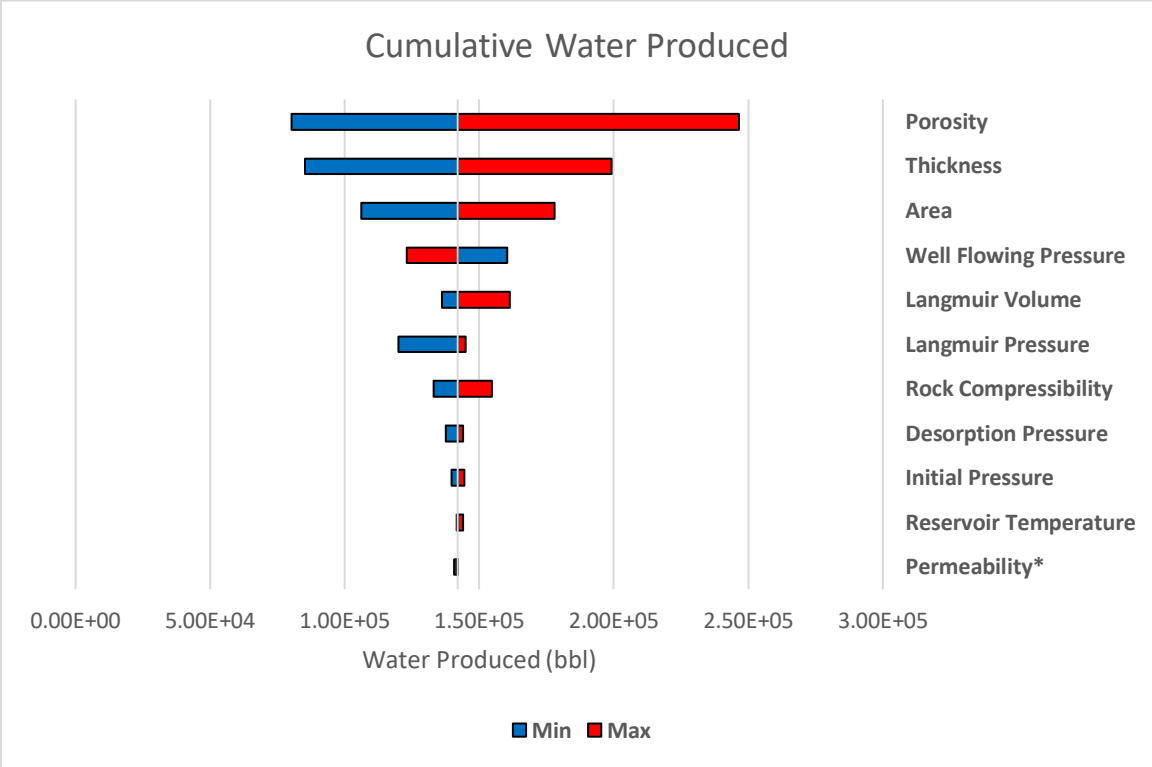


**Figure 6-47** - Tornado chart showing the effect of each parameter on the cumulative water produced in bbl.

* Permeability simulation time was increased to 20 years for a better display of results.

From the tornado charts presented above, the effect of each reservoir parameter on the specified result is ranked from top to bottom. The length of the bar for each parameter shows the sensitivity of the pursued result to a change in that parameter. It is not necessary that the output is symmetric if the input is symmetric. In fact, for non-linear problems, such as this, the output is not expected to be symmetric. This can be seen in **Figure 6-44** where the minimum permeability has a much larger effect on the time to peak rate than the maximum even though they are both 27.5 $[md]$ apart from the base case value.

Considering that the evaluated case is an undersaturated coalbed methane reservoir (100% water saturation initially), the parameters that affect the pore volume has the largest effect on the cumulative water produced. These parameters are reservoir area, thickness and porosity. This is because the pore volume is directly related to how much water is available in the reservoir. The

more water there is, the more that will be produced and vice versa. Related to this is the cumulative gas produced, this is also affected by the pore volume because as water is produced, gas is being desorbed to take its place in the pore volume and be produced as well. However, what has a larger effect on the cumulative gas produced is the Langmuir properties. The Langmuir volume is the maximum amount of gas that can be adsorbed on the rock. Thus, a greater Langmuir volume will result in more gas being available to be produced. On the other hand, the Langmuir pressure is the pressure at which half of Langmuir volume has desorbed. This is essentially the pressure sensitivity of the adsorptive rock. If the Langmuir pressure is low, a higher-pressure drawdown will be required to produce more gas. Moreover, the pressure should reach a certain value in order for gas to start to desorb. This is called the desorption pressure. From the tornado charts, desorption pressure affects gas production in general and particularly, the time to peak gas rate as it is dictated by when desorption starts.

The well flowing pressure has a large effect on production since it determines the pressure drawdown which controls production. However, it does not seem to affect the time to peak rate as much.

Production is also controlled by the parameters that affect Darcy's law. These parameters include thickness, permeability, initial pressure and well flowing pressure. While the reservoir thickness plays a large role in production in general, it does not seem to affect the time to peak gas rate as much. This is probably due to doubling thickness would double the production rate, but it would also double the OGIP. So, the time to reach the pressure for $q_g\ max$ above would roughly be the same. On the other hand, permeability has a significant impact on the gas rate and the time to peak gas rate, this is obvious. However, what seems odd is that both the increase and decrease in permeability had a negative effect on both the cumulative water and gas produced while also being not very significant. Essentially, this means is that the area under the rate versus time curve is the same for the different permeabilities. To investigate this, plots comparing the effect of

different permeabilities on the gas rate, cumulative gas produced, and change in pressure has been generated.

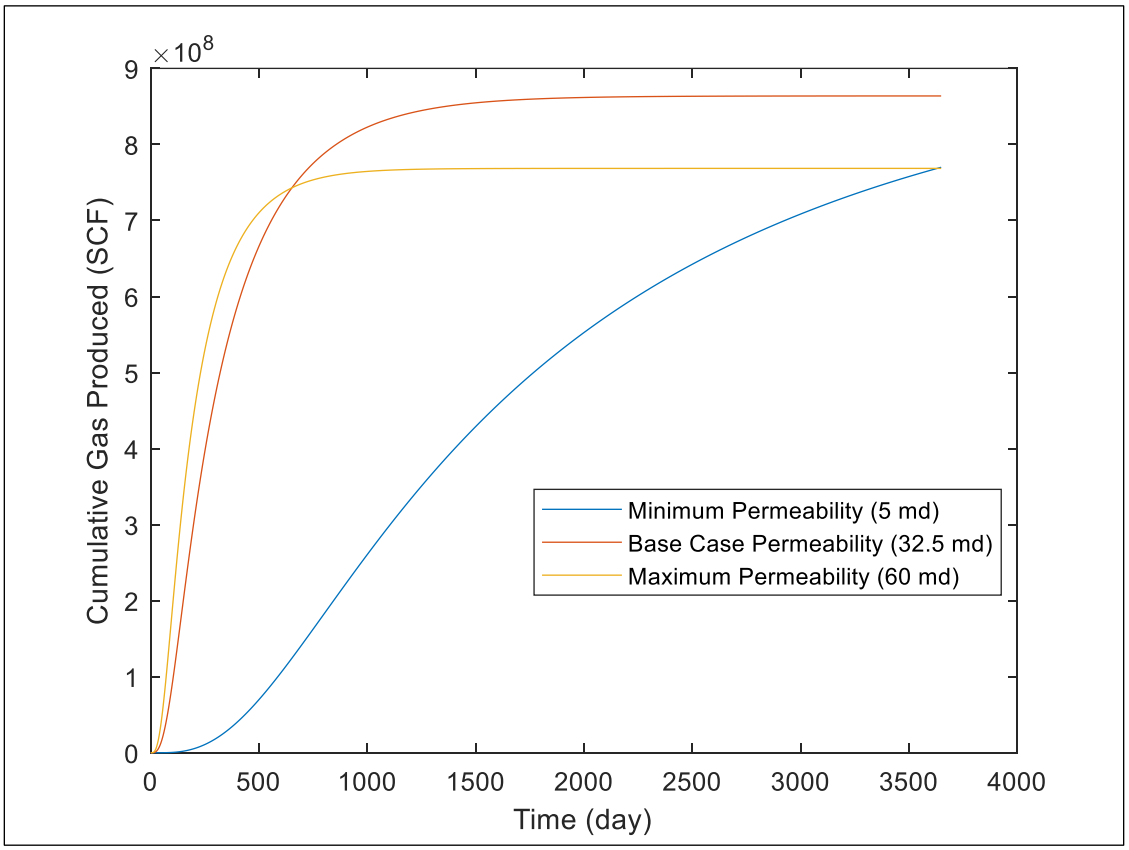


**Figure 6-48** - Cumulative gas produced for different permeability inputs.

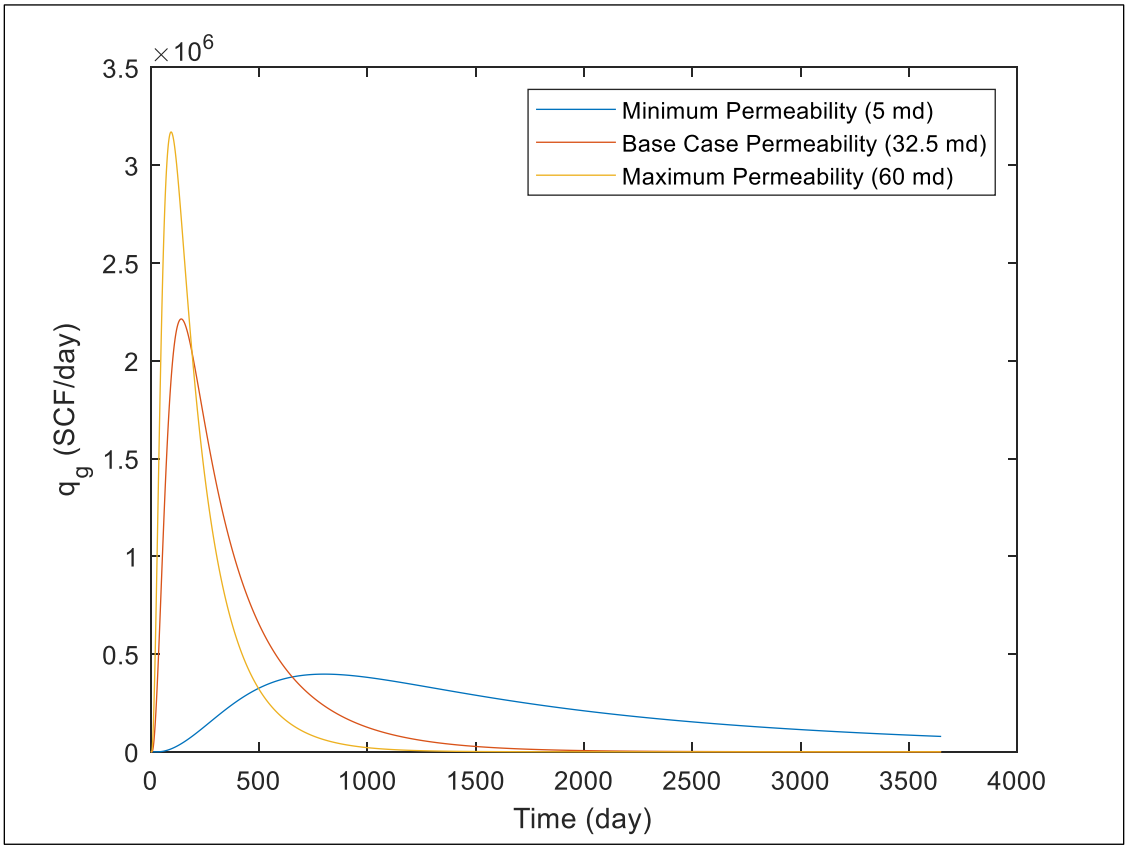


**Figure 6-49** - Gas rate for different permeability inputs.

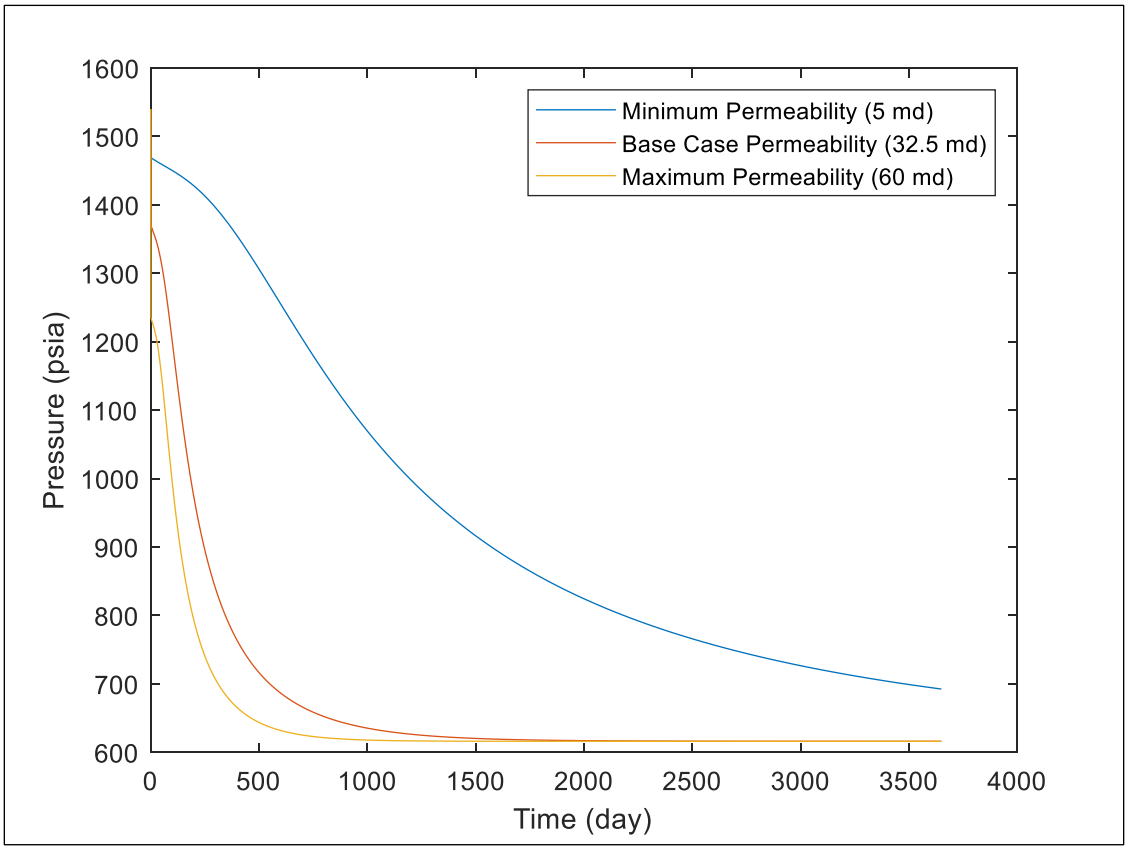


**Figure 6-50** - Pressure versus time for different permeability inputs.

It seems that a lower permeability causes a slower drop in pressure (**Figure 6-50**). This results in the drawdown being maintained over a longer period of time and thus, a higher cumulative production in the long run. Coincidentally, after 10 years of production, the amount gas that the minimum permeability produced is almost equal to the amount produced by the maximum permeability. However, judging from **Figure 6-48**, the minimum permeability should produce more and plateau at a higher amount of cumulative gas produced. To examine this, the total simulation time is increased to 20 years. **Figure 6-51** shows the results for all permeability cases after 20 years of production.

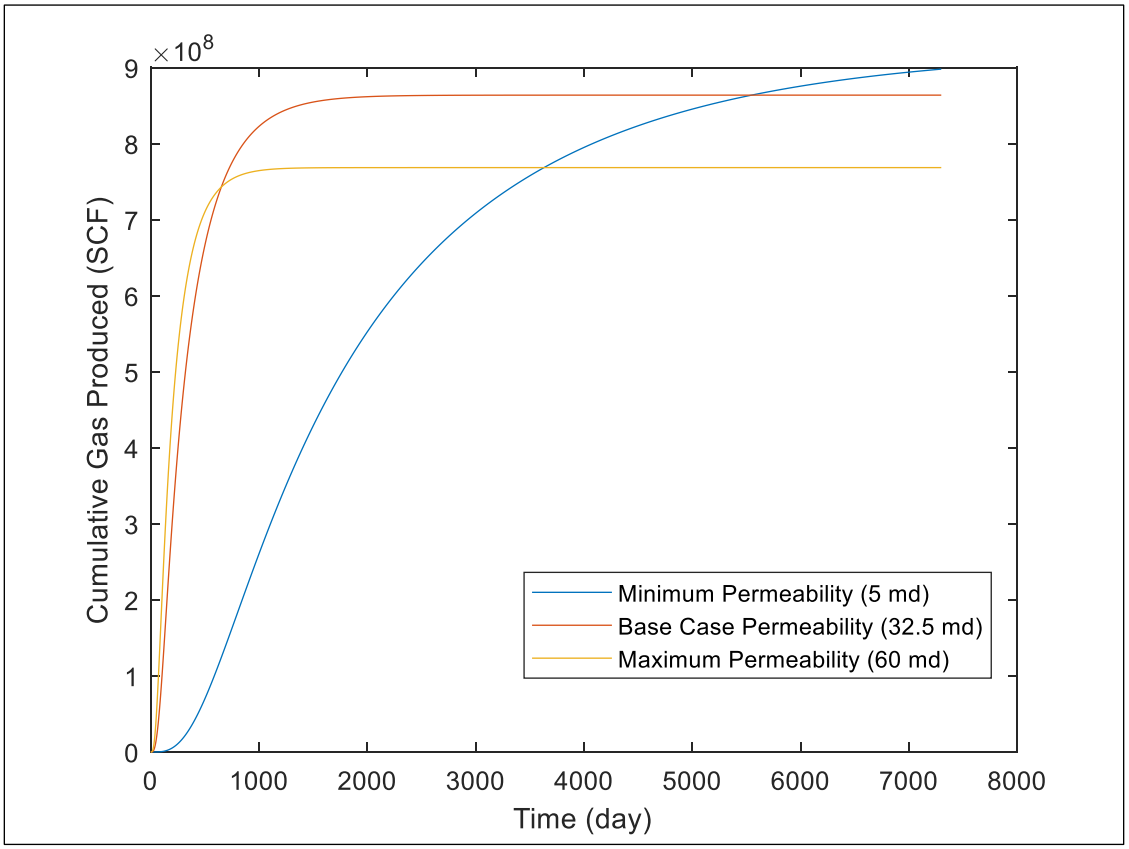


**Figure 6-51 -** Cumulative gas produced for different permeability inputs with 20 years simulation time.

Indeed, the minimum permeability case produces more gas over a longer period of time and plateaus at higher level than the base case.

Even though it seemed unlikely that a numerical simulator would produce the same effect, these cases were evaluated using a numerical simulator for comparison. However, since the numerical simulator being used does not incorporate a desorption pressure, both models were set to desorb gas at initial pressure. The results showed agreement between the two models. This led to the conclusion that the desorption pressure is the culprit for this odd behavior.

**Figure 6-52** shows the cumulative gas production for the different permeability cases, with desorption pressure set to initial pressure.

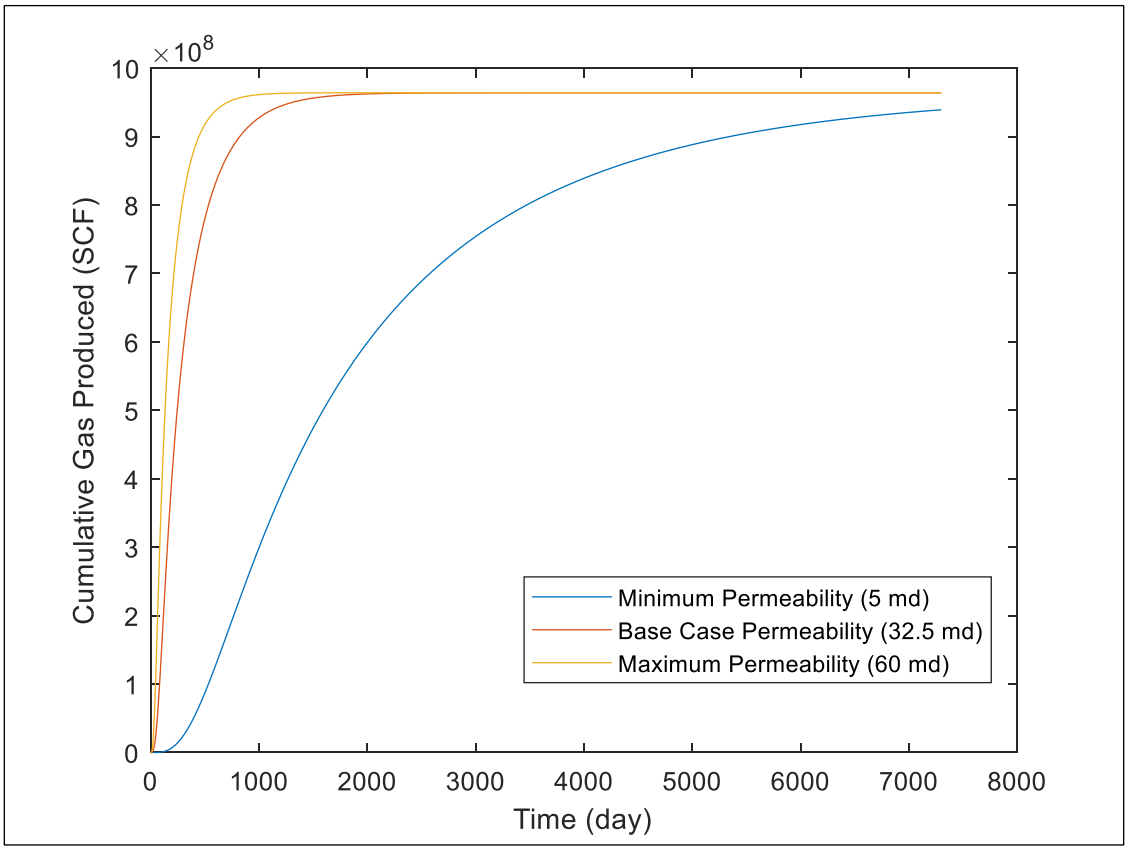


**Figure 6-52** - Cumulative gas produced for different permeability inputs with 20 years simulation time and desorption pressure set at initial pressure.

From **Figure 6-52**, it can be seen that all permeability cases plateau on approximately the same cumulative gas produced. Permeability only affects how fast it will take to reach the plateau as can be seen between the maximum case and the base case. It is expected that if the simulation

time is increased, the minimum permeability case should also plateau on the same level as the other cases.

The possible cause for this disparity is because when there is no gas desorbing after production starts, only water is being produced. However, the void space in the pore volume that is left from the produced water is not being filled up by desorbed gas. This causes a large pressure drop which would not occur if gas was desorbing from the beginning of production. Thus, the pressure drop causes a loss of drawdown and less cumulative gas is produced by the end of production.

**Table 6-5 – Pressure profile for the maximum permeability case with and without desorption pressure.**

| Maximum Permeability Case (60 md) | | |
|---|---|---|
| **Time (day)** | **Pressure, psia (Desorption Pressure = 1490 psia)** | **Pressure, psia (Desorption Pressure = Initial Pressure = 1540 psia)** |
| 0 | 1540.0 | 1540.0 |
| 1 | 1234.9 | 1537.0 |
| 2 | 1233.9 | 1534.1 |
| 3 | 1232.8 | 1531.3 |
| 4 | 1231.7 | 1528.6 |
| 5 | 1230.7 | 1525.9 |
| 6 | 1229.7 | 1523.1 |
| 7 | 1228.7 | 1520.4 |
| 8 | 1227.7 | 1517.6 |
| 9 | 1226.7 | 1514.7 |
| 10 | 1225.7 | 1511.6 |

**Table 6-5** shows the pressure readings for the maximum permeability case with and without desorption pressure. It can be seen that since there is no pressure support from the desorbed gas, the pressure drops rapidly. Thus, production is reduced. On the other hand, when the gas is desorbing as water is being produced, the pressure drops slightly and the drawdown is maintained for more gas to be produced in the long run. Additionally, it seems that the step size which is set as 1-day time steps might be causing the results to be coarse. This would mean that there is a large

amount of error in the calculated pressure value. To validate this observation, additional runs were made with 0.1 and 0.01 step sizes in the Runge-Kutta iteration. **Table 6-6** summarizes the results.

**Table 6-6 - Pressure profile calculated using different step sizes for the maximum permeability case with desorption pressure.**

| Maximum Permeability Case (60 md) (With Desorption Pressure = 1490 psia) | | | |
|---|---|---|---|
| **Time (day)** | **Pressure, psia (1-day Time Step)** | **Pressure, psia (0.1-day Time Step)** | **Pressure, psia (0.01-day Time Step)** |
| 0 | 1540.0 | 1540.0 | 1540.0 |
| 1 | 1234.9 | 1483.5 | 1486.6 |
| 2 | 1233.9 | 1481.0 | 1484.1 |
| 3 | 1232.8 | 1478.6 | 1481.7 |
| 4 | 1231.7 | 1476.2 | 1479.3 |
| 5 | 1230.7 | 1473.9 | 1477.0 |
| 6 | 1229.7 | 1471.6 | 1474.6 |
| 7 | 1228.7 | 1469.2 | 1472.3 |
| 8 | 1227.7 | 1466.8 | 1469.9 |
| 9 | 1226.7 | 1464.4 | 1467.4 |
| 10 | 1225.7 | 1461.9 | 1464.8 |

The results illustrate that step size selected can be a factor in the accuracy of the model. This coincides with what was explained earlier regarding Runge-Kutta. However, reducing the step size comes at the cost of computational time. **Figure 6-53** illustrates the change in accuracy caused by the different time steps. It also shows the difference between having a desorption pressure below initial pressure and having desorption pressure at initial pressure.

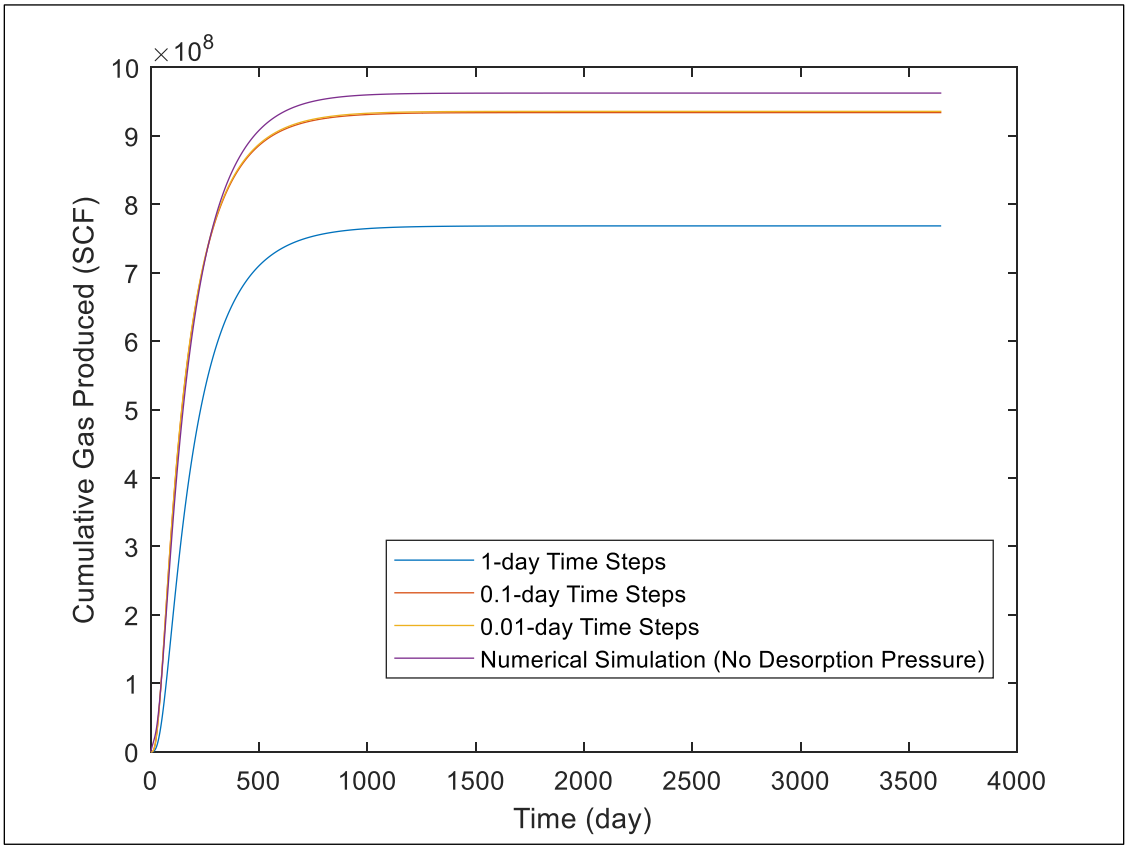


**Figure 6-53** - Cumulative gas produced comparison between different time steps. Also, numerical simulation is plotted but without desorption pressure.

### 6.6.2 Dual Peaking

Previous literatures and real field production data reports a unique behavior in gas rate curves generated for CBM. This feature is referred to as "dual peaking" (Okeke, 2005). However, there was no explanation as to why this behavior occurs. This behavior is also witnessed in the numerical simulation used to validate the developed semi-analytical model. **Figure 6-54** shows a magnified image of the early time where the first peak arises.

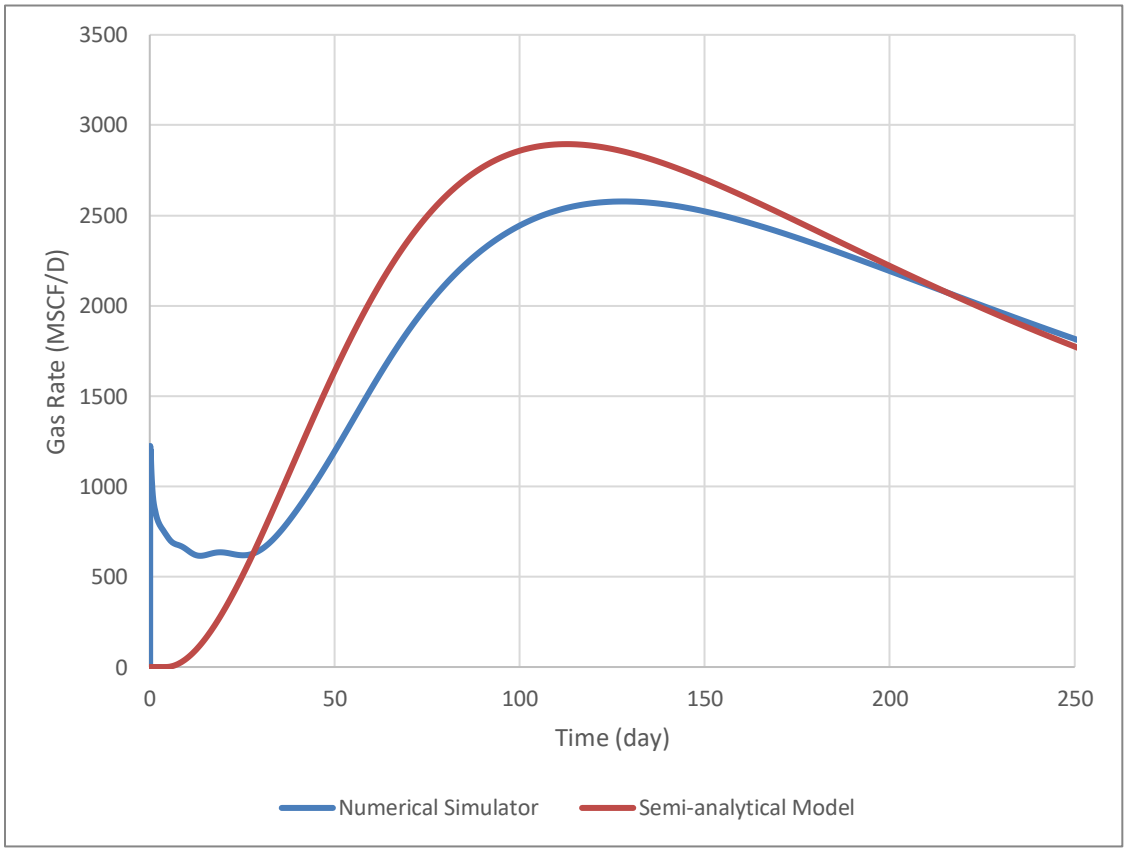


**Figure 6-54** - Dual peaking behavior in numerical simulation of case 5.

As this behavior cannot be observed in the semi-analytical model which assumes pseudo-steady state from the first day, it is safe to assume that the dual peaking behavior is caused by the transient state production that occurs at the early time region. This can be backed up through the derivative of the gas rate over time ($\frac{dq_g}{dt}$) from the semi-analytical model that shows the curve

having a zero value at a single point only which implies one peak (see **Figure 6-29**). However, for the numerical simulation, there are three points at which the derivative of the gas rate curve has a zero value. The first is at a maximum point where the first peak is, the second is at a minimum (which also has a derivative/slope of zero), and the third is at another maximum where the second peak is. **Figure 6-55** shows this observation.

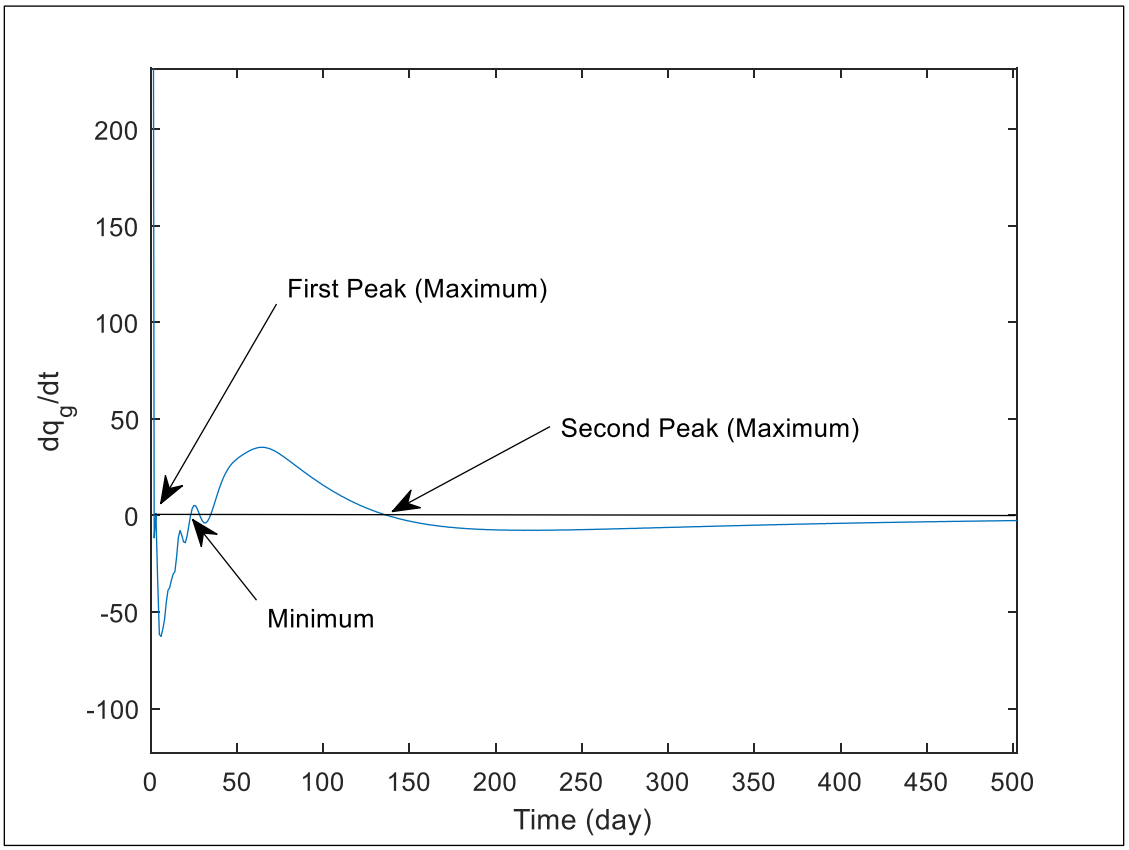


**Figure 6-55 -** Derivative of the gas rate over time (dqg/dt) for case 5 numerical simulation with annotations showing the locations of the maximums (peaks) and the minimum.

### 6.6.3 Prediction of Change of Water Saturation Over Time ($\frac{dS_w}{dt}$)

One of the observations made from the results of the semi-analytical model is that the change of water saturation over time ($\frac{dS_w}{dt}$) can be estimated using the water rate, initial water formation volume factor ($B_{wi}$) and initial porosity ($\phi_i$). The basis of this comes from the developed water rate equation.

$$q_w = \frac{V_b}{\alpha_c}\frac{d}{dt}\left(\frac{\phi\, S_w}{B_w}\right) \tag{6.31}$$

Assuming that the changes in porosity and water formation volume factor were small, the equation can be manipulated to be made in terms of the change in water saturation over time:

$$\frac{dS_w}{dt} = \frac{\alpha_c\, q_w\, B_{wi}}{V_b\, \phi_i} \tag{6.32}$$

Using the base case, this theory was tested. **Figure 6-56** shows the results from both the semi-analytical model and equation **(6.32)**.

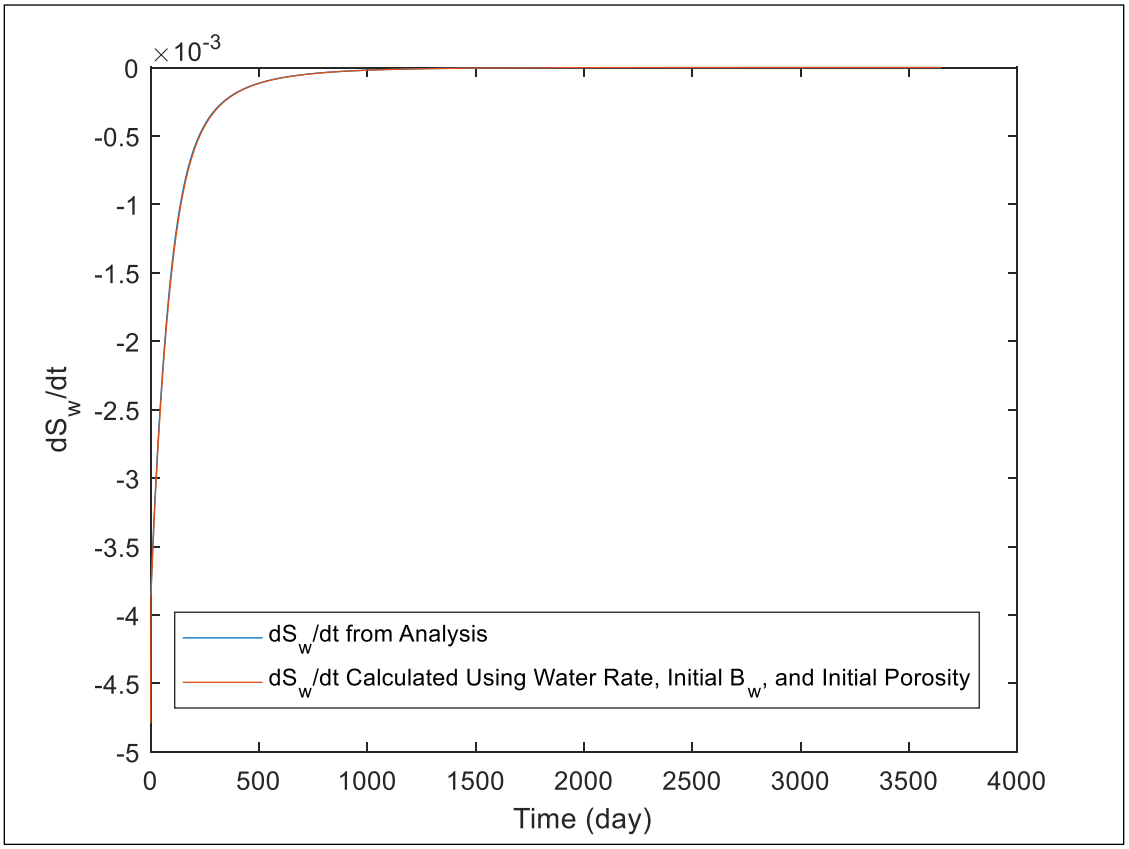


**Figure 6-56** - dSw/dt from analysis vs prediction.

However, this equation gave accurate predictions only when the rock compressibility is low. This is because both the water formation volume factor and porosity equations (equation **(4.20)** and **(4.1)** respectively) have a rock and compressibility term multiplying the pressure dependency term. Since the rock and water compressibility are small, the pressure dependency term is made negligible. Thus, the changes in water formation volume factor and porosity are considered to be very small and can be assumed to be constant at initial value.

### 6.6.4 Prediction of Gas Saturation at the End of Production

Another observation made shows that at the end of production, the gas saturation was approximately equal to the percentage of water produced from the reservoir after desorption pressure is achieved.

$$S_g \approx \frac{W_p}{W} \tag{6.33}$$

To illustrate this, **Table 6-7** shows the results from the semi-analytical model using base case values.

**Table 6-7 - Analysis of the Percentage Water Produced Compared to the Gas Saturation at the End of Production for Semi-Analytical Model**

| | |
|---|---|
| Original Water in Place (OWIP) | $310312\ bbl$ |
| Cumulative Water Produced | $140728\ bbl$ |
| Percentage of OWIP Produced | 45.35% |
| Gas Saturation at End of Production | 44.9% |
| Error Percentage | 1.00% |

To validate this observation, the same was done with the five cases developed for numerical simulation.

**Table 6-8 - Analysis of the Percentage Water Produced Compared to the Gas Saturation at the End of Production for Numerical Simulator (Case 1)**

| **Case 1** | |
|---|---|
| Original Water in Place (OWIP) | $215664\ bbl$ |
| Cumulative Water Produced | $124788\ bbl$ |
| Percentage of OWIP Produced | 57.86% |
| Gas Saturation at End of Production | 43.93% |
| Error Percentage | 31.71% |

**Table 6-9- Analysis of the Percentage Water Produced Compared to the Gas Saturation at the End of Production for Numerical Simulator (Case 2)**

| **Case 2** | |
|---|---|
| Original Water in Place (OWIP) | $286647\ bbl$ |
| Cumulative Water Produced | $139386\ bbl$ |
| Percentage of OWIP Produced | 48.62% |
| Gas Saturation at End of Production | 45.76% |
| Error Percentage | 6.25% |

**Table 6-10 - Analysis of the Percentage Water Produced Compared to the Gas Saturation at the End of Production for Numerical Simulator (Case 3)**

| **Case 3** | |
|---|---|
| Original Water in Place (OWIP) | $305575\ bbl$ |
| Cumulative Water Produced | $141634\ bbl$ |
| Percentage of OWIP Produced | 46.35% |
| Gas Saturation at End of Production | 45.68% |
| Error Percentage | 1.47% |

**Table 6-11 - Analysis of the Percentage Water Produced Compared to the Gas Saturation at the End of Production for Numerical Simulator (Case 4)**

| **Case 4** | |
|---|---|
| Original Water in Place (OWIP) | $307941\ bbl$ |
| Cumulative Water Produced | $141911\ bbl$ |
| Percentage of OWIP Produced | 46.08% |
| Gas Saturation at End of Production | 45.67% |
| Error Percentage | 0.90% |

**Table 6-12 - Analysis of the Percentage Water Produced Compared to the Gas Saturation at the End of Production for Numerical Simulator (Case 5)**

| **Case 5** | |
|---|---|
| Original Water in Place (OWIP) | $309834\ bbl$ |
| Cumulative Water Produced | $142132\ bbl$ |
| Percentage of OWIP Produced | 45.87% |
| Gas Saturation at End of Production | 45.66% |
| Error Percentage | 0.46% |

From the results of this analysis, it is concluded that rock compressibility is a factor when it comes to this observation. This could be due to the difference in water production caused by the transient-state during early production. This is also backed up by the fact that case 5 has the least time to pseudo-steady state and the least error percentage calculated. Also, as the time to pseudo-steady state decreased, the error percentage decreased. Another explanation for this phenomenon is because as the rock and water compressibility decreased (became more incompressible) then for every 1 $[bbl]$ of water produced, there is 1 $[bbl]$ of void space in the pore volume for the gas to

desorb in. This is because there is no change in pore volume due to the incompressibility of the reservoir rock and water.

# Chapter 7

## Summary and Conclusions

In this thesis, a Muskat-type equation for unconventional gas-water reservoirs impacted by adsorption has been derived in different domains; pressure, time, cumulative gas produced, and cumulative water produced domains. It has also been derived for different flow regimes such as pseudo-steady state and "pseudo-transient" state. A semi-analytical model has been developed in MATLAB that solves the Muskat-type ordinary differential equation (ODE) using the Runge-Kutta method. Using the original Muskat-type equation in the pressure domain ($\frac{dS_w}{dP}$), the semi-analytical model generates water saturation values as a function of inputted pressures. However, solving the system of two ordinary differential equations for the Muskat-type equation in the time domain ($\frac{dP}{dt}$ and $\frac{dS_w}{dt}$) results in pressure and saturation values as a function of time.

Coalbed methane was selected to be the unconventional reservoir used to test the developed semi-analytical model. This is due to its remarkable adsorption capabilities and its short transient-state period during production which allows for pseudo-steady state to be achieved. The semi-analytical model was tested on a data-driven base case and range of reservoir parameters.

Unfortunately, the "pseudo-transient" model did not produce any results. It is speculated that the resulting equations were too stiff for Runge-Kutta or they did not honor mass balance laws. However, the derivations did show that the change in bulk volume during transient-state is constant if the permeability and porosity are constant and the time steps are uniform. On the other hand, the pseudo-steady state model showed promising results.

Using the developed base case, the semi-analytical model for pseudo-steady state has been validated using finite difference, MATLAB's gradient function, and analytical equations. It was

also benchmarked against a homogenous and isotropic numerical simulator that uses the same correlations as the ones used in the semi-analytical model in order to calculate parameters such as z-factors, gas viscosities and relative permeabilities. The results showed that the time to pseudo-steady state is the most significant factor affecting the results produced from the numerical simulator. As the time to pseudo-steady state decreased, a better match was found between the semi-analytical model and the numerical simulator. The concluded reason for this is because of the transient state that takes place within the numerical simulator but not in the developed model which assumes pseudo-steady state from the beginning. Thus, decreasing the rock compressibility caused a decrease in the time it takes to achieve pseudo-steady state. At $t_{pss}$ less than 0.111 days[2], numerical simulation is almost replaceable in forecasting rates. However, at $t_{pss}$ less than 0.717 days[2], cumulative gas produced can be accurately forecasted.

Moreover, an analytical equation has been developed to identify the peak gas rate and the time to the peak gas rate. In this equation, the byproduct of the Muskat-type equation which solves for saturation as a function of pressure: $\frac{dS_w}{dP}$ , is used. This equation can be rewritten in terms of physical parameters such as rock and fluid properties. Therefore, if history matching were to be done, each property can be studied to identify those causing the peak. Furthermore, three well specifications were constructed to study their effects on the peak production: specified (constant) well flowing pressure $P_{wf}$, specified (constant) drawdown $(\bar{P} - P_{wf})$ and specified (constant) water production $q_w$. The first two well specifications resulted in a peak gas production rate; while the constant water production did not produce such a peak.

In the gas production profile of the semi-analytical model, two inflection points can be analyzed graphically. This was done through the derivative of the gas rate $(\frac{dq_g}{dt})$ which produces

[2] This is not a general recommendation but was based off the limited amount of cases analyzed within this thesis. For a more general range of applicability, more cases will need to developed and analyzed.

different maxima and minima signifying a change in the direction of curvature. The first inflection point is a maximum in the rate derivative indicating a concave (upward) production curve while the second inflection point is a minimum in the rate derivative indicating concave (downward) production. Also, the derivative goes through zero once signifying the peak production. The inflection point-locations can be altered by changing reservoir and fluid parameters. This could be especially useful when doing history matching and testing the impact of various rock and fluid properties on the shape of the production profile. Furthermore, if decline curve analysis was to be performed using Arps Decline Curves, then it should be done after the second inflection point.

The solution of the material balance is strongly dependent on the time to pseudo-steady state. Short times to pseudo-steady state are closer to the inherent assumption in the semi-analytical model and result in good agreement between the proposed model and numerical simulation. Long times to pseudo-steady state deviate from the assumptions inherent to the proposed model and result in less accurate agreement with reservoir simulation.

With a $t_{pss}$ less than 0.178 days$^2$, material balance can be used to replace decline curve analysis. The Muskat-type equation in the cumulative gas and water produced domain was used to compare late-time production between the numerical simulation and the results of the developed semi-analytical model.

Using the proposed differential material balance (Muskat-type equation), a non-iterative methodology was developed to calculate the original gas in place (OGIP) through King's integral material balance equation. It was also concluded that the use of the slope of the $P/z^*$ to calculate the OGIP is more accurate than extrapolating for the intercept.

The dual peaking phenomenon that is observed in CBM field production data and numerical simulation that occurs at the early stage of production was concluded to be purely due to the transient-state. The reasoning behind this is because this behavior has not been witnessed in

the developed semi-analytical model or its derivatives which assumes pseudo-steady state flow only.

At low rock and water compressibility, it is possible to estimate the change in water saturation over time ($\frac{dS_w}{dt}$) using the water production rate and initial values for water formation volume factor and porosity. This is because the pressure dependency term in the porosity and the water formation volume factor equations is made negligible due to it being multiplied by the low rock compressibility. Therefore, it is safe to assume they are constant at initial values and do not change with pressure.

Also, an observation has been made that shows that the gas saturation at the end of production can be estimated using the percentage of water produced after desorption pressure. However, the reservoir rock and water compressibility should be very low for an accurate prediction. This is because the pore volume should not change to allow for every barrel of water produced, one barrel of void pore volume is available for gas to desorb into. This observation holds true even in the results of the numerical simulator.

**Bibliography**


American Energy Innovation Council. (2013). Unconventional Gas Exploration & Production.

Arfken, G. B., & Weber, H.-J. (2005). *Mathematical methods for physicists* (6th ed.). Boston: Elsevier.

Ayers, W. (2001). Coalbed methane in the Fruitland Formation, San Juan Basin, Western United States: A giant unconventional gas play. *AAPG Memoir*, 159 - 188. doi:10.1306/8626D4D7-173B-11D7-8645000102C1865D

Camacho-V, R. G. (1991). Constant-Pressure Production in Solution-Gas-Drive Reservoirs: Transient Flow. *SPE Formation Evaluation, 6*(02), 199-208. doi:10.2118/17118-PA

Dake, L. P. (1978). *Fundamentals of reservoir engineering* (Vol. 8;8.;). New York;Amsterdam;: Elsevier Scientific Pub. Co.

Dune, K., & Bright N, O. (2012). *A NEW COMPUTERIZED APPROACH TO Z-FACTOR DETERMINATION* (Vol. vol 2).

Ertekin, T., Abou-Kassem, J. H., & King, G. R. (2001). *Basic applied reservoir simulation* (Vol. 7). Richardson, Tex: Society of Petroleum Engineers.

Fatoorehchi, H., Abolghasemi, H., Rach, R., & Assar, M. (2014). An improved algorithm for calculation of the natural gas compressibility factor via the Hall-Yarborough equation of state. *The Canadian Journal of Chemical Engineering, 92*(12), 2211-2217. doi:10.1002/cjce.22054

Fekete Associates Inc. (2012). Material Balance Analysis Theory. Retrieved from http://www.fekete.com/SAN/TheoryAndEquations/HarmonyTheoryEquations/Content/HTML_Files/Reference_Material/Analysis_Method_Theory/Material_Balance_Theory.htm

Holditch, S. A. (2003). The increasing role of unconventional reservoirs in the future of the oil and gas business. *Journal of Petroleum Technology, 55*(11), 34-+. doi:10.2118/1103-0034-jpt

King, G. R. (1993). Material-Balance Techniques for Coal-Seam and Devonian Shale Gas Reservoirs With Limited Water Influx. *SPE Reservoir Engineering, 8*(01), 67-72. doi:10.2118/20730-PA

King, G. R., Ertekin, T., & Schwerer, F. C. (1986). Numerical Simulation of the Transient Behavior of Coal-Seam Degasification Wells. *SPE Formation Evaluation, 1*(02), 165-183. doi:10.2118/12258-PA

Lee, A. L., Gonzalez, M. H., & Eakin, B. E. (1966). The Viscosity of Natural Gases. *Journal of Petroleum Technology, 18*(08), 997-1000. doi:10.2118/1340-PA

Lee, J. (1981). *Well Testing*. Richardson, UNITED STATES: Society of Petroleum Engineers.

Liu, S., & Harpalani, S. (2012). *Gas Production Induced Stress And Permeability Variations In Coalbed Methane Reservoirs*. Paper presented at the 46th U.S. Rock Mechanics/Geomechanics Symposium, Chicago, Illinois. https://doi.org/

Mattar, L., & McNeil, R. (1998). The "Flowing" Gas Material Balance. *Journal of Canadian Petroleum Technology, 37*(02), 4. doi:10.2118/98-02-06

Matthews, C. S. (1986). Transient, Semisteady-State, and Steady-State Flow. *Journal of Petroleum Technology, 38*(04), 385-386. doi:10.2118/15278-PA

Mavor, M. J., Owen, L. B., & Pratt, T. J. (1990). *Measurement and Evaluation of Coal Sorption Isotherm Data*. Paper presented at the SPE Annual Technical Conference and Exhibition, New Orleans, Louisiana. https://doi.org/10.2118/20728-MS

Moghadam, S., Jeje, O., & Mattar, L. (2011). Advanced Gas Material Balance in Simplified Format. *Journal of Canadian Petroleum Technology, 50*(01), 90-98. doi:10.2118/139428-PA

Mosobalaje, O. O., Onuh, C. Y., & Seteyeobot, I. (2015). *A New Solution Methodology to the Material Balance Equation, for Saturated Reservoirs*. Paper presented at the SPE Nigeria Annual International Conference and Exhibition, Lagos, Nigeria. https://doi.org/10.2118/178392-MS

Okeke, A. N. (2005). *SENSITIVITY ANALYSIS OF MODELING PARAMETERS THAT AFFECT THE DUAL PEAKING BEHAVIOR IN COALBED METHANE RESERVOIRS* (Petroleum Engineering Master of Science), Texas A&M University Retrieved from http://hdl.handle.net/1969.1/4196

Palmer, I., & Mansoori, J. (1996). *How Permeability Depends on Stress and Pore Pressure in Coalbeds: A New Model*. Paper presented at the SPE Annual Technical Conference and Exhibition, Denver, Colorado. https://doi.org/10.2118/36737-MS

Poston, S. W., & Poe, B. D. (2007). *Analysis of Production Decline Curves*. Richardson, UNITED STATES: Society of Petroleum Engineers.

Press, W. H. (2007). *Numerical recipes: the art of scientific computing* (3rd ed.). Cambridge, UK;New York;: Cambridge University Press.

Seidle, J. (2011). *Fundamentals of Coalbed Methane Reservoir Engineering*. Tulsa, UNITED STATES: PennWell Corporation.

Slider, H. C. (1966). *Application of Pseudo-Steady-State Flow to Pressure-Buildup Analysis*. Paper presented at the SPE Amarillo Regional Meeting, Amarillo, Texas. https://doi.org/10.2118/1403-MS

# Appendix A

Appendix A presents different results from the semi-analytical model using base case values. This was done by scaling the x-axis to show the relationship between different results.

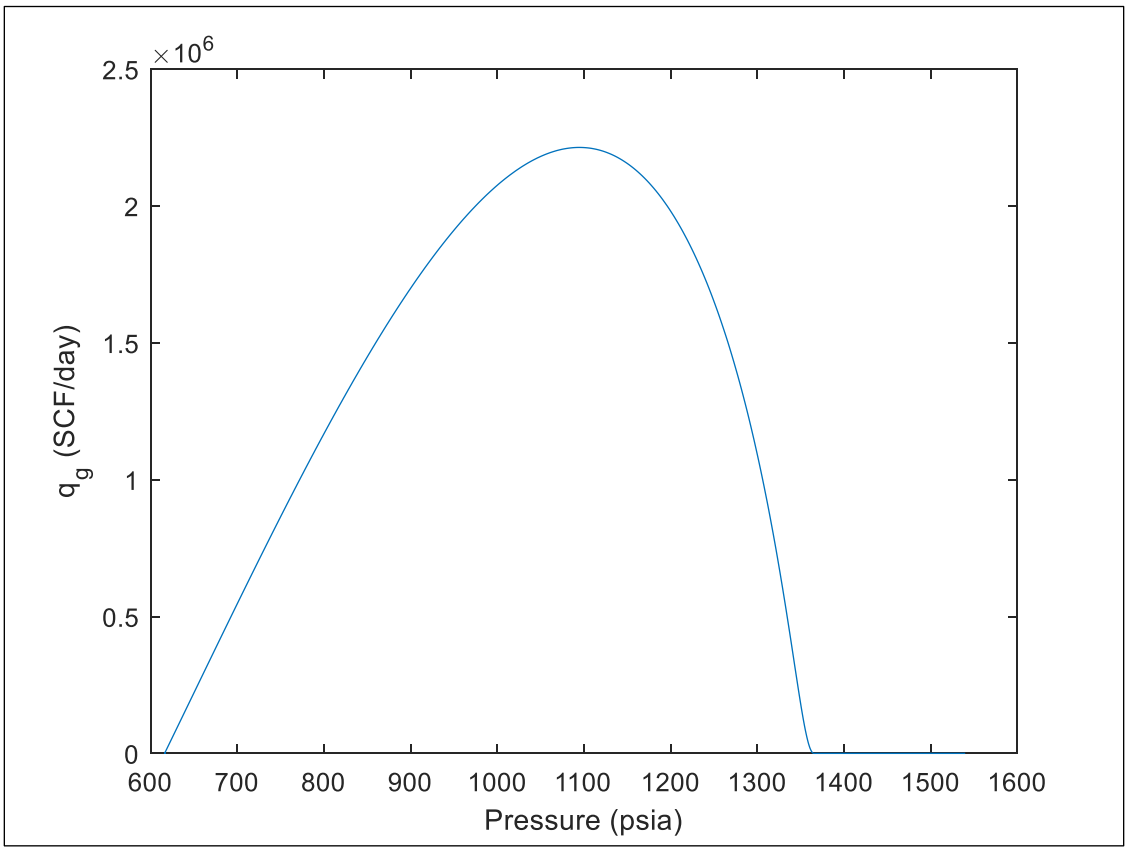


**Figure A-1** – Pressure vs gas rate (base case).

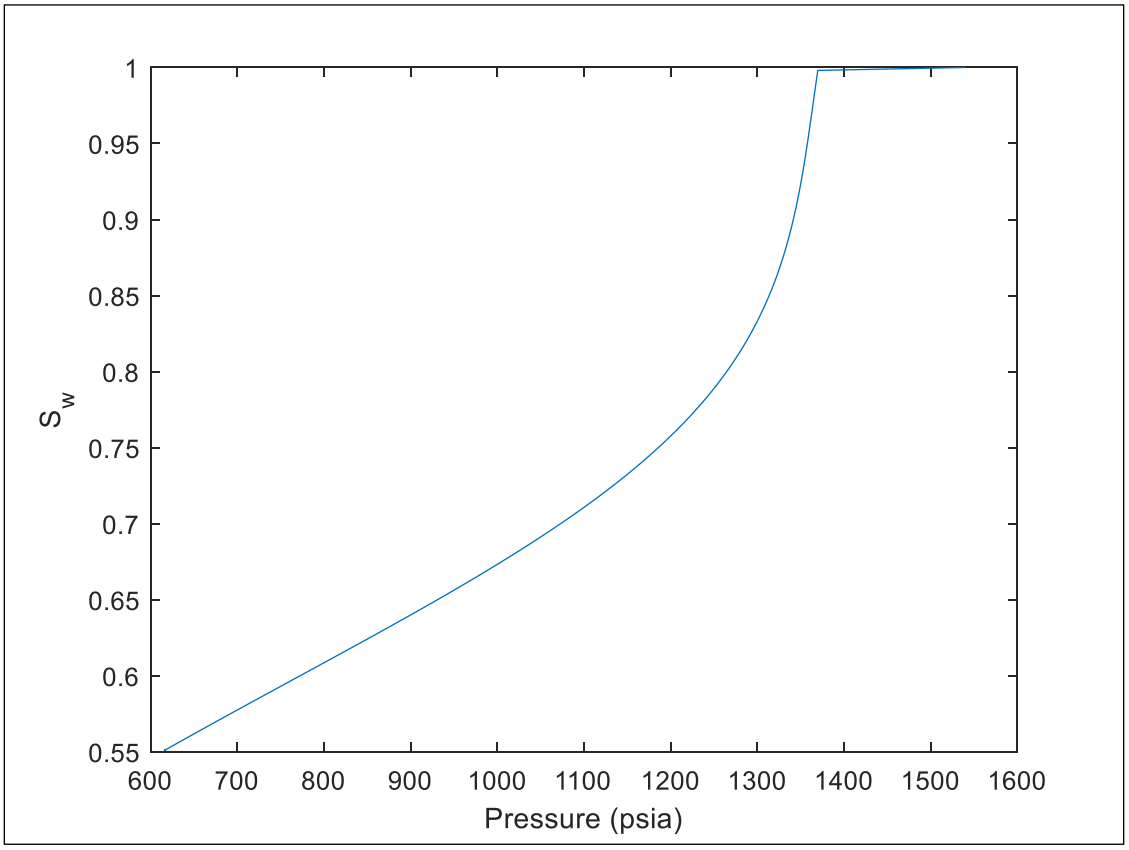


**Figure A-2** – Pressure vs water saturation (base case).

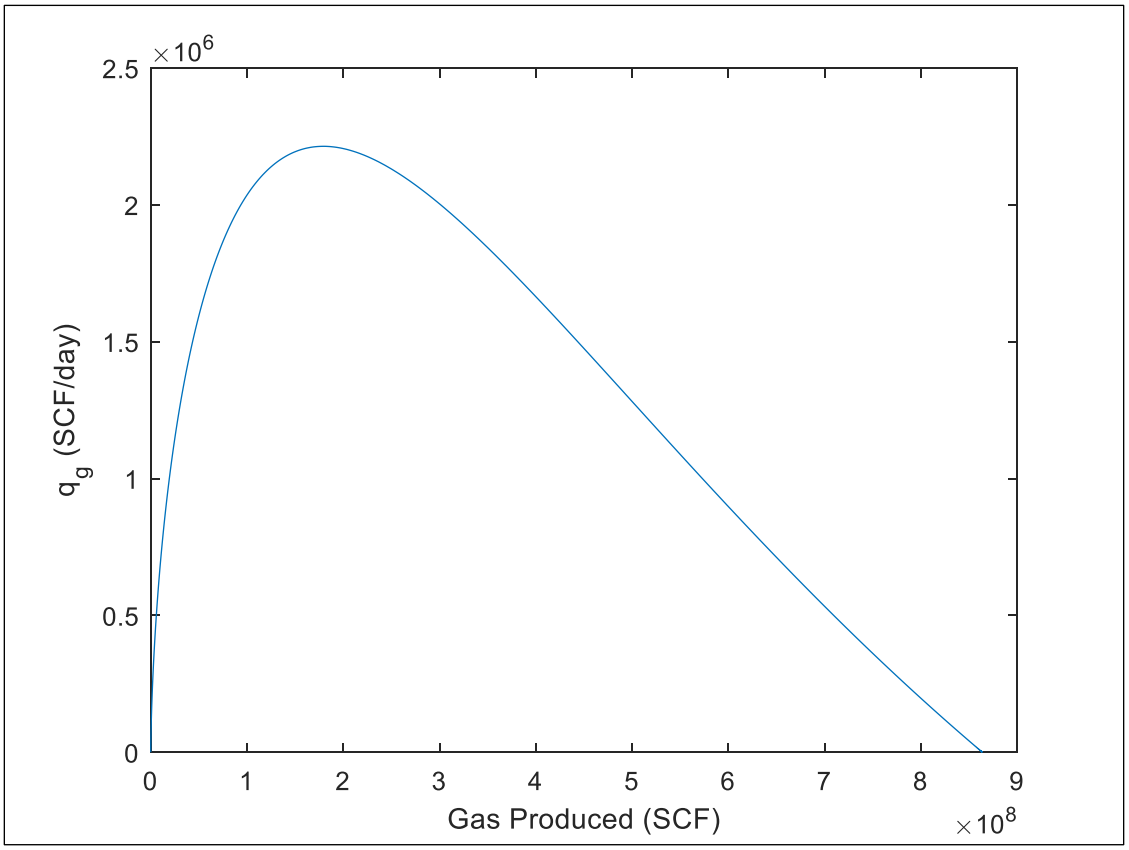


**Figure A-3** – Cumulative gas produced vs gas rate (base case).

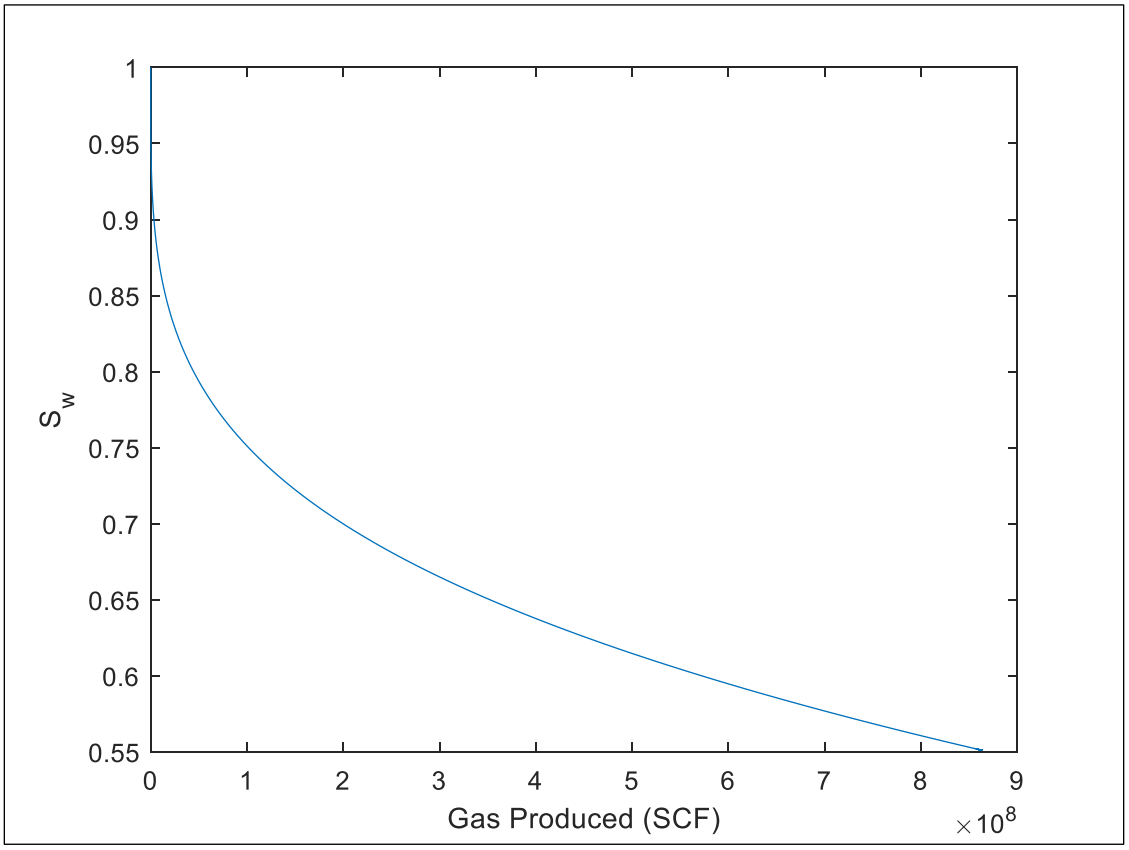


**Figure A-4** – Cumulative gas produced vs water saturation (base case).

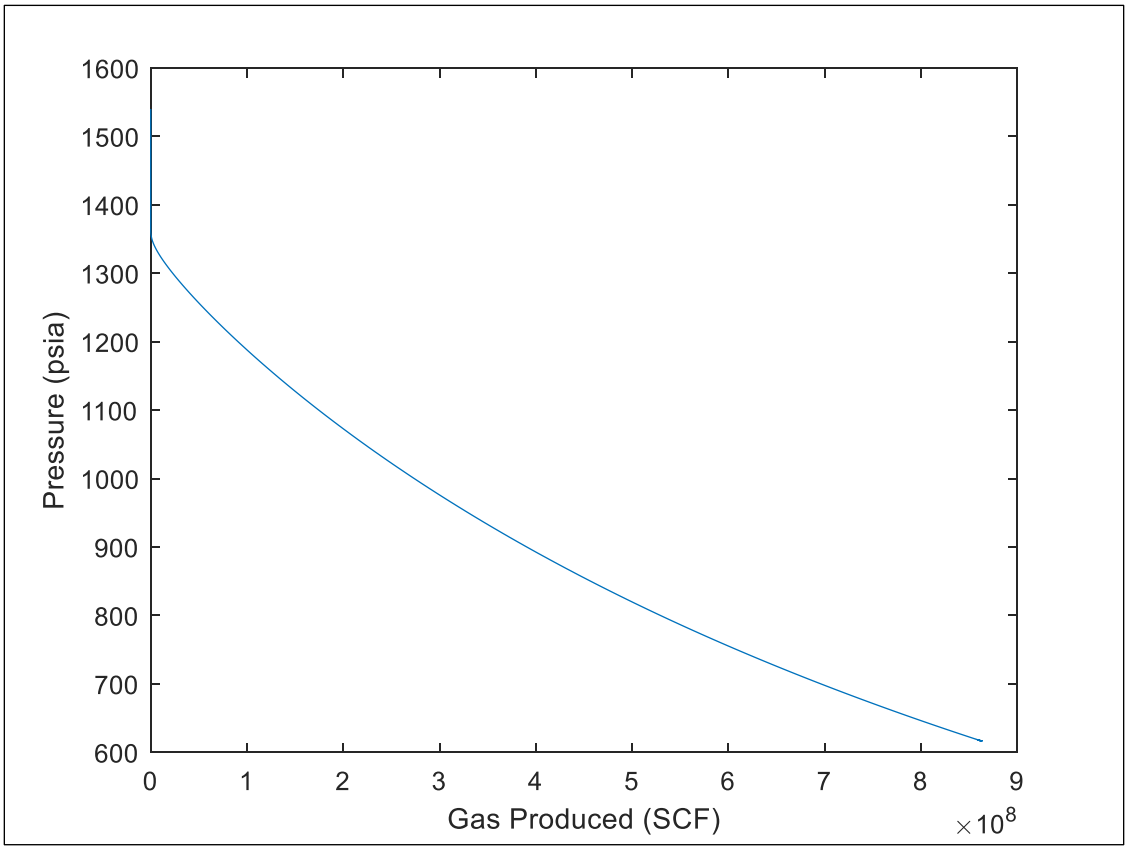


**Figure A-5** – Cumulative gas produced vs pressure (base case).

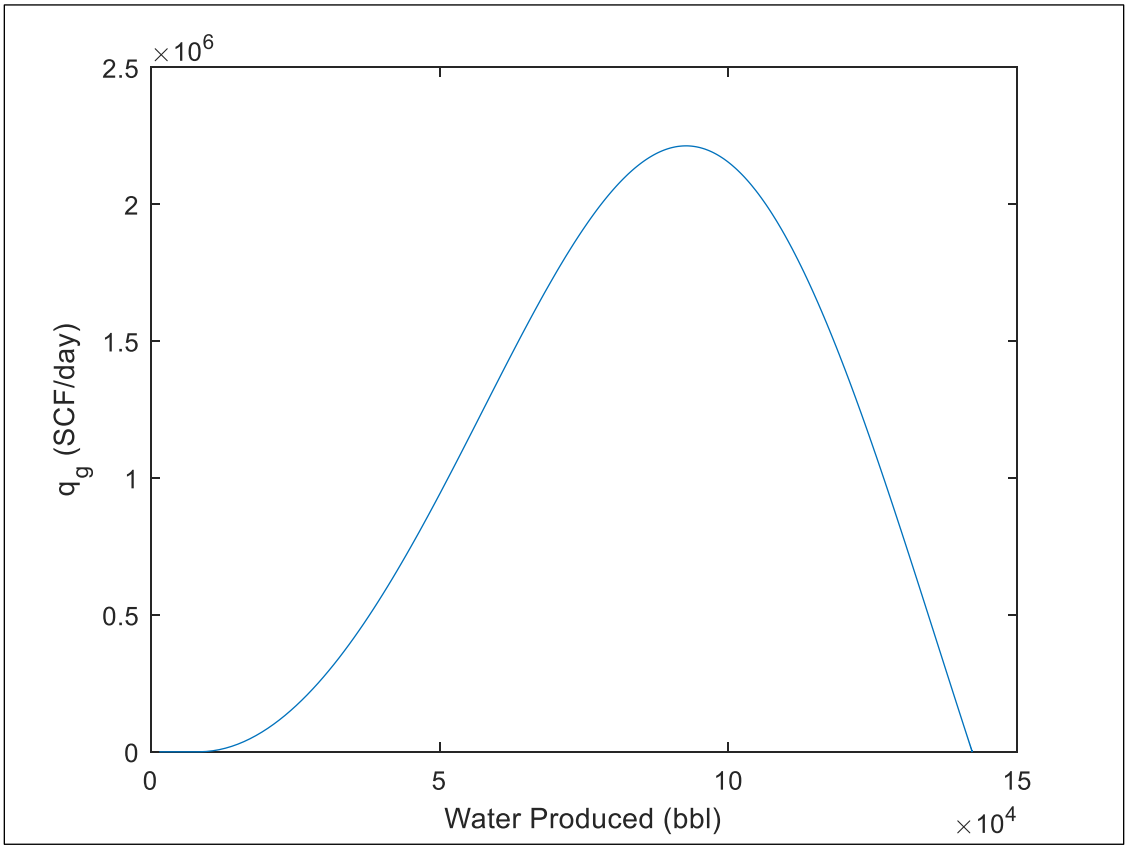


**Figure A-6** – Cumulative water produced vs gas rate (base case).

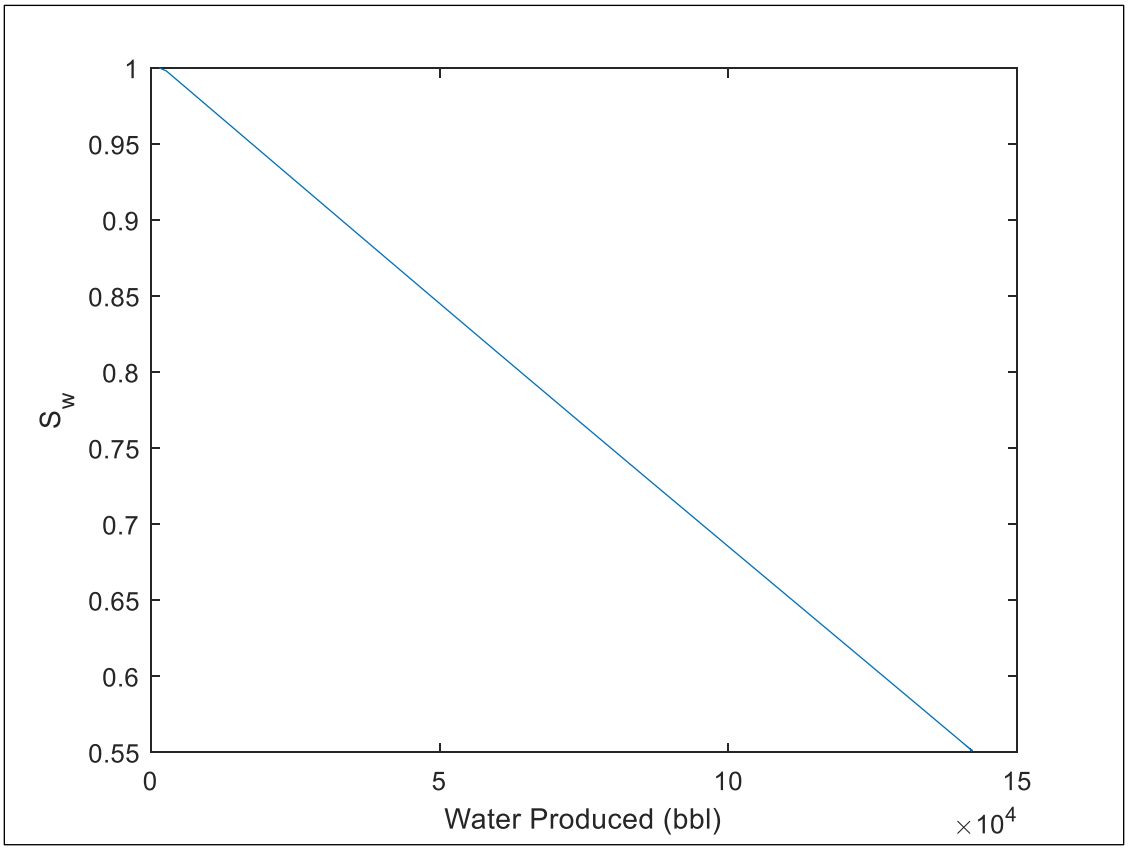


**Figure A-7** – Cumulative water produced vs water saturation (base case).

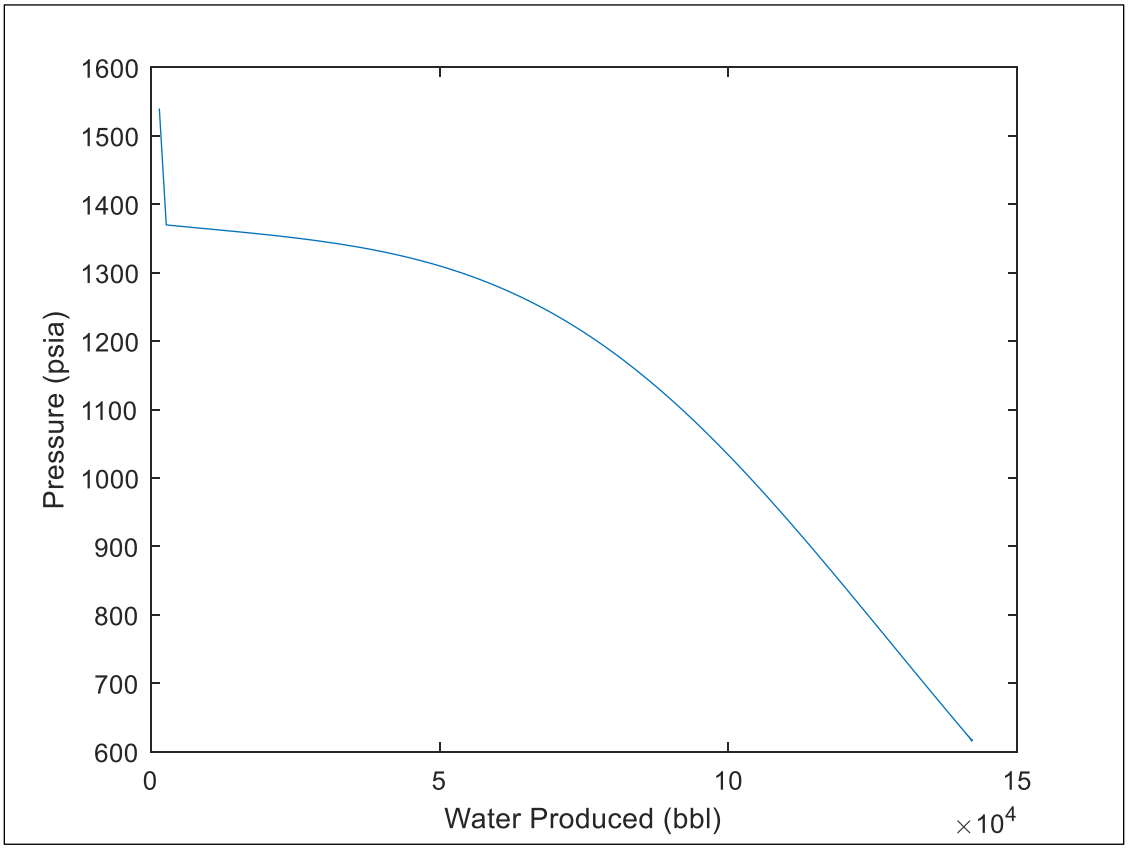


**Figure A-8** – Cumulative water produced vs pressure (base case).